

Reports



MSE Technology Applications, Inc.
P.O. Box 4078
Butte, MT 59702
(406) 494-7100
FAX (406) 494-7230

November 18, 1999

99MSE-1790



John Kieling
New Mexico Environmental Department
2044 A Galisteo Street
Santa Fe, New Mexico 87505

Dear John:

Enclosed is a copy of the "Final Report - Cold Demonstration of NonTraditional In Situ Vitrification at the Los Alamos National Laboratory" (ECCP-11), prepared by MSE Technology Applications, Inc. (MSE) and Geosafe Corporation.

Should you have any questions or require additional information, please contact me at (406) 494-7382, fax - (406) 494-7230, or e-mail - hudgj@mse-ta.com. You can also visit MSE's web site at: www.mse-ta.com.

Sincerely,

Gordon Huddleston
Project Manager

GJH/LKI

Enclosure

cc: Andrea Hart, MSE Technology Applications, Inc.



8179

TV

FSWA
LANL
1/1106/zi



MSE Technology Applications, Inc.
P.O. Box 4078
Butte, MT 59702
(406) 494-7100
FAX (406) 494-7230

November 18, 1999

99MSE-1790

Report
Scott McMullin
U. S. Department of Energy
Savannah River Operations Office
P. O. Box A, Bldg 703-A Room E118N
Aiken, SC 29802

Subject: *"Final Report - Cold Demonstration of NonTraditional In Situ Vitrification at the Los Alamos National Laboratory"* (ECCP-11)

Dear Scott:

Enclosed is a copy of the *"Final Report - Cold Demonstration of NonTraditional In Situ Vitrification at the Los Alamos National Laboratory"* (ECCP-11), prepared by MSE Technology Applications, Inc. (MSE) and Geosafe Corporation. This report was completed under TTP #FT10WE21.

Should you have any questions or require additional information, please contact me at (406) 494-7382, fax - (406) 494-7230, or e-mail - hudgj@mse-ta.com. You can also visit MSE's web site at: www.mse-ta.com.

Sincerely,

Gordon Huddleston
Project Manager

GJH/LKI

Enclosure

Cc w/attachment: Scott McMullin
Mel Shupe
Bruce Erdal
Missy Clem
Brett Campbell
Skip Chamberlain
Bob Seidel

Mike Serrato
Gene Ashby
Deba Daymon
George Rael
Jody Plum
Leo Makovsky
Andrea Hart

Marja Springer
Tom Baca
Julie Canepa
Tony Trujillo
Tom Longo
R. Schreiber

Tc



MSE Technology Applications



Western Environmental Technology Office

P.O. Box 4078 Butte, Montana 59702 (406) 494-7100

**FINAL REPORT—COLD
DEMONSTRATION OF NONTRADITIONAL
IN SITU VITRIFICATION AT THE
LOS ALAMOS NATIONAL LABORATORY**

Submitted by:

MSE Technology Applications, Inc.
200 Technology Way
P.O. Box 4078
Butte, Montana 59702

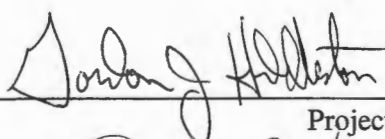
Prepared for:

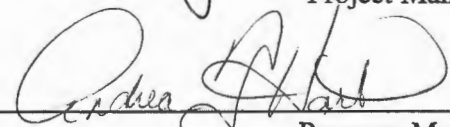
U.S. Department of Energy
Federal Energy Technology Center
Pittsburgh, Pennsylvania 15236
Contract No. DE-AC22-96EW96405

November 1999

REVIEWS AND APPROVALS:

Reviewed by: 
Project Engineer

Reviewed by: 
Project Manager

Approved by: 
Program Manager

EXECUTIVE SUMMARY

MSE Technology Applications, Inc. (MSE) in Butte, Montana, is being funded by the U.S. Department of Energy Subsurface Contaminant Focus Area to conduct two sequential demonstrations of Nontraditional In Situ Vitrification (NTISV) technology at a National Laboratory. The attached two-part report reviews the first NTISV demonstration that was conducted at the Los Alamos National Laboratory (LANL) in April 1999. Part 1 of the report describes the nonintrusive imaging techniques that were used by MSE to determine the size and shape of the resultant subsurface vitrified monolith; Part 2 discusses the actual NTISV demonstration as conducted by Geosafe Corporation of Richland, Washington, under subcontract to MSE.

In situ vitrification (ISV) is a process designed specifically to remediate problematic buried wastes containing organic contaminants, heavy metals, and/or radionuclides. Basically, the ISV process uses electricity to heat and melt contaminated soils to form magma that dissolves radionuclides and heavy metals, while also destroying any organic contaminants by pyrolysis. When an ISV melt has reached the desired size, power is shut off, and the magma begins to cool, thereby, solidifying and trapping heavy metals and radionuclides in solid-solution in a glass-like vitrified product that exhibits the same retentive properties as natural obsidian.

Because ISV can remediate subsurface contaminants in-place, underground, it can theoretically provide significant advantages over ex-situ remediation systems as follows: 1) enhance public and worker safety by eliminating any opportunity for contaminants to become airborne during excavation, transport, and reburial; 2) immobilize contaminants at a molecular level in synthetic obsidian, a material whose natural counterpart has proven stable over geologic time; and 3) cost reductions of ten times or more are believed possible once ISV becomes a proven and accepted means to remediate problematic mixed/buried wastes and/or deeply buried contaminants.

It should be noted that ISV has been used successfully to remediate a variety of buried wastes by applying it in the *traditional* mode, i.e., with the melt proceeding downward, starting at the ground surface. Traditional ISV systems, however, exhibit problems and limitations that have precluded its use as a remediation tool in: 1) contaminated sites where groundwater is present; and 2) sites with contaminants that extend 20 ft or more below ground surface.

Because ISV appears to offer tremendous potential as a remediation tool, several companies have made efforts to extend its usefulness by *nontraditional* means. In contrast to traditional *top-down* melts, NTISV melts are started underground to: 1) minimize the explosion risk that can occur when volatile materials become trapped under molten magma; and 2) facilitate surgical immobilization of contaminants buried deeper than 20 ft. The LANL demonstrations will provide customers, regulators, and stakeholders with accurate information about the capabilities, costs, and potential of NTISV to facilitate intelligent decision making about future deployment.

The NTISV demonstrations at LANL involve two large-scale melts, the first of which has been termed a *cold* demonstration because the selected site contained no radioactive materials. The primary objective of this cold test was to show that the system was ready to demonstrate at an adjacent *hot* absorption bed containing radioactive contaminants. The attached reports show why the cold demonstration was successful and how it met or exceeded all operational, safety, and technical objectives. As a result of this success, the NTISV hot demonstration is scheduled to take place at LANL TA-21 on the MDA-V absorption bed in February 2000.

ACKNOWLEDGMENTS

This work was conducted through the U.S. Department of Energy (DOE) Environmental Management Office of Science and Technology, Subsurface Contaminants Focus Area and administered through the Western Environmental Technology Office in Butte, Montana, under DOE Contract No. DE-AC22-96EW96405. Direct, indirect, and in-kind support for this project was also provided by Los Alamos National Laboratory (LANL) operated by the University of California, DOE Albuquerque Operations Office, and DOE Los Alamos Area Office (DOE-LAAO).

Individuals from many different organizations have been involved in the planning, preparation, coordination, and implementation of the Nontraditional In Situ Vitrification Project at Los Alamos National Laboratory since its inception in March 1998. The core project team consisted of MSE Technology Applications, Inc. (MSE), Geosafe Corporation, and Los Alamos National Laboratory. LANL lead organizations for this project are the LANL Science and Technology Program and the LANL Environmental Restoration Project who provided the host site for the demonstration at Technical Area 21. The interest, cooperation, and assistance of LANL management and staff and DOE-LAAO were instrumental in the timely and successful performance of this technology demonstration. The involvement of the New Mexico Environmental Department and their continued interest in vitrification technology has also contributed greatly to the overall success of this project.

CONTENTS

PART 1 GEOPHYSICAL VERIFICATION AND MONITORING RESULTS FOR THE
NONTRADITIONAL IN SITU VITRIFICATION COLD DEMONSTRATION AT THE
LOS ALAMOS NATIONAL LABORATORY (prepared by MSE Technology Applications, Inc.)

PART 2 NONTRADITIONAL IN SITU VITRIFICATION AT THE LOS ALAMOS NATIONAL
LABORATORY—COLD DEMONSTRATION REPORT (prepared by Geosafe Corporation)

PART 1

**GEOPHYSICAL VERIFICATION AND
MONITORING RESULTS FOR THE
NONTRADITIONAL IN SITU VITRIFICATION
COLD DEMONSTRATION AT THE
LOS ALAMOS NATIONAL LABORATORY**

Prepared by:

MSE Technology Applications, Inc.
200 Technology Way
P.O. Box 4078
Butte, Montana 59702

November 1999

CONTENTS

	Page
1. INTRODUCTION	1
1.1 Purpose	1
1.2 Scope of Work	1
1.3 Methods Investigated for Verification of Vitrification	1
1.3.1 Seismic Velocity Tomography	2
1.3.2 Ground Penetrating Radar (GPR) Tomography	2
1.3.3 Ground Penetrating Radar (GPR) Zero-Offset Profile (ZOP)	2
1.3.4 Electrical Resistance Tomography (ERT)	2
2. SITE PREPARATION	4
2.1 Site Location/Description	4
2.2 Geophysical Access Port Installation	5
3. GEOPHYSICAL VERIFICATION AND MONITORING	7
3.1 Baseline Geophysical Surveys	7
3.1.1 Seismic Tomography Baseline	7
3.1.2 GPR Tomography	9
3.1.3 GPR ZOP	9
3.1.4 ERT	11
3.2 Geophysical Monitoring of the NTISV Melt	13
3.2.1 Seismic Tomography	13
3.2.2 GPR ZOP	15
3.3 Postmelt Geophysical Surveys	16
3.3.1 Seismic Tomography	17
3.3.2 GPR Tomography	19
3.3.3 GPR ZOP	21
3.3.4 ERT	21
4. CORRELATION OF GEOPHYSICAL DATA	24
4.1 Correlation Study	24
4.1.1 Data Analysis	24
4.1.2 Results	24
5. CONCLUSIONS	26
6. REFERENCES	27

FIGURES

	Page
2-1. Los Alamos National Laboratory (LANL)	4
2-2. Plan View of MDA-V Site at LANL	5
2-3. Plan View of Cold Demonstration Site Showing Geophysical Access Port Locations	6
3-1. Premelt Seismic Tomography Setup	7
3-2. North-South Premelt Seismic Velocity Distribution	8
3-3. East-West Premelt Seismic Velocity Distribution	9
3-4. Premelt GPR ZOP Results for the North-South Cross-Section	10
3-5. Premelt GPR ZOP Results for the East-West Cross-Section	11
3-6. Premelt ERT Results for the North-South Cross-Section	12
3-7. Premelt Results for the East-West Cross-Section	12
3-8. Seismic Tomography Setup for Data Acquisition During the Melt	13
3-9. North-South Seismic Velocity Distribution for April 21, 1999 Shutdown	14
3-10. North-South Seismic Velocity Distribution for the April 22, 1999 Shutdown	15
3-11. Baseline and Shutdown GPR Pseudo-Velocity Logs for the North-South Cross-Section	16
3-12. Baseline and Shutdown GPR Pseudo-Velocity Logs for East-West Cross-Section	16
3-13. Postmelt Seismic tomography Setup	17
3-14. North-South Postmelt Seismic Velocity Distribution	18
3-15. East-West Postmelt Seismic Velocity Distribution	19
3-16. GPR ZOP and MOP Postmelt Tomography Data	20
3-17. Postmelt GPR Tomography Results	20
3-18. Premelt and Postmelt GPR ZOP Results for the North-South Cross-Section	21
3-19. Premelt and Postmelt GPR ZOP Results for the East-West Cross-Section	22
3-20. Postmelt ERT Results for the North-South Cross-Section	23
3-21. Postmelt ERT Results for the East-West Cross-Section	23
4-1. Correlation Results for the North-South Cross-Section	25
4-2. Correlation Results for the East-West Cross-Section	25

1. INTRODUCTION

MSE Technology Applications, Inc. (MSE) is funded by the U.S. Department of Energy Subsurface Containment Focus Area under TTP FT18SS21 to coordinate and facilitate a demonstration of Nontraditional In Situ Vitrification (NTISV) technology. The purpose of this demonstration is to provide data suitable to support a Comprehensive Environmental Response and Compensation Liability Act Treatability Study designed to illustrate the feasibility and applicability of NTISV technology to immobilize buried radioactive and hazardous waste. As part of MSE's task to demonstrate the use of in situ vitrification for waste stabilization, a method of verifying the vitrified waste's integrity must be developed and demonstrated.

1.1 PURPOSE

This report describes the geophysical verification work completed during the NTISV Cold Demonstration that took place in March and April 1999. The geophysical methods employed prior to, during, and after the melt are discussed as well as the results that were obtained. The geophysical verification methods are also evaluated based on information obtained from an excavation and destructive examination of the vitrified mass.

1.2 SCOPE OF WORK

The primary objectives for the first phase (Cold Demonstration) of the in situ vitrification (ISV) demonstration included investigating the use of geo-tomography to:

- Determine the most effective method(s) of verifying that complete vitrification has taken place;
- Design a system for using geo-tomography to verify that complete vitrification has taken place; and
- Implement the system design for verifying that complete vitrification has taken place.

The primary objectives for the second phase (Hot Demonstration) of the ISV demonstration included:

- Based on lessons learned from the cold demonstration, design a system for verifying that complete vitrification has taken place for the hot demonstration; and
- Implement the system design for verifying that complete vitrification has taken place for the hot demonstration.

1.3 METHODS INVESTIGATED FOR VERIFICATION OF VITRIFICATION

Geo-tomography was investigated for the purpose of imaging the vitrified mass. The methods considered for the Cold Demonstration included:

- Seismic Tomography;
- Ground Penetrating Radar (GPR) Tomography; and
- Electrical Resistance Tomography (ERT).

Tomography is the process of forming images of the interior of an object from measurements made outside the object along rays passed through the object (Ref. 1).

1.3.1 Seismic Velocity Tomography

Field methods for acquiring seismic tomography data typically entail placing a series of seismic receivers (in this case, hydrophones) into a borehole and a seismic source in an adjacent borehole or at the ground surface and recording the travel time for the seismic energy from source to receiver locations. The source is moved to a new location, and the process repeated until a sufficient number of travel times have been recorded along ray paths through the area of interest.

The travel time data are inverted to estimate a velocity distribution over the area of interest. The velocity distribution is related to the material property distribution (primarily density) within the area of interest, thus, providing an image of the interior of the area of interest. The denser the material, the faster seismic waves will travel through it. Assuming it is denser than the surrounding host soil, the melt should appear as an increase in velocity.

1.3.2 Ground Penetrating Radar (GPR) Tomography

GPR tomography data are taken in a similar manner to seismic tomography data. Several travel time measurements are made outside of the area of interest along ray paths through the area of interest. The measurements can be made from adjacent boreholes or from the ground surface to a borehole. Instead of a mechanical wave moving through the subsurface, GPR uses an electromagnetic wave that propagates through the subsurface.

An estimate of the GPR velocity distribution is obtained from the tomographic inversion. This velocity distribution is also a function of the material properties within the area of interest; however, rather than density, it is more closely related to electrical properties. More conductive materials tend to slow and attenuate the electromagnetic wave. It is expected that the melt will have such an effect on the GPR signal.

1.3.3 Ground Penetrating Radar (GPR) Zero-Offset Profile (ZOP)

GPR ZOP data are acquired in the same manner as the GPR tomography data. However, the transmitter and receiver antenna are simultaneously moved along the length of the borehole at a given increment.

Data are used to calculate an average velocity at each depth increment. Since the distance between the boreholes is known and the travel time is measured, an average velocity can be calculated. A change in the average velocity indicates a change in the subsurface material. The melt is expected to have a lower GPR velocity than the surrounding host soil.

2. SITE PREPARATION

The NTISV Cold Demonstration, was completed at the Los Alamos National Laboratory (LANL) in Los Alamos, New Mexico, in March and April 1999.

2.1 SITE LOCATION/DESCRIPTION

LANL is located on the Pajarito Plateau about 35 miles northwest of Santa Fe. The lab covers more than 43 square miles (see Figure 2-1). The site chosen for the Cold Demonstration is located to the north of the MDA-V site, off the southwest corner of the parking lot (see Figure 2-2).

Geology at the LANL Cold Demonstration site consists of volcanic units. These units include, from top to bottom, the Tshirege Unit (~350 ft thick), the Cerro Toledo Interval (~45 ft thick), the Otowi Member (~270 ft thick), the Guaje Pumice Bed (~25 ft thick), and the Puye Formation. The Tshirege Unit and Otowi Member are primarily nonwelded to partially welded tuff. ISV work for the Cold Demonstration will be completed in the upper portion of the Tshirege Unit.

The NTISV process for the Cold Demonstration was completed by Geosafe Corporation. As part of the site preparation, Geosafe had an area approximately 60 ft in diameter leveled. The center of the area was located directly over the center position of the Cold Demonstration bed. Geosafe's off-gas collection hood was also centered on the leveled area.

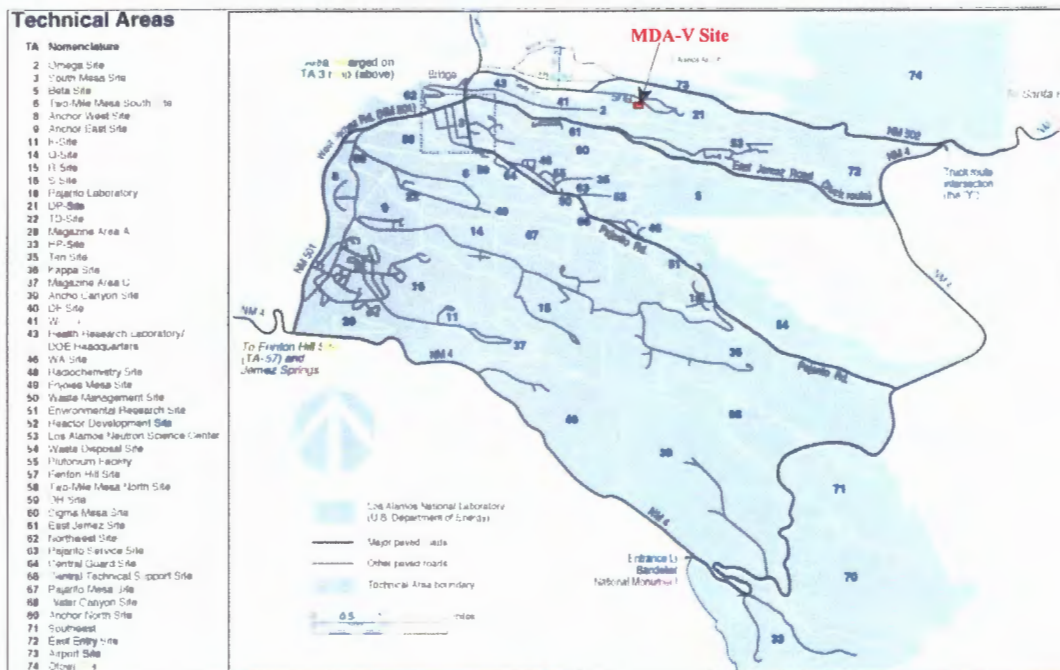


Figure 2-1. Los Alamos National Laboratory (LANL).

1.3.4 Electrical Resistance Tomography (ERT)

Electrical resistivity is a fundamental property of rock materials and is closely related to the rock type. The determination of the subsurface distribution of resistivity from measurements on the ground surface or from boreholes can yield useful information on the structure or composition of the subsurface. The most common method of making these types of measurements involves the passage into the earth of direct (or very low frequency) current and measuring the electrical potential between different locations using a pair of receiver, or potential, electrodes. The electrical resistivity is then determined from the magnitude of the current and voltage and the geometric factor for the electrode configuration.

Electrical resistivity methods can be used in a cross-structure tomographic mode, commonly called ERT, in which the measurements are made from both current and potential electrodes located in the subsurface. The electrodes can be installed in boreholes or using a push type of technology.

The ERT data are inverted to estimate a two-dimensional planar distribution of electrical resistance between a pair of boreholes (this is the traditional tomographic format), or the data can be inverted to estimate a three-dimensional volumetric distribution of the electrical resistance for the area of interest.

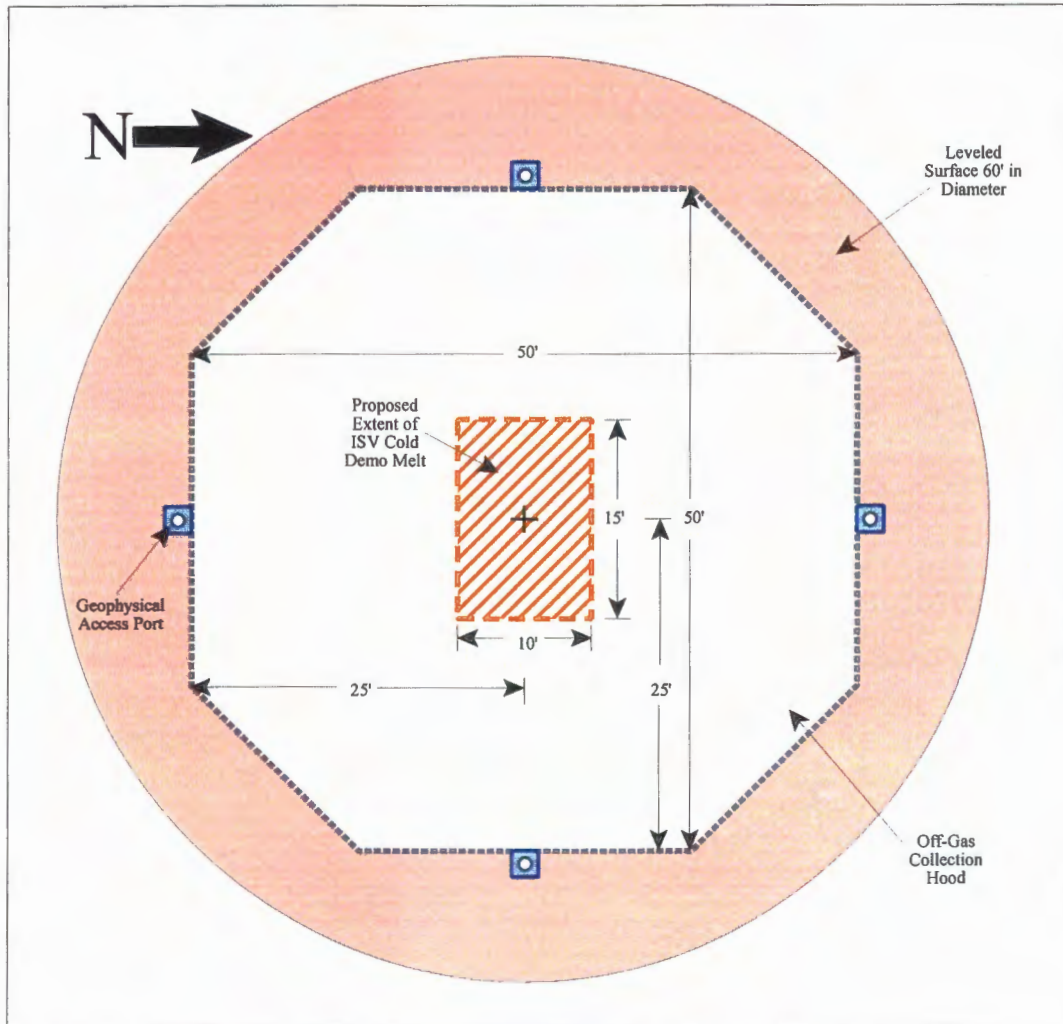


Figure 2-3. Plan view of Cold Demonstration site showing geophysical access port locations.

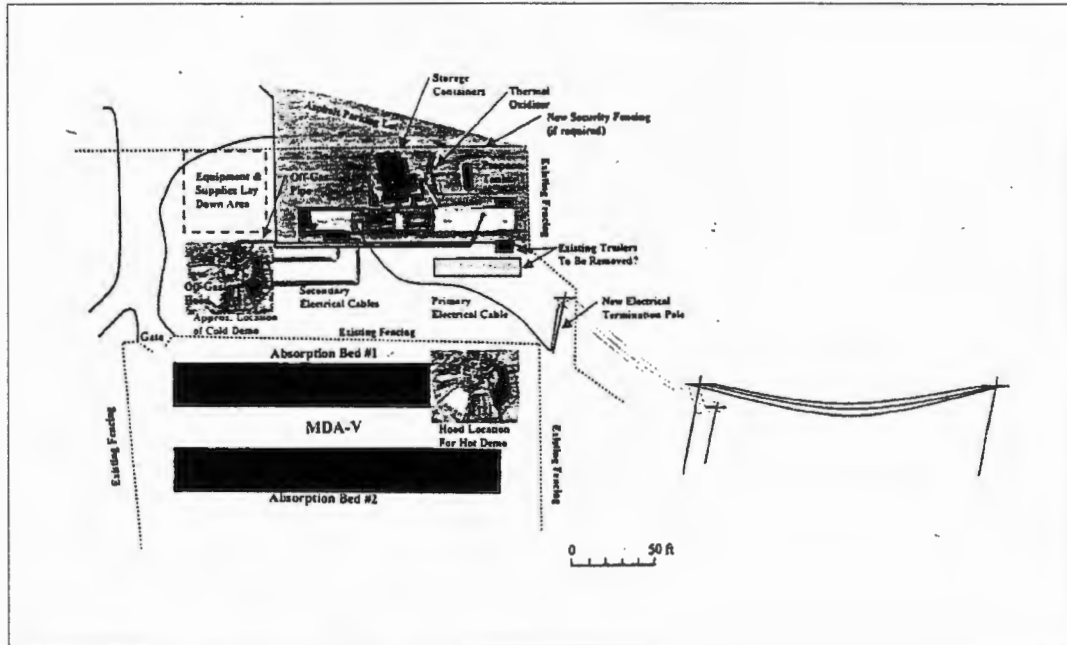


Figure 2-2. Plan view of MDA-V site at LANL.

2.2 GEOPHYSICAL ACCESS PORT INSTALLATION

Geophysical verification data acquisition for the NTISV Cold Demonstration required installing four geophysical access ports or boreholes. These ports provided a means for acquiring the necessary seismic, electrical resistance, and GPR data. The access ports were installed approximately 25 ft from the center position of the Cold Demonstration bed and offset from each side of the proposed melt area (see Figure 2-3.) Once completed, the access ports were surveyed for x, y, and z locations of the top at the ports, and the deviation of the ports was also measured. The survey was done using a localized grid system established for the project with an arbitrary elevation datum.

Boreholes were 4 in. in diameter and installed to a depth of approximately 50 ft below ground surface (bgs). Boreholes were completed with a flush threaded 2-in. PVC well casing sealed at the bottom with a threaded PVC plug. A series of electrodes were attached to the outside of the PVC casing from the ground surface to the bottom of the casing. The electrodes were used for acquiring ERT data and consisted of a 3/8-in. diameter multiconductor electrical cable with stainless steel screen electrodes attached every 3 ft along the length of the cable. The electrodes were emplaced so that each string of electrodes was at the same elevation, regardless of the depth of the hole.

3. GEOPHYSICAL VERIFICATION AND MONITORING

Data for the geophysical verification and monitoring of the NTISV Cold Demonstration melt were acquired prior to, during, and after the melt process. Data acquired prior to the melt were used as a baseline and were compared to the data acquired during and after the melting process. Data acquired during the melting process were used to determine the progress of the melt. Once the melt was completed, a suite of geophysical measurements were made in attempt to image the final melt, including its size, shape and extents.

3.1 BASELINE GEOPHYSICAL SURVEYS

Baseline geophysical surveys were completed at the NTISV Cold Demonstration site using seismic tomography, GPR tomography, and ERT methods.

3.1.1 SEISMIC TOMOGRAPHY BASELINE

Surface to borehole seismic data were acquired along the two planes between the access port pairs spaced 50 ft apart. Seismic source points were positioned between each access port pair at 5-ft increments (see Figure 3-1). Seismic receivers, spaced 1 ft apart, were placed in each geophysical access port. Travel times were recorded along the length of the boreholes for each surface source position. The surface source locations were surveyed for x, y, and z locations following the data acquisition to provide accurate distances from source to receivers.

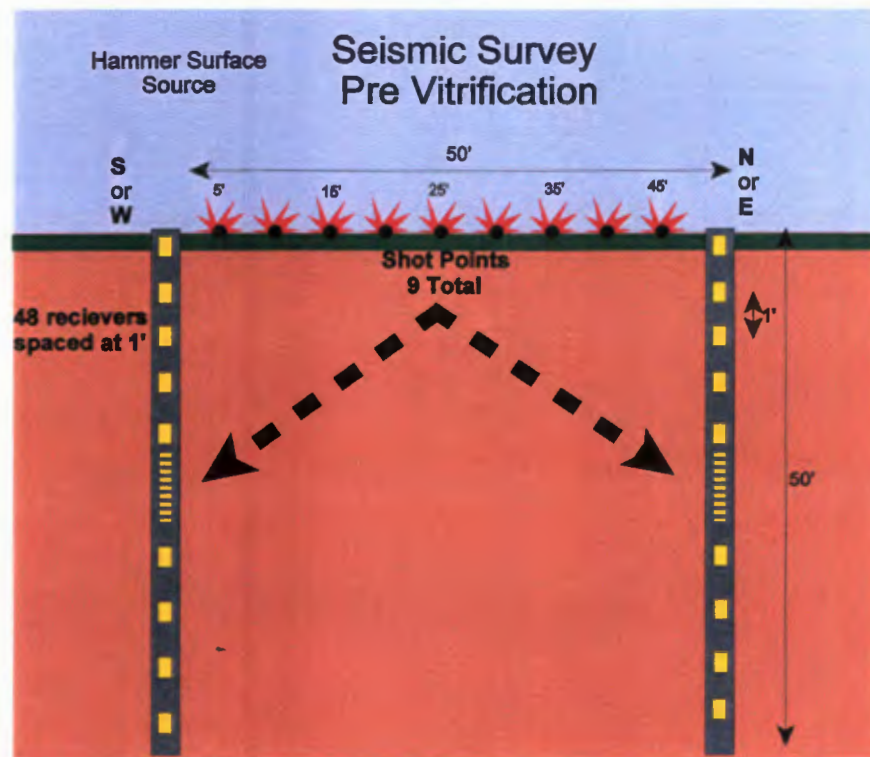


Figure 3-1. Premelt seismic tomography setup.

The baseline seismic velocity data were processed as two profiles. Travel times and distances were determined for each source receiver pair to create the tomography data set. Seismic tomography data were processed using GEOTOMAN, a computer program developed for three-dimensional tomographic imaging. The inversion routine was allowed to continue until the residuals (values indicating how much the model has changed) approached a constant value.

The north-south and east-west results from the premelt seismic tomography modeling are shown in Figures 3-2 and 3-3, respectively. Areas that had no data coverage are shaded. Ground surface is at approximately 98 ft.

A high velocity anomaly is present in the center of the north-south tomogram (see Figure 3-2) where the test pit was constructed. Dimensions of the anomaly are approximately equal to those of the test pit. There are several other high velocity anomalies present along the boreholes and data boundaries. These anomalies are most likely artifacts of the inversion caused by an insufficient amount of data at the edges of the tomogram.

The premelt seismic velocity distribution for the east-west cross-section is shown in Figure 3-3. A high velocity anomaly is present in the center of the tomogram, but it is not as refined as the anomaly in the north-south cross-section. The high velocity anomaly also appears to have a greater lateral extent in this plane. There are several other high velocity anomalies present along the boreholes and data boundaries. These anomalies are most likely artifacts of the inversion caused by an insufficient amount of data at the edges of the tomogram.

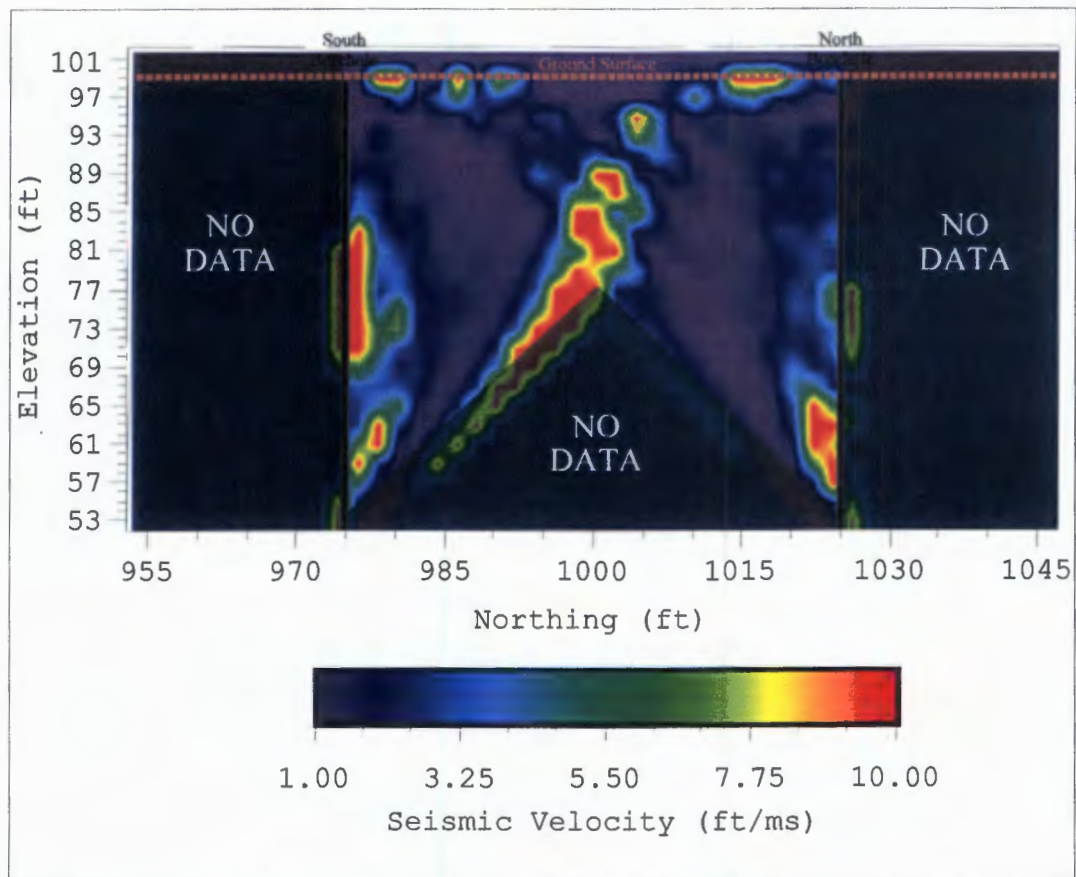


Figure 3-2. North-south premelt seismic velocity distribution.

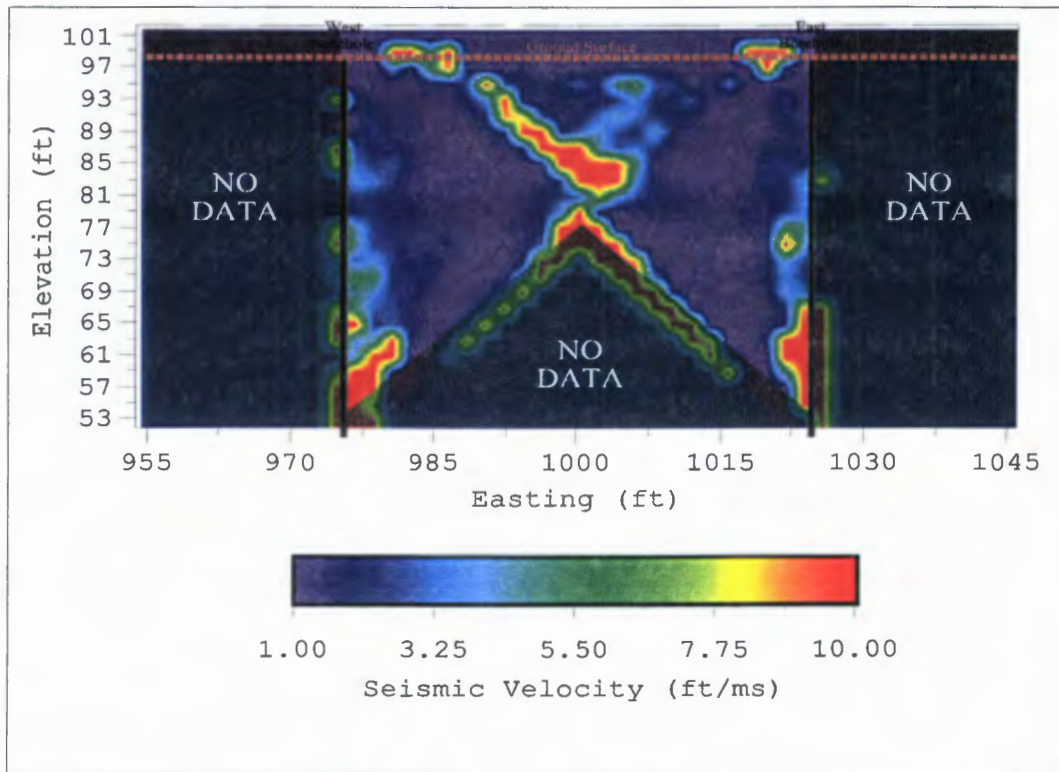


Figure 3-3. East-west premelt seismic velocity distribution.

3.1.2 GPR Tomography

Borehole to borehole GPR tomography data were acquired to determine the GPR velocity distribution in the subsurface and test trench prior to the NTISV melt. However, problems with the calibration data files prevented the processing of the tomography data. As a result, no premelt GPR tomograms were completed.

3.1.3 GPR ZOP

Borehole to borehole GPR ZOP data were acquired using 50-MHz antennas to determine the average GPR velocity as a function of depth in the subsurface and test trench prior to the NTISV melt. The purpose of this data was to be able to estimate the lower boundary of the melt based on a decrease in velocity caused by the melt. Data taken during the melt could be compared to this baseline data and any changes in velocity noted. ZOP data were acquired along both the north-south and east-west planes.

The GPR ZOP data were acquired by simultaneously moving the transmitter and receiver antennas along the length of opposite boreholes. The antennas were moved at 0.25-meter increments from the top of the casings (100-ft elevation) to a depth of 14 meters below the top of the casings.

Data were acquired twice for each plane (north-south and east-west) and the travel times were averaged. An average velocity was calculated using the distance between boreholes (calculated from survey data) and the averaged travel times. The average velocities were then plotted against the depth below the top of the casings to create a pseudo-velocity log for each cross-section.

The premelt pseudo-velocity logs for the north-south and east-west cross-sections are shown in Figures 3-4 and 3-5, respectively. Average GPR velocities in the north-south cross-section (see Figure 3-4) range from approximately 310 meters/nanosecond (m/ns) to 115 m/ns. The high velocities near the surface are most likely a result of the electromagnetic wave traveling through the air from the transmitter to the receiver. The velocity decreases steadily (140 m/ns) to a depth of about 14 ft and gradually decreases (115 m/ns) to a depth of approximately 26 ft. At 26 ft below the top of the casings, the velocity slowly increases and becomes rather constant (135 m/ns) around 34 ft.

Average velocities in the east-west cross-section (see Figure 3-5) range from approximately 700 m/ns to 170 m/ns. The average velocity decreases steadily (300 m/ns) to approximately a depth of 10 ft. Between depths of 10 to 16 ft, the velocity remains fairly constant (230 m/ns). At approximately 16 ft below the top of the casings, the velocity drops to 170 m/ns and remains fairly constant.

Results from the GPR ZOP surveys indicate that the average velocity in the east-west direction is greater than in the north-south direction. This difference in average velocity suggests that the subsurface geology is not constant over the site. Seismic refraction data, acquired prior to the borehole installation, showed a near surface layer of varying thickness may exist at the site. The change in thickness would increase or decrease the average GPR velocity.

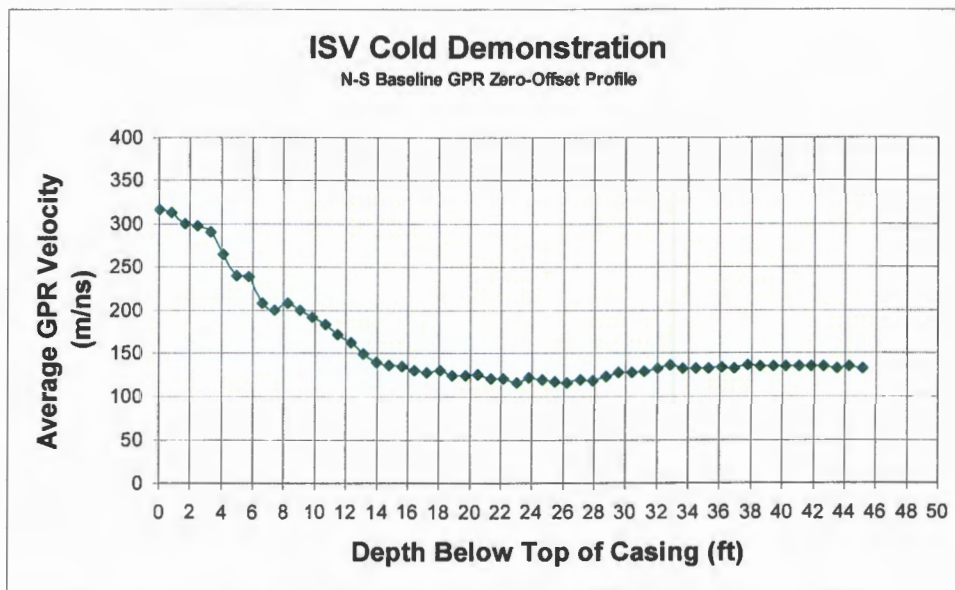


Figure 3-4. Premelt GPR ZOP results for the north-south cross-section.

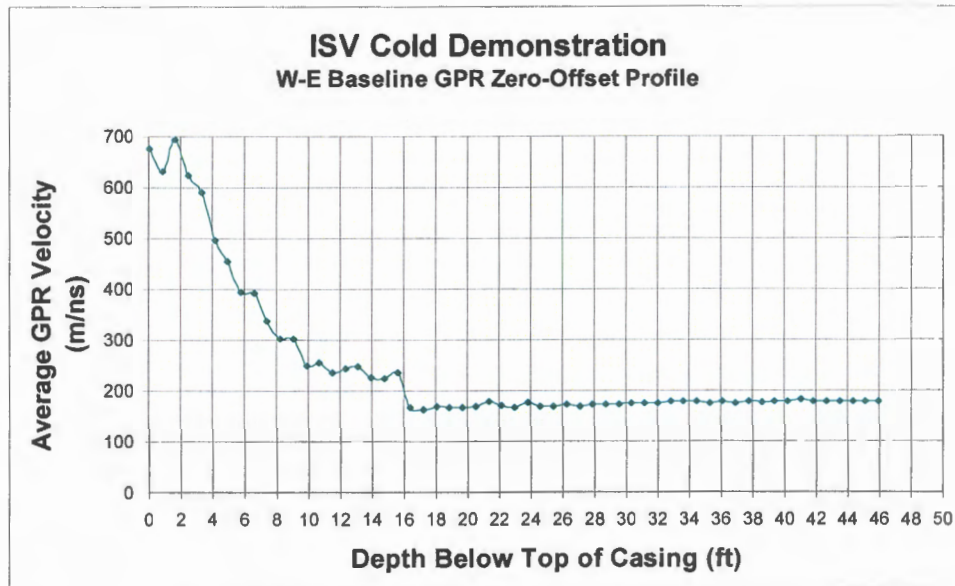


Figure 3-5. Premelt GPR ZOP results for the east-west cross-section.

3.1.4 ERT

Surface to borehole and borehole to borehole ERT data were acquired to determine the resistivity distribution in the subsurface and test trench prior to the NTISV melt. Data were acquired along a north-south plane and an east-west plane.

Premelt ERT data were acquired using the borehole electrodes installed during the geophysical borehole construction and surface electrodes emplaced between the north and south and east and west borehole pairs. Each borehole consisted of 15 electrodes spaced 3 ft apart starting approximately 3 ft below the ground surface. Fifteen surface electrodes, spaced 3 ft apart, were centered between the borehole pairs.

Current and voltage measurements were recorded using surface and borehole electrode pair combinations.

Processing the ERT data required determining the geometric factor for each electrode combination. Apparent resistivities were then calculated current, voltage, and corresponding geometric factor values.

Prior to inverting the data and resistivity, values less than zero were removed. The resulting data set was inverted using OCC2D3D, a three-dimensional source and two-dimensional plane ERT modeling program.

The premelt ERT results for the north-south and east-west cross-sections are shown in Figures 3-6 and 3-7, respectively. Premelt ERT results appear to have been affected by the cement-bentonite mixture used to complete the geophysical boreholes. It is possible that premelt data were acquired before the cement-bentonite had cured enough. As a result, the mixture, being highly conductive, created a *short circuit* for the system.

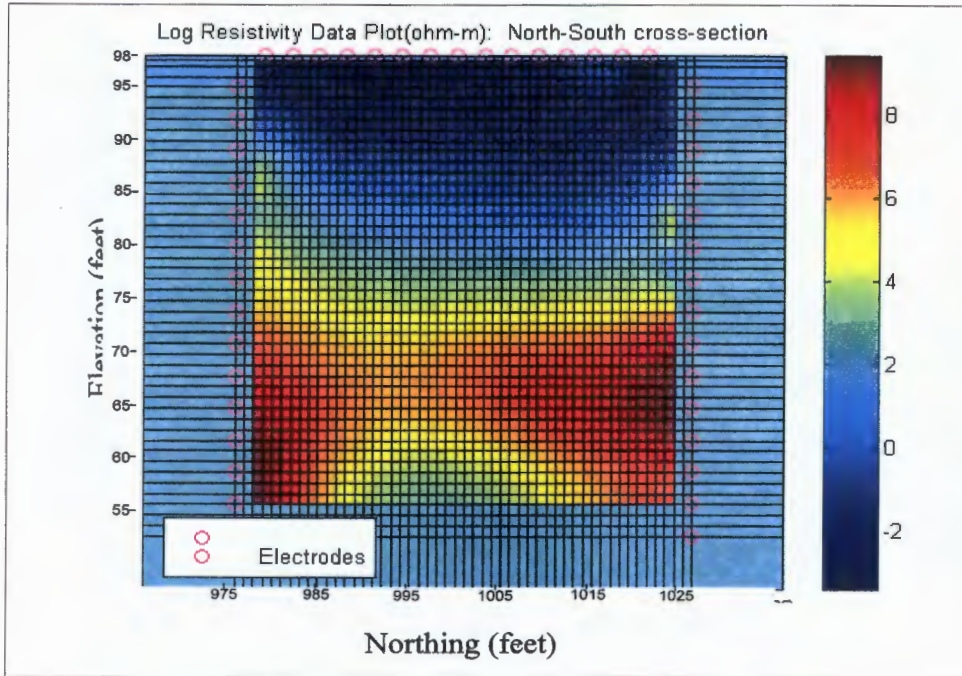


Figure 3-6. Premelt ERT results for the north-south cross-section.

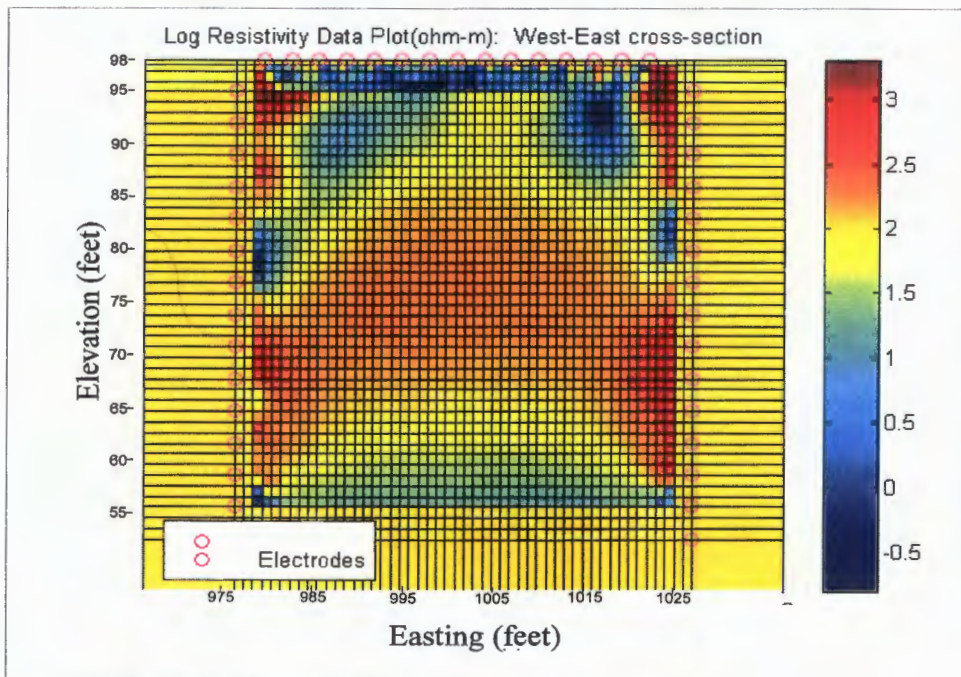


Figure 3-7. Premelt results for the east-west cross-section.

3.2 GEOPHYSICAL MONITORING OF THE NTISV MELT

In an attempt to monitor the progress of the NTISV melt, geophysical data were acquired during two periods in which the *ISV system* was powered down to feed electrodes into the melt. Data were acquired on April 21 and April 22, approximately 5 and 6 days after the melt had begun, respectively.

Geophysical data acquired during the melt included surface to borehole seismic tomography and GPR ZOP data. These methods were chosen primarily because the data could be acquired quickly, reducing the amount of time the *ISV system* would need to remain powered down.

3.2.1 Seismic Tomography

Because the off-gas collection hood was in place over the melt site, it was not possible to take seismic data from shot locations on the surface between the boreholes. To compensate for this, data were taken from shot locations outside the borehole pairs as shown in Figure 3-8. The shot points were spaced 5 ft apart.

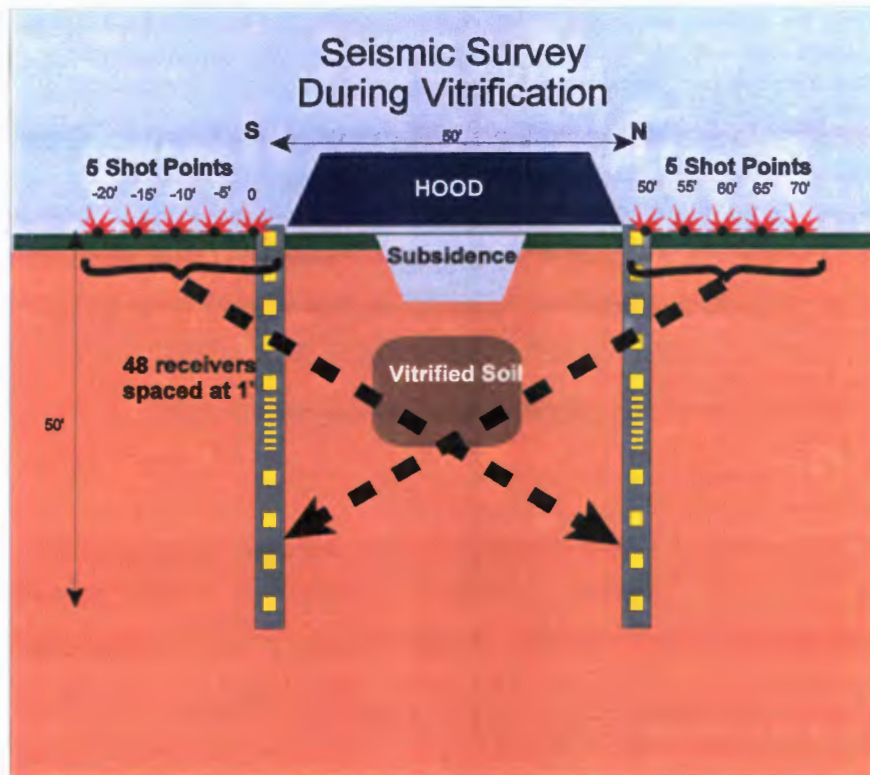


Figure 3-8. Seismic tomography setup for data acquisition during the melt.

Due to the limited down time of the ISV system, data were only taken for the north-south cross-section. Seismic receivers, spaced 1 ft apart, were placed in each geophysical access port. Travel times were recorded along the length of the boreholes for each surface source position. The surface source locations were surveyed for x, y, and z locations following the data acquisition to provide accurate distances from source to receivers.

Seismic tomography data were processed using GEOTOMAN, a computer program developed for three-dimensional tomographic imaging. Travel times and distances were determined for each source receiver pair to create the tomography data sets. Curved ray processing was employed in the inversion of the travel time data sets. Prior to beginning the inversion, a starting model was constructed for each data set. A starting model provides the inversion routine with a velocity distribution, based on a prior knowledge of the site, to begin iterating on. The inversion routine was allowed to continue until the residuals (values indicating how much the model has changed) approached a constant value.

Seismic tomography results for the data acquired on April 21, 1999, are shown in Figure 3-9. A high velocity [4.0 to 5.5 feet/millisecond (ft/ms)] anomaly, believed to represent the melt, is present in the center of the tomogram. The top of the anomaly does not appear to be as uniform as the bottom. The lower extent of the anomaly extends to an elevation of 79 ft (19 to 20 ft below ground surface). The extent of the anomaly in the north-south direction is approximately 14 ft.

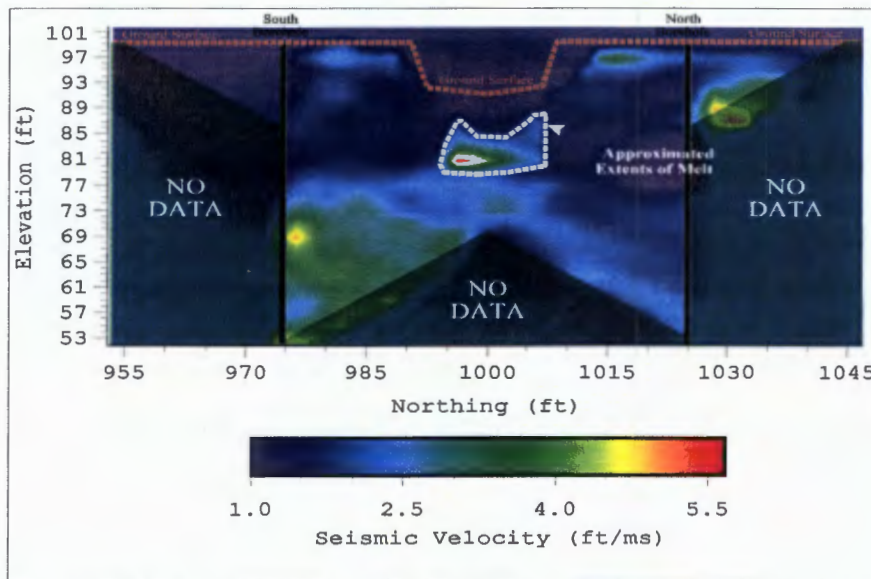


Figure 3-9. North-south seismic velocity distribution for April 21, 1999 shutdown.

Figure 3-10 shows the seismic velocity distribution produced from the data acquired during the April 22, 1999 shutdown. A high velocity (4.0 to 5.5 ft/ms) anomaly, believed to represent the melt, can be seen in the center of the tomogram. The top of the anomaly does not appear to be as uniform as the bottom. The lower extent of the anomaly extends to an elevation of 79 ft (19 to 20 ft below ground surface). The extent of the anomaly in the north-south direction is approximately 14 ft.

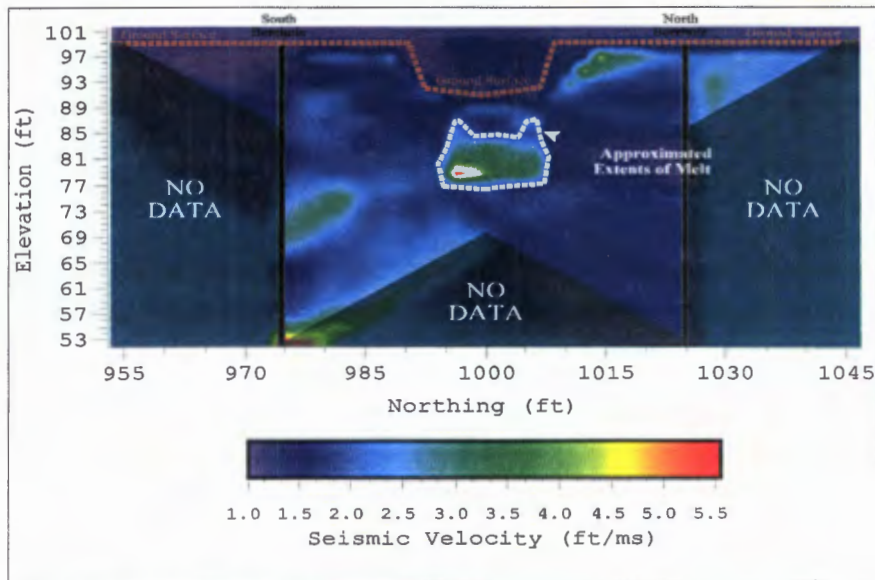


Figure 3-10. North-south seismic velocity distribution for the April 22, 1999 shutdown.

3.2.2 GPR ZOP

GPR ZOP data were acquired along the north-south and east-west cross-sections during the April 21 and 22 shutdowns to attempt to estimate the location of the bottom of the melt to be compared with the baseline data.

The GPR ZOP data acquired during the shutdown periods were taken at the same depth intervals and frequencies as the premelt GPR ZOP data. The antennas were moved at a constant increment of 0.25 meters from the top of the casings (100-ft elevation) to a depth of 14 meters below the top of the casings.

The data processing followed the premelt GPR ZOP data processing steps. Data were acquired twice for each plane (north-south and east-west) and the travel times were averaged. An average velocity was calculated using the distance between boreholes (calculated from survey data) and the averaged travel times. The average velocities were then plotted against the depth below the top of the casings to create a pseudo-velocity log for each cross-section.

The results of the GPR ZOP survey for the north-south cross-section are shown in Figure 3-11. The two pseudo-velocity logs created from the shutdown data are plotted with the baseline pseudo-velocity log.

Average velocities for the two *shutdown* data sets decrease slightly, indicating the presence of a more conductive zone (the melt). Below the melt, velocities should reflect those seen in the baseline data set. The April 21 shutdown data indicates the bottom of the melt is at approximately 22.5 ft below the top of the casings (20 ft below the ground surface). Data from the April 22 shutdown indicate a slightly greater depth of around 24.5 ft below the top of the casings (22 ft below the ground surface).

Figure 3-12 shows the GPR ZOP data for the east-west cross-section. The baseline pseudo velocity log has been plotted with the two pseudo-velocity logs from the shutdown data.

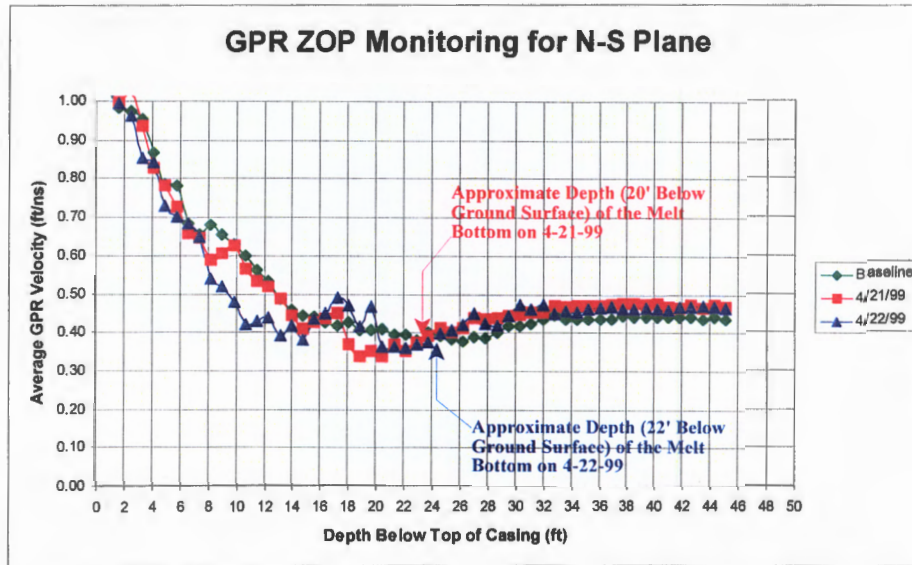


Figure 3-11. Baseline and shutdown GPR pseudo-velocity logs for the north-south cross-section.

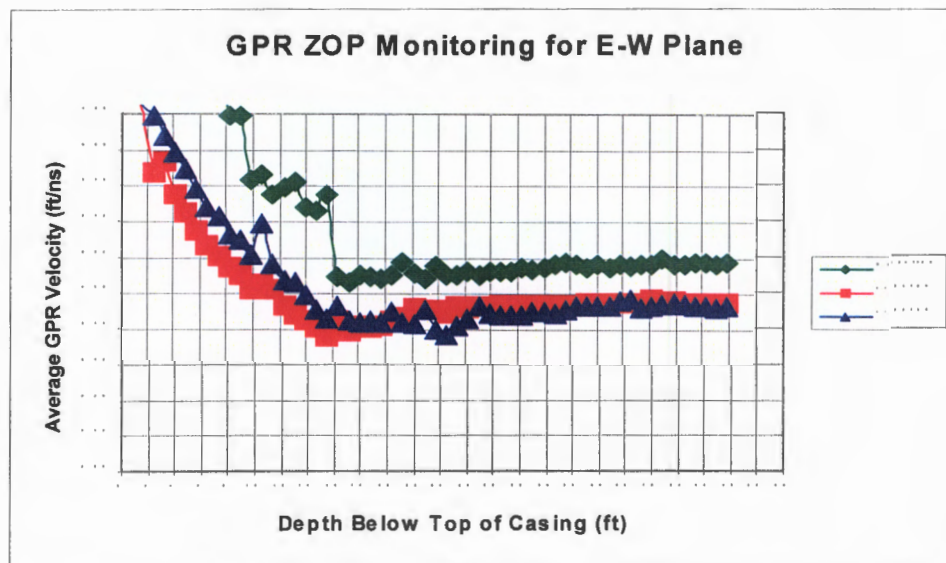


Figure 3-12. Baseline and shutdown GPR pseudo-velocity logs for east-west cross-section.

Both sets of shutdown data indicate a decrease in the average velocity. However, it is difficult to ascertain where the bottom of the melt is from this data set.

3.3 POSTMELT GEOPHYSICAL SURVEYS

After the melt had been completed, geophysical measurements were acquired along the north-south and east-west cross-sections. Postmelt geophysical methods used included seismic tomography, GPR tomography, and ERT methods.

In May 1999, the vitrified block was excavated as part of the destructive examination. During the excavation, survey data were acquired along the upper surface of the vitrified mass. Survey data were used to assess the performance of the geophysical verification methods.

3.3.1 Seismic Tomography

Surface to borehole seismic tomography data were acquired along the north-south plane to determine the seismic velocity distribution in the subsurface.

Seismic tomography data were acquired using a combination of premelt and during-melt surface source positions. Since an area approximately 20 ft in diameter had subsided due to the melting volume reduction caused by the melting process, several of the surface source positions between the boreholes could not be used (see Figure 3-13).

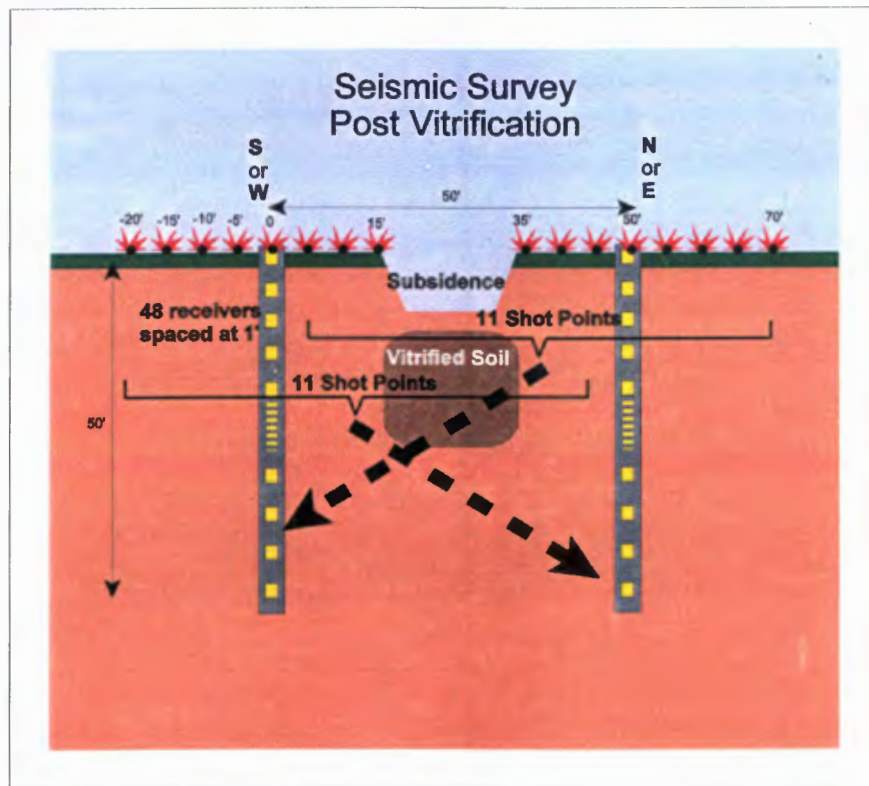


Figure 3-13. Postmelt seismic tomography setup.

Seismic tomography data obtained after the melt was completed were processed using GEOTOMAN and the same inversion parameters used for the shutdown seismic data. Travel times and distances were determined for each source receiver pair to create the tomography data sets; and prior to beginning the inversion, a starting model was constructed for each data set. As with the shutdown seismic tomography inversion, the inversion routine was allowed to continue until the residuals (values indicating how much the model has changed) approached a constant value.

The north-south and east-west results from the postmelt seismic tomography modeling are shown in Figures 3-14 and 3-15, respectively. Areas that had no data coverage are shaded.

The postmelt results from the north-south cross-section (Figure 3-14) show a distinct high velocity (outlined) anomaly in the area where the melt was expected to be. Survey points acquired from the top of the vitrified mass during the excavation are also shown. The upper extent of the velocity anomaly and the actual survey points do not correlate well.

Figure 3-15 shows the postmelt seismic velocity distribution for the east-west cross-section. A distinct increase in velocity (outlined) is present in the east-west postmelt seismic velocity distribution. The upper boundary of the velocity anomaly correlate well with the excavation survey data.

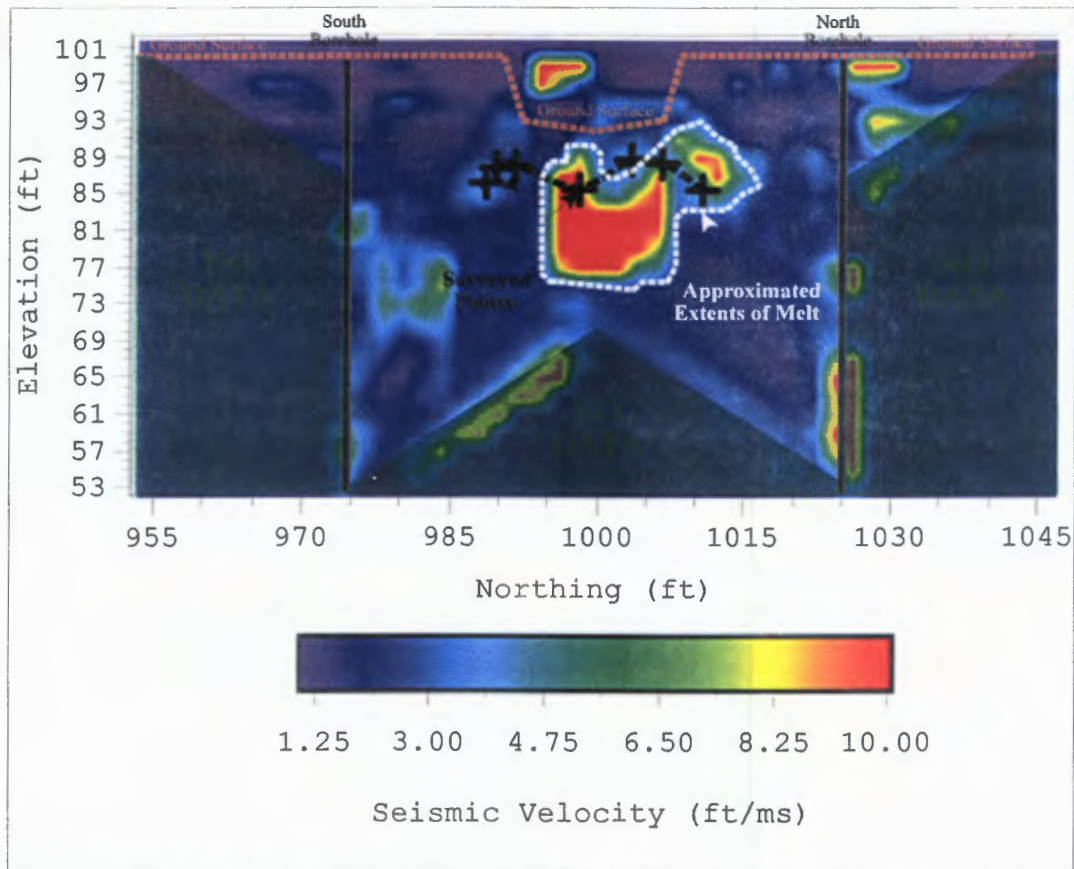


Figure 3-14. North-south postmelt seismic velocity distribution.

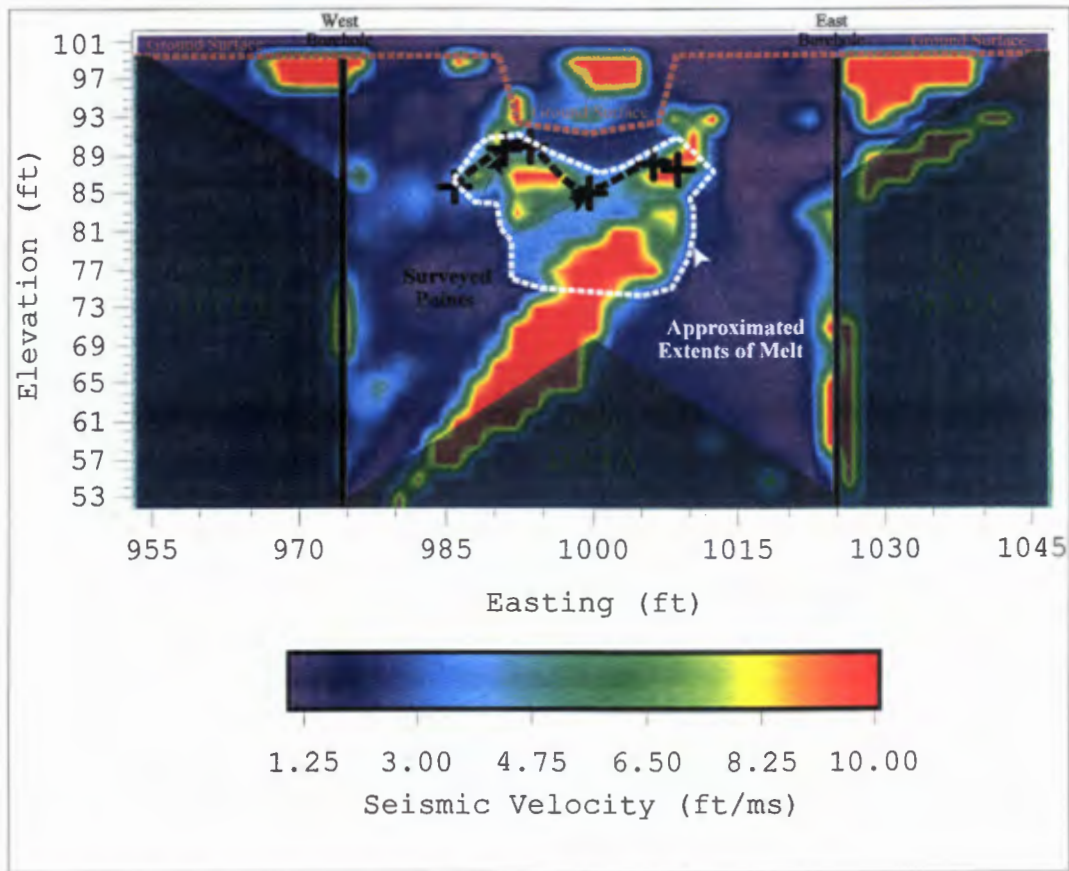


Figure 3-15. East-west postmelt seismic velocity distribution.

3.3.2 GPR Tomography

Borehole to borehole GPR tomography data were acquired to determine the GPR velocity distribution in the subsurface after the NTISV melt had been completed. Tomography data were used to image the vitrified mass.

Using a 100-MHz transmitter and receiver, multiple-offset profiles (MOP) and ZOP data were acquired between the geophysical boreholes. ZOP data were acquired between each borehole pair and MOP data were acquired between selected borehole pairs (see Figure 3-16).

ZOP data were acquired from 1 to 14 meters below the top of the casings at a 0.25-meter increment. At each depth, five measurements were made. MOP data were acquired from 1 to 14 meters below the top of the casings at a 1-meter increment.

GPR MOP and ZOP data from the north-south and east-west cross-sections were processed separately using GEOTOMAN. Travel times and distances were determined for each source receiver pair to create the tomography data sets; and prior to beginning the inversion, a starting model was constructed for each data set. The inversion routine was allowed to continue until the residuals (values indicating how much the model has changed) approached a constant value.

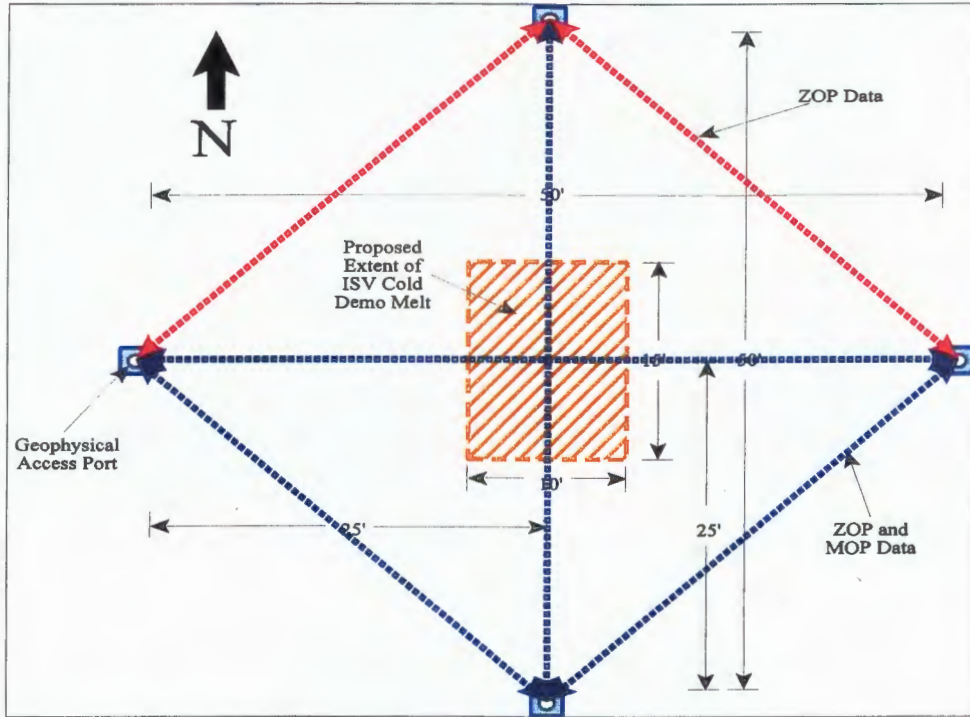


Figure 3-16. GPR ZOP and MOP postmelt tomography data.

GEOTOMAN was also used to process the entire set of GPR MOP and ZOP postmelt tomography data. Travel times and distances were compiled into a common data set and inverted using straight ray processing techniques. A starting model was constructed prior to inverting the data set.

Postmelt GPR velocity distributions for the north-south and east-west cross-sections are shown in Figure 3-17. After processing the data, it was found that many of the ray paths traveling through the melt had been severely attenuated, resulting in an insufficient amount of data to image the vitrified mass. Consequently, the GPR velocity distributions are primarily an artifact of the starting models.

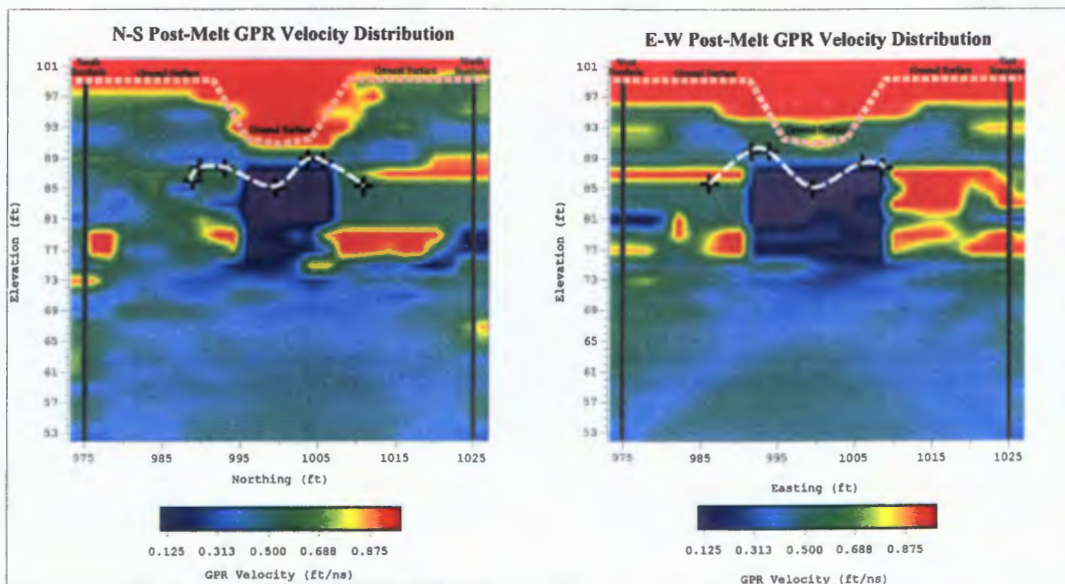


Figure 3-17. Postmelt GPR tomography results.

3.3.3 GPR ZOP

GPR ZOP data were acquired along the north-south and east-west cross-sections after the melt had been completed.

GPR ZOP data were acquired by simultaneously moving the transmitter and receiver antennas along the length of opposite boreholes. The 50-MHz antennas were moved at a constant increment of 0.25 meters from the top of the casings (100 ft elevation) to a depth of 14 meters below the top of the casings.

Data were acquired twice for each plane (north-south and east-west), and the travel times were averaged. An average velocity was calculated using the distance between boreholes (calculated from survey data) and the averaged travel times. The average velocities were then plotted against the depth below the top of the casings to create a pseudo-velocity log for each cross-section.

Figures 3-18 and 3-19 show the premelt and postmelt GPR ZOP for the north-south and east-west cross-sections, respectively. Since the GPR signal was severely attenuated by the conductive melt, travel times could not be discerned at a number of depths. It is reasonable to estimate that the signal is useable once the transmitter and receiver antennas have moved below the melt. Consequently, the loss of signal could be used to estimate the vertical extent of the melted mass.

3.3.4 ERT

Surface to borehole and borehole to borehole ERT data were acquired to determine the resistivity distribution in the subsurface after the NTISV melt was complete. Data were acquired along a north-south plane and an east-west plane.

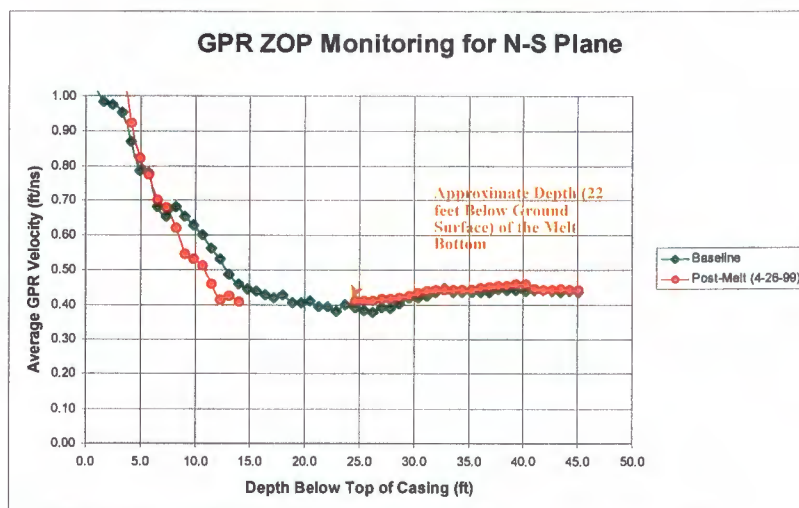


Figure 3-18. Premelt and postmelt GPR ZOP results for the north-south cross-section.

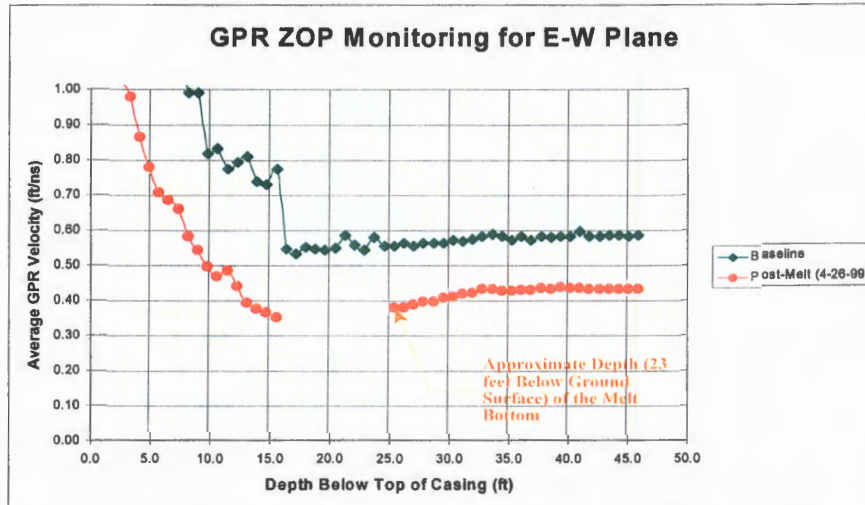


Figure 3-19. Premelt and postmelt GPR ZOP results for the east-west cross-section.

Premelt ERT data were acquired using the borehole electrodes installed during the geophysical borehole construction and surface electrodes emplaced between the north and south and east and west borehole pairs. Each borehole consisted of 15 electrodes spaced 3 ft apart starting approximately 3 ft below the ground surface. Surface electrodes between the north and south boreholes were placed 3, 6, 9, 12, 15, 18, 35, 38, 41, 44, and 47 ft from the north borehole. Surface electrodes between the east and west boreholes were placed 3, 6, 9, 12, 15, 18, 35, 38, 41, 44, and 47 ft from the west borehole.

Current and voltage measurements were recorded using surface and borehole electrode pair combinations.

Processing the ERT data required determining the geometric factor for each electrode combination. Apparent resistivities were then calculated using current, voltage, and corresponding geometric factor values.

Prior to inverting the data and resistivity, values less than zero were removed. The resulting data set was inverted using OCC2D3D, a three-dimensional source and two-dimensional plane ERT modeling program.

Postmelt ERT results for the north-south and east-west cross-sections are shown in Figures 3-20 and 3-21, respectively. The north-south cross-section shows a conductor located beneath a resistor approximately midway between the boreholes. The north-south cross-section appears to have resolved both the vitrified mass target and either a steam pocket or the hole in the ground. The vitrified mass is interpreted to be the conductive body, and the steam pocket or hole in the ground is interpreted to be the resistive body. The dimensions of the conductive body are similar to the dimensions of the melt measured at the site.

The west-east values shows a very strong conductor surrounded by a less conductive material. The west-east cross-section may have been affected by one of the carbon-graphite electrode left in the ground.

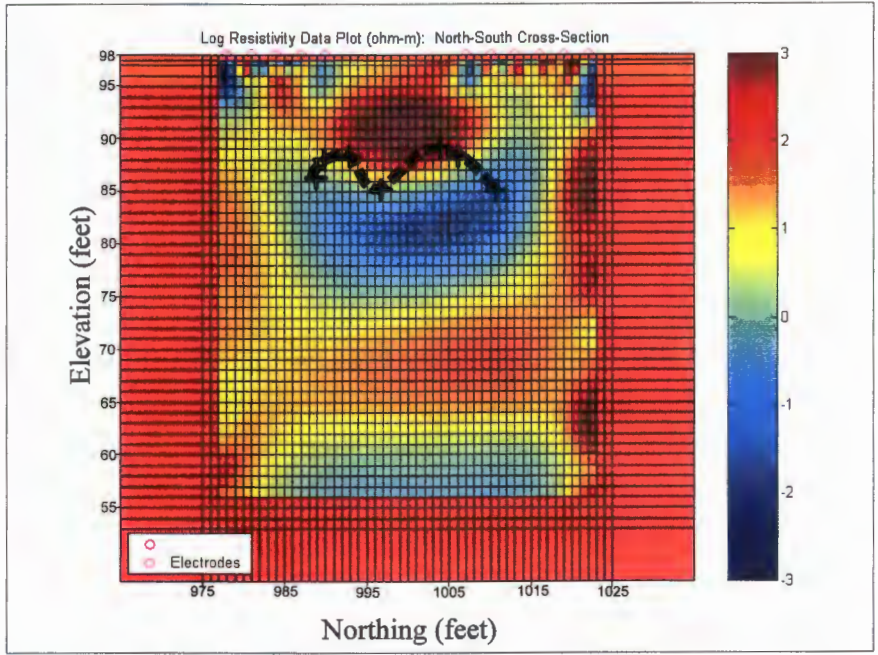


Figure 3-20. Postmelt ERT results for the north-south cross-section.

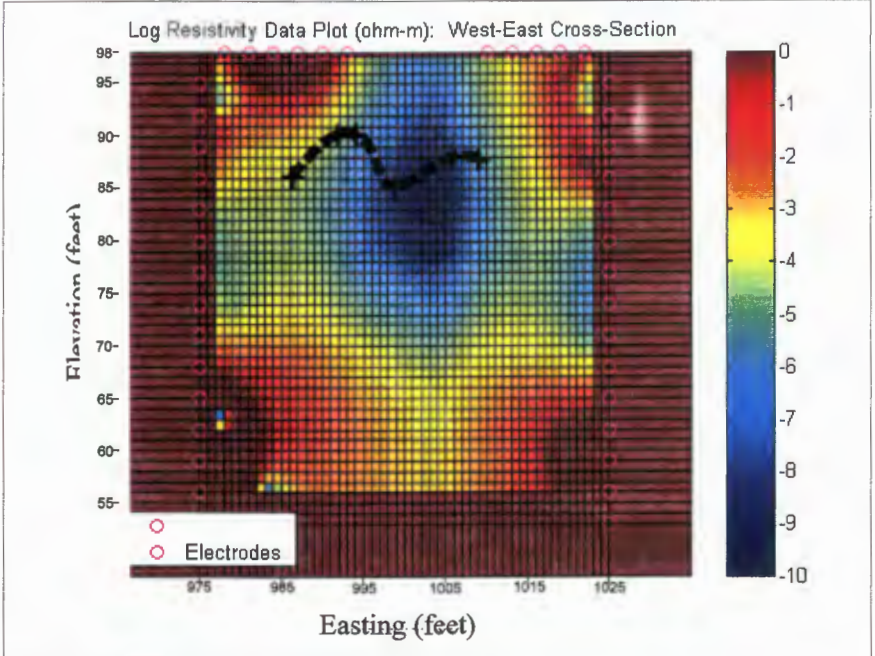


Figure 3-21. Postmelt ERT results for the east-west cross-section.

4. CORRELATION OF GEOPHYSICAL DATA

Analysis of the postmelt geophysical data indicated that results from the applied methods appeared capable of discriminating the vitrified mass from the host soil. To further image the vitrified mass, a correlation study using the postmelt seismic tomography and ERT data was completed. The correlation study was used to define the vitrified mass as an object that was electrically conductive and seismically fast.

4.1 CORRELATION STUDY

Postmelt seismic tomography and ERT data from the north-south and east-west cross-sections were analyzed using a simple correlation technique. From this technique, the mutual relation of the data sets can be ascertained.

4.1.1 Data Analysis

The correlation analysis of the postmelt seismic tomography and ERT data involved reducing the two data sets to a common grid. Seismic velocity and electrical resistivity values were then scaled using the following formulas:

$$\rho_s = 1 / (\rho_v / \rho_{\max});$$

and

$$V_s = V_v / V_{\max}.$$

Where ρ_s is the scaled resistivity, ρ_v is the resistivity value, ρ_{\max} is the maximum resistivity, V_s is the scaled velocity, V_v is the velocity value being scaled, and V_{\max} is the maximum velocity. The resulting scaled values create data sets in which a value of 1 indicates a high probability of the presence of the melted mass and a value of 0 indicates a low probability of the presence of the melted mass.

Using a simple correlation technique, the two scaled data sets were multiplied, and a single correlated data set was created. This type of correlation produces higher values when the individual data points from the data sets are similar and lower values when the data points are dissimilar.

4.1.2 Results

Postmelt seismic tomography and ERT correlation results from the north-south and east-west cross-sections are shown in Figures 4-1 and 4-2, respectively. These distributions have been smoothed, and the location of the melted mass has been estimated (outlined).

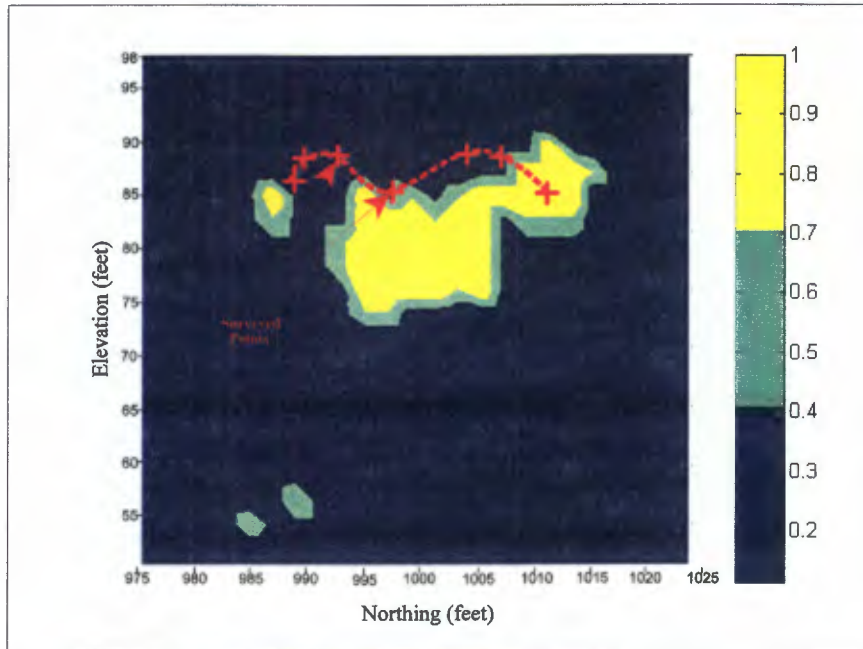


Figure 4-1. Correlation results for the north-south cross-section.

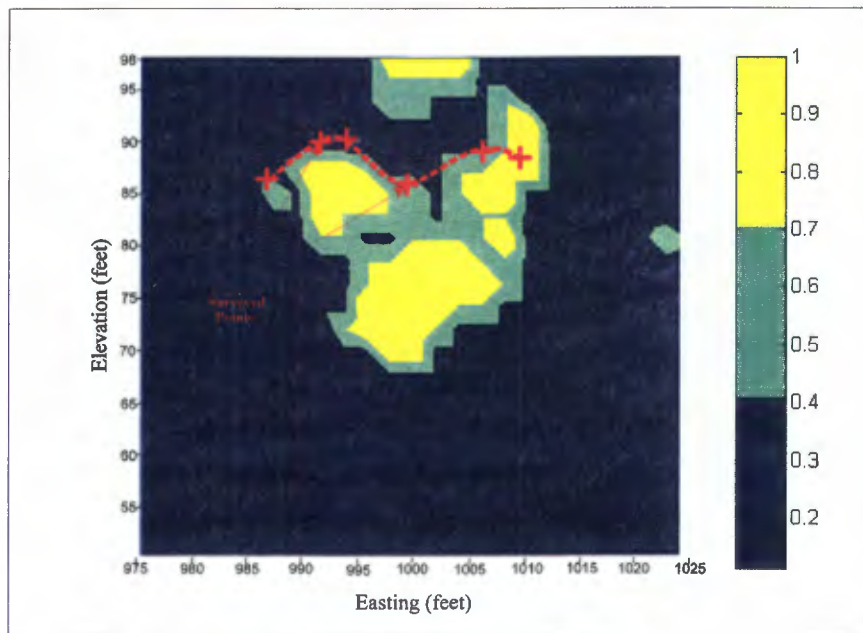


Figure 4-2. Correlation results for the east-west cross-section.

The correlation results, in particular the east-west cross-section, appear to correlate well with the survey data obtained during the excavation. The upper lateral extents of the melt as indicated by the correlations also match the upper lateral extents determined during the excavation.

5. CONCLUSIONS

Analysis of the geophysical verification data for the NTISV Cold Demonstration has provided significant information that will be useful for designing and implementing a verification system for the NTISV Hot Demonstration. Results indicate that seismic tomography and ERT methods can be used to image the vitrified mass in the subsurface. Although not as successful as the seismic tomography and ERT methods, GPR tomography could possibly be used in conjunction with the other methods to further define the vitrified mass.

Seismic tomography methods appear to have had success imaging the vitrified mass. Data analysis suggests that more detailed images could be obtained using better starting models and more model iterations. Starting models can be more accurately constructed with the aid of more prior information and site characterization data. Forward modeling suggests that borehole to borehole seismic data would also improve the tomographic image. Future seismic tomography verification work should incorporate surface to borehole data with borehole to borehole data.

Premelt ERT results were not as successful as the postmelt results. Problems were most likely caused by the uncured, highly conductive grout used to complete the boreholes. If more time had been given for the grout to cure, results could have been more indicative of what was in the subsurface. Postmelt results indicate that ERT methods can be used to image the vitrified mass. Forward modeling has demonstrated the need for surface electrodes and careful borehole positioning. Data analysis should be completed carefully due to the sensitivity of the ERT method. Postmelt ERT data suggest the graphite electrodes left in the ground may interfere with data acquisition.

GPR tomography methods appear to have had the most problems imaging the NTISV Cold Demonstration vitrified mass. GPR signals from the 100-MHz and 50-MHz antennas were severely attenuated by the conductive, vitrified mass. As a result, data were sparse in the area in which the vitrified mass was located. Results from the GPR ZOP data indicate that the attenuation could be used to determine the depth of the melt. As the borehole antennas are transmitting through the melt, the signal is lost. However, it appears that the signal may return once the antennas are below the melt.

The correlation analysis completed on the seismic tomography and ERT postmelt data sets suggests that combining the results of multiple data sets will increase the ability of geophysical verification methods to image the vitrified mass. In addition to geophysical data, this method could be applied to other sets of data that characterize the melt.

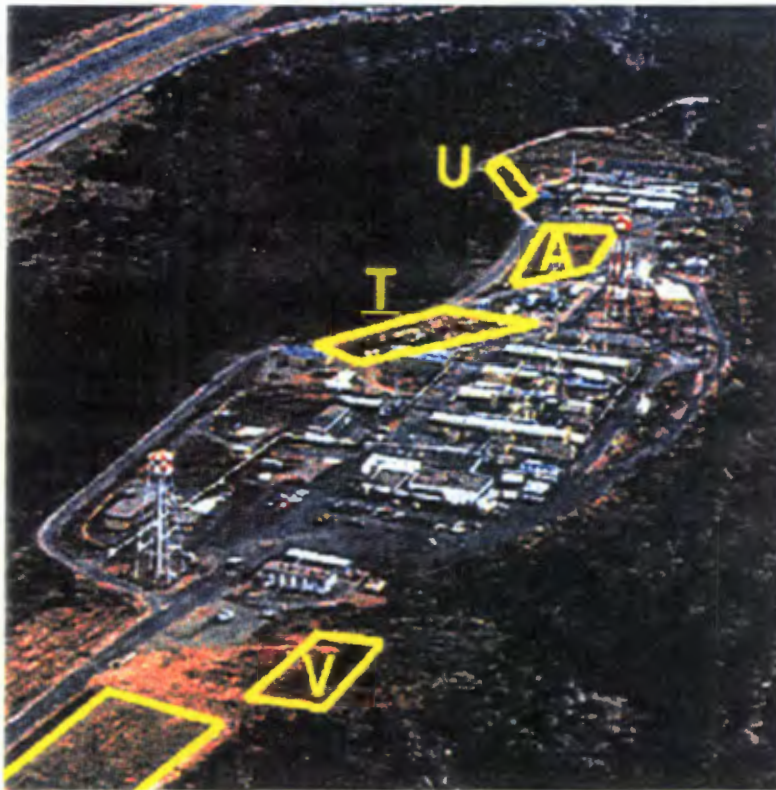
6. REFERENCES

1. Menke, W., *Geophysical Data Analysis: Discrete Inverse Theory*, Academic Press, Inc., 1989.

PART 2

GSC 363
October 13, 1999

**NON-TRADITIONAL IN SITU VITRIFICATION AT THE
LOS ALAMOS NATIONAL LABORATORY
COLD DEMONSTRATION REPORT**



Submitted to:

MSE Technology Applications Inc.
P.O. Box 4078
Butte, MT 59702

Prepared by:

Geosafe Corporation
2952 George Washington WAY
Richland, WA 99352

GSC 363
October 13, 1999

**NON-TRADITIONAL IN SITU VITRIFICATION AT THE
LOS ALAMOS NATIONAL LABORATORY
COLD DEMONSTRATION REPORT**

Submitted to:

MSE Technology Applications Inc.
P.O. Box 4078
Butte, MT 59702

Prepared by:

Geosafe Corporation
2952 George Washington WAY
Richland, WA 99352

EXECUTIVE SUMMARY

The cold demonstration phase of the NTISV project was highly successful based upon the results obtained. The demonstration confirmed that the subsurface GeoMelt-planar ISV process is capable of meeting the depth and treatment effectiveness objectives for the MDA-V site, in an efficient and reliable manner. The demonstration was productive in generating field scale data that could be used to evaluate the approach for use on the MDA-V absorption beds as well as other similar applications at LANL and other DOE sites. The process converted the simulated absorption bed into a vitrified product that exhibits excellent durability (resistance to leaching) and stability, which will maximize the long-term performance of the waste form. In addition, because of the excellent leach resistance property of the product, the need for long-term monitoring should be minimized.

The following conclusions are based upon the results of the cold demonstration:

- The starter path injection method utilized was highly successful. Two seven-ft long vertical starter planes were installed by injection below the simulated absorption bed at the depth of 6.5 to 9.5-ft below grade. The installation of these two starter planes was conducted safely and to the specifications required to enable initiation of subsurface melting. The initial GeoMelt process start-up and continued processing of the simulated absorption bed proceeded smoothly. The ability to successfully inject the starter material into the subsurface is an approach, which could greatly increase the depth capabilities of GeoMelt applications. Injection of the starter path materials had previously not been performed prior to this project.
- A simulated absorption bed was configured according to the specifications identified in as-built drawings of the actual MDA-V beds. An increase in the size range of the cobbles placed in the simulated bed (relative to the drawings) was made based upon observations made during actual excavation activities within the MDA-V beds. Some minor differences in the surrounding soil stratigraphy of the cold demonstration area existed as compared to the actual MDA-V, due to limited availability of uncontaminated areas near the site selected for the hot demonstration. However, the small variations in the soil stratigraphy did not affect the melting process or the quality of the product.
- Post-test examinations indicated that the entire target volume and its contents were successfully treated and incorporated into the resulting vitrified monolith. A volume 10-ft wide by 15-ft long and 22-ft deep was established as the target treatment volume for the cold demonstration. The 10-ft by 15-ft area was configured from grade down to a depth of 6 ft to represent the absorption beds found within the MDA-V.

A subsidence volume of 16-ft by 16-ft wide at the surface with a depth of 8.5-ft existed after completion of the cold demonstration. The subsidence volume was created from the incorporation of the absorption bed materials and the subsequent volume reduction of these materials as they are converted into a vitreous product.

In addition, the majority of a 2.5-ft layer of overburden gravel (that existed above grade prior to treatment) was also incorporated into the melt. Thus, the entire target volume was incorporated downward into the melt, which resulted in the development of a large subsidence volume that was later backfilled with clean soil.

Observations made when the completed product was exhumed indicated that all of the contents of the simulated absorption bed comprising the target treatment volume were incorporated into the vitrified product, including the large (up to 2-ft diameter) cobble.

- The entire top surface of the vitrified product was exposed one month after processing was completed. In addition, two sides of the cooled melt were exposed down to a depth of approximately 18-ft. The dimensions of the vitrified product were measured to be 25-ft in the east/west direction and 23-ft in the north/south direction. In addition to the data provided above, this also confirms that the target treatment area (10 ft by 15 ft) was treated and incorporated into the melt. In regards to the depth of treatment, all four of the electrodes used in the melting process exceeded the target depth of 22-ft.
- Data was gathered in many areas during the cold demonstration that will facilitate the successful completion of the hot demonstration. Many activities associated with the cold demonstration were being performed for the first time on the media specific to the LANL site. Because sites vary significantly from one to another, the need to gather operational data to allow "fine tuning" is a typical requirement. The approach used during the cold demonstration was to simulate the hot demonstration application in as many ways as possible such that the data produced would be representative for use on the subsequent hot demonstration. In this way, Geosafe was able to gain the maximum amount of knowledge in regards to the operation and application of the system on the hot demonstration.
- An excellent vitrified product was produced by the cold demonstration. The product was sampled such that various analyses could be performed to evaluate product quality. The analyses included the determination of the quantities of surrogates (cesium and cerium) that are present within the product, the degree of mixing (or homogeneity) of the surrogates within the product, and the degree of leachability of the surrogates out of the product.

Samples of the vitrified product were analyzed to determine the concentration of the cesium and cerium surrogates immobilized within the product. During the preparation of the simulated absorption bed, surrogates representing radionuclides contained within the MDA-V were added to the bottom of the simulated bed (at the 6-ft depth). Cesium for (Cs^{137}) and cerium (for transuranics) were added in concentrations sufficient to allow the determination of mixing efficiency of the surrogates within the vitrified product. Enough of the cesium and cerium were added to raise the concentration from background concentrations of 3.5 ppm and 110 ppm, respectively in the soil, to concentrations of 33-ppm cesium and 248-ppm cerium in the vitrified product. The concentrations of surrogates found within the vitrified product also indicates that all of the surrogates were retained

within the vitrified product and not volatilized to the off gas or transported into the surrounding soil.

To determine how well the surrogates were incorporated into and distributed within the resulting vitrified product, five samples were collected from a portion of the melt and submitted for complete digestion and analysis. Homogeneity testing of these samples resulted in a values of 33 ± 0.7 ppm for cesium and 248 ± 3 ppm for cerium. This indicates that all of the surrogates present in the simulated absorption bed were incorporated downward into the developing melt and distributed uniformly through out the resulting product. This is typical within a GeoMelt-created product due to the convective flow patterns that develop within the melt. Hotter regions within the melt, which occur around the four electrodes, cause molten material to flow upward and then outward and downward into the cooler regions. This flow pattern is the reason that contaminants (or surrogates), that may be localized initially in the soil column, become effectively distributed through out the entire melt volume.

Leach testing was also performed on the cold demonstration product to evaluate its resistance to leaching. Five random samples were submitted for product consistency and toxic characteristic leach procedure testing. In all cases, the results indicated that none of the surrogate compounds were present in the leachate at or above the detection limits of the analytical procedures. For the TCLP analysis, all five of the samples were reported at less than 0.29 ppm for cerium and less than 0.056 ppm for cesium. Likewise, the results of the PCT analyses indicated that the concentration within the leachate was less than 0.002 ppm for cerium and less than 0.006 ppm for cesium. The data gathered from the two leach tests exceeds the criteria established for the test as well as that of any other type of immobilization technology, including high-level waste melters. The high level of product quality is possible due to the fact that no melt additives are required to lower the melting temperature during GeoMelt processing. In addition, the soils present at the LANL site contain a very high concentration (>90 wt %) of glass forming compounds, which serve to make a very high quality and durable vitrified waste form.

- All major components of the GeoMelt ISV system operated as designed throughout the duration of the demonstration. Only two minor equipment problems were encountered during the cold demonstration. Both of the equipment problems were minor and were resolved easily without hindering the cold demonstration.

Performance data was gathered on individual pieces of equipment such that "fine tuning" or minor modifications can be made prior to initiating the hot demonstration. The adjustments that have been identified will allow for an efficient, safe and cost effective application during the hot demonstration.

- Gases exiting the thermal oxidizer were sampled continuously during the cold demonstration for oxygen (O₂), carbon monoxide and dioxide (CO and CO₂), and total hydrocarbons (THC). These compounds are routinely monitored when treating hydrocarbons as they either measure:
 - a component required for combustion (O₂)
 - a combustion product (CO and CO₂), or
 - the presence of any untreated organics (THC).

The O₂ and the CO₂ levels were typical discharge levels when measuring at the discharge of the thermal oxidizer. The propane fuel combustion process depletes the O₂ level from 20.9 wt % down to approximately 15-wt %. Likewise, 5 to 8 wt % CO₂ is generated from the combustion of the fuel. The total hydrocarbons measured were between 0 and 1 ppm during the demonstration.

The level of carbon monoxide, which is generated as a result of partial combustion, was evolved at a level typically between 15 and 65 ppm, which is approximately equivalent to the emission coming from one standard automobile. Typically, these levels are of no concern from a health and safety and environmental release standpoint.

- All phases of the cold demonstration were conducted safely and according to all of the applicable components of LANL's integrated safety management program. Although the GeoMelt process uses high levels of power, generates significant amounts of molten soil subsurface, and requires the use of cranes, drill rigs and high-pressure injection equipment, no accidents or near accident occurred during the cold demonstration.
- Cost data collected during the cold demonstration indicated that the direct costs of the cold demonstration operations amounted to \$684/ton (this includes the labor, equipment costs, consumables, propane, and electrical energy used during the 8-day run). This cost per ton is below the established unit cost criteria established for the hot demonstration of \$800/ton of treated soil. It is expected that the cost/ton of the hot demonstration will be equal to or less than that of the cold demonstration due to increased efficiency with larger scales of application. The planned target volume for the hot demonstration is twice the volume than that of the cold demonstration.

TABLE OF CONTENTS

	<u>Page</u>
1. INTRODUCTION.....	1
2. GEOSAFE GEOMELT-ISV SYSTEM.....	5
2.1 Electrical Power Supply System.....	5
2.2 Electrode System.....	6
2.3 Off-Gas Treatment System.....	7
2.3.1 Off-Gas Hood.....	7
2.3.2 Off-Gas Processing System.....	8
2.4 Auxiliary System.....	10
3. NTISV COLD DEMONSTRATION AREA PREPARATION.....	12
3.1 Simulated Absorption Bed Activities.....	12
3.1.1 Simulated Absorption Bed Excavation and Lateral Thermocouple Placement.....	12
3.1.2 Simulated Absorption Bed Construction.....	16
3.2 Installation of Melt Profile Monitoring Wells.....	20
3.3 Site Pre-Conditioning By Dynamic Disruption.....	22
3.4 Electrode Installation.....	25
3.5 Starter Plane Installation.....	28
3.6 Installation of the Overburden Layer.....	31
3.7 Sampling and Analysis of the Simulated Absorption Bed Materials and Surrounding Soils.....	31
3.7.1 Whole Rock Analyses.....	31
3.7.2 Presence of Surrogates in the Simulated Absorption Bed Materials and Surrounding Soils.....	34
4. NTISV COLD DEMONSTRATION TEST OPERATIONS.....	36
4.1 Cold Demonstration Operations Overview.....	36
4.2 Electrical Performance.....	36
4.3 Off-Gas Treatment Performance.....	39
4.3.1 Particulate Generation and Removal.....	39
4.3.2 Thermal Oxidizer Operation.....	41
4.3.3 Off-Gas Emission Sampling.....	41
4.4 System Reliability and Improvements.....	43
4.5 Electrode Performance.....	44
5. NTISV COLD DEMONSTRATION PRODUCT EVALUATION.....	47
5.1 Post-Test Condition of Treatment Zone and Overburden.....	47
5.1.1 Subsidence Volume.....	47
5.1.2 Vitrified Monolith Size and Shape.....	48
5.1.3 Melt Depth.....	51

TABLE OF CONTENTS

	<u>Page</u>
5.2 Vitrified Monolith Sampling	52
5.2.1 Bulk Chemistry Testing.....	52
5.2.2 Homogeneity of the Radionuclide Surrogate Distribution	55
5.2.3 Surrogate Retention Efficiency	56
5.2.4 Product Quality Testing.....	58
5.2.4.1 PCT Evaluation of the Vitrified Product.....	59
5.2.4.2 TCLP Testing of the Vitrified Product.....	60
5.2.5 Geochemical Evaluation	61
6. PRELIMINARY COST INFORMATION.....	62
7. REFERENCES.....	63
APPENDIX A – Sample and Analysis Plan.....	65
APPENDIX B – Cold Demonstration Operations Chronology	66
APPENDIX C – Geochemical Evaluation	67

LIST OF FIGURES

	<u>Page</u>
1-1 Illustration of planar melting as applied to the cold demonstration.....	3
2-1 NTISV off-gas hood, electrodes, and electrode feeder assemblies	6
2-2 Off-gas treatment schematic	7
2-3 NTISV HEPA pre-filter	9
2-4 Thermal oxidizer used during the cold demonstration	11
3-1 Cold demonstration simulated absorption bed configuration	12
3-2 Area excavated for the simulated absorption bed	13
3-3 Photo of the completed excavation	13
3-4 Position of lateral TC as viewed from the east side of the bed looking west	14
3-5 Position of lateral TCs as viewed from the south side of the bed looking north	15
3-6 Placement of the lateral thermocouples	15
3-7 Placement of the surrogate chemicals on the floor of the simulated absorption bed.....	17
3-8 Placement of the cobbles with attached thermocouples	18
3-9 Addition of soil to fill voids within the cobble layer	18
3-10 Placement of a 1-ft layer of gravel within the simulated absorption bed	19
3-11 Installation of the sand layer in the simulated absorption bed.....	19
3-12 The completed simulated absorption bed prior to final grading	20
3-13 Pneumatic rotary drill rig used to install the melt shape monitoring boreholes	21
3-14 Completed melt monitoring borehole (minus the cement apron)	21
3-15 Vertical plumbness verification of the melt shape monitoring boreholes	22
3-16 Location of preconditioning performed in and around the cold demonstration area.....	23
3-17 Dynamic disruption pre-conditioning of the simulated absorption bed area	24
3-18 Photograph showing the area influenced around each preconditioning point	24
3-19 Pre-conditioning and installation of vertical TCs in the simulated absorption bed	25
3-20 Location of vertical thermocouples	26
3-21 Installation of the electrode casings	26
3-22 Withdrawal of electrode casing over the placed electrode	27
3-23 Starter path injection segment created during field testing within the tuff.....	29
3-24 Injection of the west starter plane	30
3-25 Simulated absorption bed after the electrode and starter plane installation.....	32
4-1 Cold demonstration voltage and amperage	37
4-2 Resistances of A and B phases during the cold demonstration	37
4-3 Cold demonstration voltage and amperage	38
4-4 HEPA filter loading rate	40
4-5 Thermal oxidizer operating temperature.....	42
4-6 Result of off-gas monitoring during the cold demonstration.....	43
4-7 Electrode depth during the cold demonstration	43
5-1 Cold demonstration subsidence area.....	48
5-2 Surface of the cold demonstration vitrified monolith	49

LIST OF FIGURES

	<u>Page</u>
5-3 Shape of the vitrified product produced during the cold demonstration	50
5-4 Location of the vitrified product compared to the original location of the simulated absorption bed	51
5-5 Breaking of the vitrified product during sampling activities	53
5-6 Section of the vitrified product removed for sampling.....	53
5-7 Representative sample of the vitrified product	54

LIST OF TABLES

	Page
3-1 Resistance of starter planes	31
3-2 Whole Rock Results of Soils and Materials In and Around the Simulated Absorption Bed	33
3-3 Background Levels of Surrogates in the Simulated Absorption Bed Soils and Materials	35
5-1 Post-test glass product sample bulk chemistry results (normalized)	54
5-2 Results of radionuclide surrogate analyses in the vitrified product	55
5-3 PCT results for the cold demonstration product	59
5-4 Results of TCLP testing of the cold demonstration product	60

1. INTRODUCTION

Geosafe, in conjunction with MSE Technology Applications, Inc. (MSE-TA), the Department of Energy's (DOE) Subsurface Contamination Focus Area (SUBCON), and the Los Alamos National Laboratory (LANL) is conducting a demonstration and evaluation of non-traditional in situ vitrification (NTISV) technology as a potential remedy for treatment of mixed-waste-contaminated absorption beds at LANL's MDA-V site, as well as other applications within the DOE complex. A competitive procurement of NTISV technologies resulted in the selection of an advanced NTISV technology offered by Geosafe Corporation, termed GeoMelt™ Planar ISV, which involves joule-heated melting within the subsurface. The technology is an advancement based on Geosafe's GeoMelt vitrification technology which has been widely demonstrated and very successfully applied on a commercial basis within the U.S., Australia and Japan.

The demonstrations are being performed using Geosafe's commercial large-scale equipment on two areas at the LANL site. The successful demonstration of NTISV at LANL is expected to provide a useful technology for the general remediation needs of EM-40 (complex-wide) including some specific site remediation needs of LANL for remediating buried waste.

The project involves the performance of two large-scale demonstration melts. The first "cold" demonstration was performed in a simulated absorption bed, which contained no radioactive contamination. The simulated absorption bed was designed and constructed to represent the actual MDA-V absorption beds as closely as possible. This simulation included the use of similar construction materials, as well as the use of surrogate chemicals for the radionuclides of interest. It is planned that a second "hot" (radioactive) demonstration melt will be performed within MDA-V's Absorption Bed #1 if the results of the first demonstration are determined to meet the performance criteria. A target treatment depth of 22-ft has been established for both demonstrations, which will demonstrate the GeoMelt technology's capability to treat both the contaminated bed contents and underlying contaminated soil. The melting process will result in the destruction and removal of all organic contaminants within the target treatment zone, and immobilization of heavy metals and radionuclides within a high integrity vitrified monolith. The process produces a product similar in appearance to natural obsidian with outstanding physical and chemical characteristics, weathering and leaching resistance, and life expectancy.

The demonstrations involve monitoring to gather performance data pertinent to evaluation of the technology for various applications at LANL and throughout the DOE Complex. Specific performance data is being gathered relative to the technology's treatment effectiveness on the contaminants present at the site. In addition, data is being gathered relative to reliability of equipment and all aspects of costs related to application of the NTISV technology.

The specific objectives established for the cold demonstration include:

- configure a simulated absorption bed including subsurface conditions that are expected for the hot demonstration

- demonstrate the ability to safely and successfully install planar starter paths within the Bandelier Tuff formation in the subsurface
- demonstrate the ability to process the materials placed into the demonstration bed using NTISV to achieve a vitrified mass depth similar to that anticipated in the hot demonstration
- verify the physical dimensions of the vitrified mass by excavating and exposing a portion of it
- obtain process performance information necessary to optimize the processing configuration and parameters for the hot demonstration
- gather geochemical data by collecting and analyzing samples of the various components that will be processed and; compare this data to the anticipated geochemical conditions in the hot demonstration
- characterize the vitrified product by performing homogeneity evaluations, as well as product quality (TCLP & PCT) leach tests,
- obtain costing data to enable estimation of large-scale remediation costs of the MDA-V, and to compare costs to the target level of \$800/ton or less
- generate data that will assist in developing evaluation criteria for the hot demonstration
- provide information that will be input into health and safety, work control, regulatory, NEPA and RCRA requirements for the hot demonstration

Historically, conventional (or traditional) ISV involved processing the soil/waste matrix in a top-down fashion. A horizontally oriented melt is established between four electrodes using a series of starter tubes placed in the soil near the surface to pass electrical current and dissipate the joule heat necessary to melt the surrounding soil. Once molten, the soil becomes sufficiently conductive to support the flow of electrical current, thereby dissipating enough joule heat to propagate the melting process. By the application of continued power through the melt, the soil adjacent to and below becomes molten. The addition of power is continued to the melt until such time that the melt has encompassed the entire treatment volume from grade down to the desired depth.

This traditional ISV approach was originally developed by Battelle Pacific Northwest National Laboratory for the Department of Energy. The Department of Energy received a patent for the process in 1983 (Brouns, et al. 1983). The commercial application of ISV has been exclusively licensed to Geosafe Corporation. The operating experience of traditional ISV is extensive, including 80 large-scale melts covering a wide array of contaminants, soil types, and inclusions. In 1994 Geosafe participated in a TSCA permit application process, and in 1995 was granted a National TSCA Permit for the use of GeoMelt ISV nationwide to remediate PCB-contaminated wastes in a soil/waste matrix at concentrations up to 17,860-ppm.

Due to limitations of traditional ISV in processing either soils that possess an extremely low permeability or contain sealed containers filled with gas generating materials, Geosafe has developed an enhancement to the traditional ISV technology. This advancement, called planar-ISV, allows the safe, effective processing of these and other problematic applications. In addition, it is expected that the planar-ISV approach will significantly extend the depth capability beyond its current limits.

In this process, the horizontal array of starter tubes used between four electrodes in traditional ISV is replaced with vertically-oriented planes of starter material between two pairs of electrodes. The planes can be positioned at the desired depth and separation within the subsurface. The separation of the starter planes allows two relatively independent melts to form during the initial stages of the process. This allows significant control of the initial melt process so that it can be focused for optimal treatment of the waste zone. Moreover, because the melts are separated laterally during their initial stages of development, the treatment volume can initially be processed without the build-up of large gas volumes, which potentially could pass through the melt possibly causing a melt disturbance and overheating event. This approach allows for the maintenance of approximately twice the amount of permeable zone around the two melts, which aids in the controlled transport of any gases generated during processing to the off-gas treatment system. Any gases generated from hazardous materials during processing are either pyrolyzed during melting, or are removed to the off-gas treatment system. By the time the melts have grown sufficiently to merge, all volatile materials (e.g. – mainly water) will have been effectively and safely removed from the treatment zone. Figure 1-1 illustrates the basic planar-ISV melting technique as applied during the NTISV Cold Demonstration.

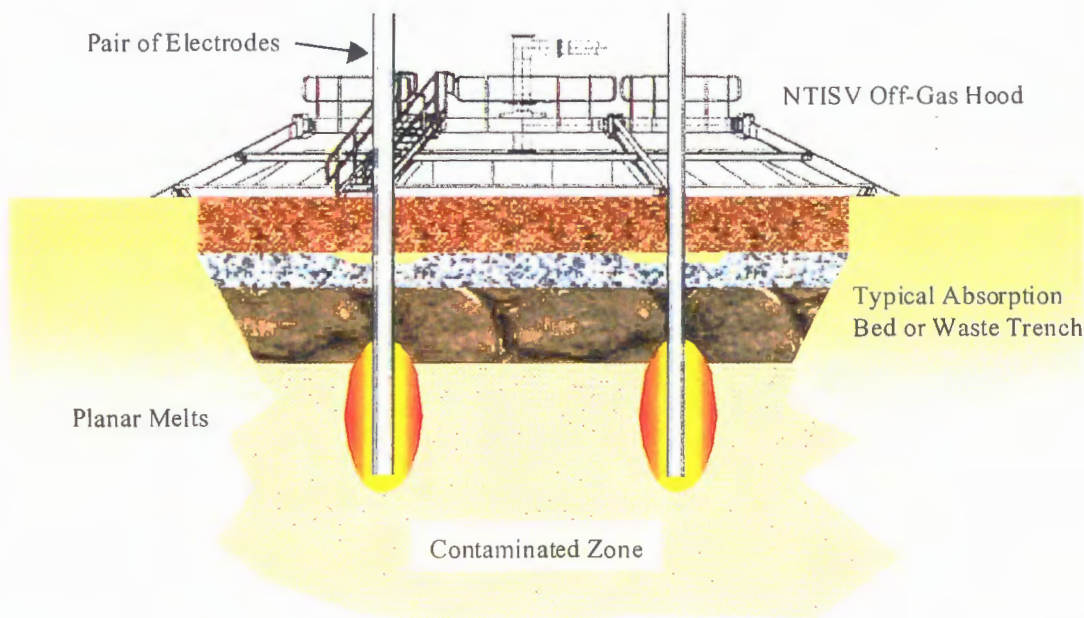


Figure 1-1. Illustration of planar melting as applied to the cold demonstration

The planar-ISV approach has previously been tested by Geosafe at various scales ranging from engineering- to large-scale. In addition, this technique has been demonstrated as an effective method for treating underground tanks containing sludge and/or liquid heels.

To qualify for the non-traditional aspect of the ISV procurement, Geosafe chose to employ the planar-ISV approach coupled with a subsurface start-up, which had not previously been tested on an application like the MDA-V absorption beds. Other innovative applications being demonstrated during both the cold and hot demonstrations included the use of overburden and dynamic disruption.

Overburden, as used in this application, serves to increase the efficiency of the melting process. Heat losses, which otherwise would escape in the plenum area of the hood and then be removed through the off-gas treatment system in a conventional top-down approach are minimized by the overburden. Use of overburden has been shown to increase the thermal efficiency of the melting process by up to 30%. This can provide significant cost savings both by reducing the power costs and by shortening the amount of run time to complete a given treatment volume. The use of overburden also provides protection from the effects of a melt disturbance that may occur when treating highly heterogeneous or liquid-bearing wastes.

Dynamic disruption of the soil surrounding the target treatment volume is a method employed to ensure that the contents of the simulated absorption bed are completely incorporated into the melt during the treatment process. Disruption of the surrounding soil is accomplished by using a hydraulic hammer to vibrate a steel probe down into the soil column. By disrupting or loosening the surrounding soil, it is enabled to feed into the surface of the developing melt(s). When treating soils that are structurally strong, such as the native tuff at the LANL site, it is possible for vertical walls to be formed as the melt progresses downward. By breaking up the tuff prior to treatment, the sloughing of the adjacent soil into the melt is promoted, as well as eliminating the potential for a steep wall of soil to cleave off and fall into the subsided area.

This report documents all of the information pertinent to the cold demonstration, including: the ISV system used, site preparation activities, operational activities, product excavation and sampling, and discussion of results.

2. GEOSAFE GEOMELT-ISV SYSTEM

The Geosafe GeoMelt-ISV system consists of two major subsystems – the power supply system and the off-gas treatment system. The basic features and capabilities of these subsystems are described in this section. The off-gas treatment system, which is composed of several different unit operations, can be operated with select portions of this system in service. The unit operations used during a given melt are dependent upon the particular application and the materials being treated. For instance, during the cold demonstration it was only necessary to pass the off gases through the pre-filter, the final high efficiency particulate (HEPA) filter and the thermal oxidizer to properly treat the off gases. However, operation of the entire system was performed to ensure its operability in the case that it may be needed during the hot demonstration phase of the NTISV project.

2.1 Electrical Power Supply System

The main component of the power supply system is the Scott-Tee-configured transformer. This transformer converts the three-phase line power to two single-phase outputs on the secondary side of the transformer. The output from the secondary side of the transformer is applied to the electrode system which, in turn, provides the electrical energy to the melt.

The Scott-Tee transformer is designed to accept standard nominal input voltages in the range of 12.47-kV to 13.80-kV. The transformer is rated at a maximum of 3750-kW and can deliver output voltages in the range of 0 to 4160 volts AC. The corresponding amperage output range on secondary-side AC current is 4000 to 0 amps.

As the size and temperature of the melt increases with increasing power input, the resultant electrical resistance experienced during processing decreases. This creates a constantly changing load on the transformer. The variation in load is a result of a constant decrease in the voltage required to drive the desired amperage through the melt. In order to maintain a desired power input to the melt as the voltage drops, it is necessary to periodically increase the amperage flow. To accommodate a continual variation in load, the transformer is equipped with sixteen taps that allow adjustment of the voltage and current supplied to the melt. Matching the transformer tap with that appropriate for the melt resistance and the desired power level helps insure optimal performance of the transformer.

The voltage and amperage generated on the transformer secondary side is supplied to the electrodes through a set of 1000 MCM electrical cables. Each cable is rated at 1000 amps. Typically, four cables are connected to each electrode. These four cables can therefore accommodate the peak current draw of 4000 amps. The length of the cables is adequate to allow placement of the hood a distance of 160 ft radially in any direction from the transformer.

The Scott-tee transformer can either be connected directly to a 12.47-kV or higher power grid, or be supplied power by diesel generators. For these demonstration tests, the LANL-Environmental Remediation (ER) division provided a dedicated 13.1 kV power drop.

2.2 Electrode System

The electrode system consists of four graphite electrodes and their associated electrode feeder assemblies. These are shown in Figure 2-1. The electrodes are indicated in this figure by the four vertical rods projecting above the ISV hood. The electrical power output from the Scott-Tee transformer is delivered to the melt through these electrodes. Each phase of the transformer secondary-side output is connected to a pair of electrodes. Therefore, four electrodes are used to supply power to the two planar melts.

Each individual electrode is composed of several electrode segments. Six electrode segments were used to construct each electrode during the cold demonstration. Each segment has a diameter of 12 in. and a length of 6 ft. The segments have threaded couplings on each end. The couplings allow a number of electrode segments to be joined to form the desired overall electrode length. The electrodes can either be gravity-fed into the melt or gripped and periodically lowered using a crane. Both operations were used during the cold demonstration. As the electrodes are lowered into the melt, additional electrode segments can be added to the top of each electrode to accommodate this feeding process.

The electrodes are held in position by electrode feeders. Each feeder maintains the vertical orientation of the electrode during processing, while also providing the electrical connection between the electrical cables and the electrode. The electrical connection is achieved by means of a set of copper contactor pads. The pads have mounting plates to accept the lug on each electrical cable, and are spring loaded to insure that contact between the contactor and electrode is maintained during operation.

Each electrode feeder contains a set of pneumatically operated grippers. These grippers are used to control the insertion depth of the electrode. When the gripper is open, the



Figure 2-1. NTISV off-gas hood, electrodes, and electrode feeder assemblies

electrode is able to gravity-feed into the developing melt. In this situation, the bottom of the electrode rides on the bottom of the melt. In this way the electrodes can be used as a depth gage. By closing the gripper via a remote control station, the downward progression of the electrode will cease.

Raising the electrodes can be accomplished with the aid of a crane and lifting bail affixed to the top segment of an electrode. Similarly, precise lowering of the electrode can also be accomplished with the use of a crane.

2.3 Off-Gas Treatment System

The off-gas treatment system is composed of two modular subsystems – the off-gas hood and off-gas treatment unit. The off-gas hood serves to collect and then to route the off gases to the treatment portion (see Figure 2-1). A schematic of the off-gas treatment system used during the cold demonstration is provided in Figure 2-2.

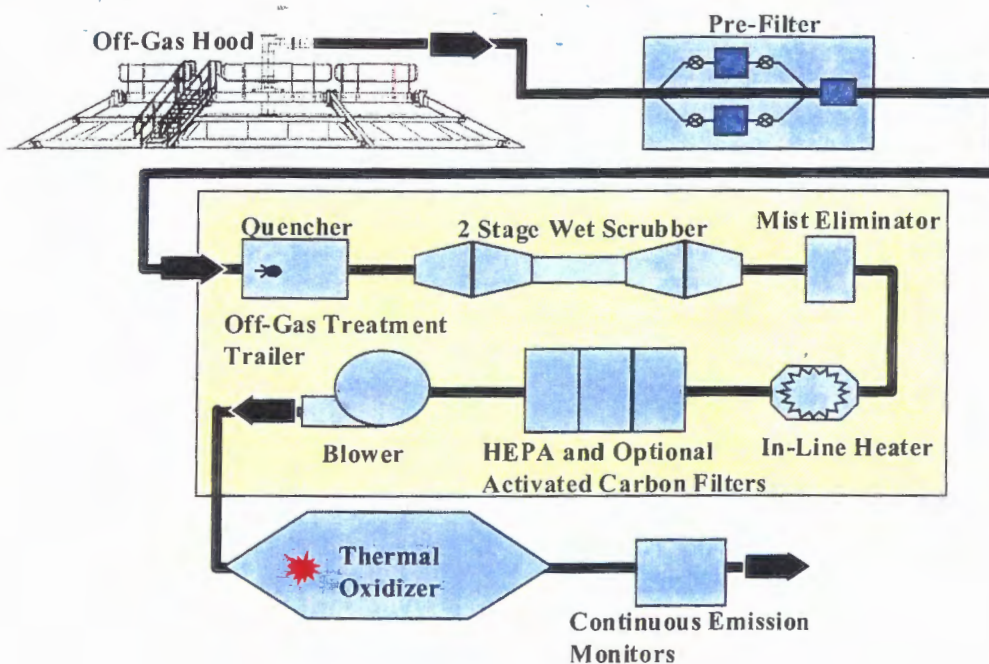


Figure 2-2. Off-gas treatment schematic

2.3.1 Off-Gas Hood

An off-gas collection hood is typically staged over the target vitrification zone prior to processing. The hood is composed of a skin of stainless steel panels supported by a steel superstructure. This structure also provides a working platform and supports the electrode feeder and associated electrode loads.

During operation, the plenum space beneath the off-gas hood is maintained at a slight vacuum to prevent the release of any gases generated during or released during process-

ing. The off-gas hood collects and routes these gases for subsequent treatment by the off-gas treatment system. The vacuum within the hood, as well as within the rest of the off-gas treatment system is established by means of a blower.

Off gases collected within the off-gas hood are transported to the off-gas processing system through a 12-in diameter stainless steel line.

2.3.2 Off-Gas Processing System

The off-gas processing system is designed to collect and/or destroy any potentially hazardous materials present in the off-gas stream. These can be volatile, semi-volatile, non-volatile, or particulate in nature. The system consists of several stages including: 1) a HEPA pre-filter, 2) a quencher, 3) a two-stage hydrosonic scrubber, 4) a mist eliminator, 5) an in-line heater, 6) a final HEPA filter, and 7) a thermal oxidizer. Depending upon the configuration and the materials to be treated, various components can be added or removed from the above system.

Flow from the off-gas hood through each of the components of this system is established by means of a high volume blower located near the end of the off-gas treatment system. This blower also develops the slight vacuum needed to insure in-leakage into the off-gas hood. The current system is designed to pull flow from the off-gas hood at a rate of 50 standard m^3/min . A backup blower in the system provides vacuum to the off-gas hood in case of a failure of the main off-gas blower, as well as during the loss of utility-fed power. The backup blower is designed to provide approximately the same volumetric off-gas flow rate as the main blower. The off-gas passing through this back-up system is processed by two separate HEPA filtration units and a thermal oxidizer unit before being exhausted to atmosphere.

The first component of the off-gas treatment system is a pre-filter (see Figure 2-3). The pre-filter is designed to remove particulate from the off-gas stream. The unit is fitted with two parallel banks of HEPA filters, each containing two filters. The minimum particulate removal efficiency of each filter is 99.97% for particles 0.3 μm in diameter and larger. By employing parallel banks of filters, it is possible to change out loaded filters while continuing to treat the off-gas by passing it through the other bank. The unit is also designed with a by-pass that allows gases to be directed through the unit unfiltered. Routing of the off gases through the two filter banks or the by-pass line is accomplished by opening and closing 12-in pneumatic gate valves.

Once gases pass through the pre-filter, they enter the off-gas treatment trailer where they can undergo wet scrubbing. The first component of the scrub system is a quencher. Water spray nozzles inside the quencher cool the incoming off-gas flow. The spray pattern promotes good mixing, condensation, and heat transfer between the spray and off-gas flow stream. In addition to removing particulates in the off-gas flow, the wet scrubbing nature of the quencher also serves to remove soluble components from the flow stream (e.g. - fluoride and chloride). Any trace concentrations of semivolatile materials still present in the off-gas stream are condensed into liquids or particles by the wet scrubbing action and consequently may also be collected at this stage. Condensate from the quencher is cooled with a water-to-glycol heat exchanger during its transfer to the scrub



Figure 2-3. NTISV HEPA pre-filter

tanks. Any acid gases that may have formed are also removed and neutralized via contact with the slightly basic scrub solution.

A two-stage hydrosonic scrubber is located just downstream of the quencher. The cooled gases leaving the quencher enter the first stage of the hydrosonic scrubber system. The off-gas is passed through a very fine circular spray, which serves to remove most entrained particulate at an efficiency of greater than 97% for particulates in the range of 0.5 micron and larger. A second hydrosonic scrubber spray nozzle is located just downstream of the first stage to further process the off-gas flow. As with the quencher system, the wet scrubbing nature of these scrubbers also serves to remove soluble components from the flow stream (e.g. – fluoride and chloride). Again, any trace concentrations of semivolatile materials still present in the off-gas stream may be condensed into liquids or particles by the wet scrubbing action and be collected at this stage.

Liquids that have been entrained and/or injected into the flow stream to this point are then removed to prevent wetting of the HEPA filters located in the final filtering unit of the treatment system. A chevron-vane mist eliminator is located downstream of the hydrosonic scrubbers to perform this dewatering function. The resulting condensate is transferred to the scrub tanks for further processing. At the design flow rate of 50 standard m^3/min , the mist eliminator removes 99.9% of all water droplets from the flow stream.

Two scrub tanks are employed to hold the scrub water and to collect the condensate from the quencher, scrubbers, and mist eliminator. The pH of the condensate in the scrub tanks is typically maintained between 6.0 and 8.0 to minimize solids formation during operation. The condensate in these tanks is recycled to provide the water for the quencher and venturi spray systems. Therefore, by maintaining the condensate in the slightly caustic range, acid gases (e.g., HCl) are effectively removed from the off-gas flow. The scrub

tanks are equipped with a transfer pump and line to allow transfer of the scrub solution between tanks during operation.

Following treatment by the mist eliminator, the off-gas is then passed through a heater to raise the dew point of the off-gas stream. The desired temperature rise of the off-gas is achieved by increasing the output of the heater, which is performed automatically by inputting the desired output temperature into the process control system.

The purpose of raising the temperature of the off-gas is to prevent condensate from forming within the final filter bank, which is the next step in the off-gas treatment. The final bank used during the NTISV cold demonstration consisted of three parallel-flow 12-in HEPA filters. Alternatively, various other sizes and types of filters including activated carbon filters can be inserted into the filter housing depending upon the application.

After passing through the final filters, the off-gas stream exits the off-gas trailer and then passes through a thermal oxidizer. The thermal oxidizer was employed due to the low levels of organic contamination found in the area in and around the location selected to construct the simulated absorption bed. The thermal oxidizer is used as a final polishing step for the: 1) treatment of any residual organic compounds, 2) conversion of carbon monoxide to carbon dioxide, and 3) the elimination of any odors that may be present due to the thermal treatment process.

The thermal oxidizer contains a large gas burner, which the off-gas flow passes directly through. Fuel for the flame is provided by a propane tank, but can also be supplied in the form of natural gas. A controller on the thermal oxidizer maintains the set point of the combustion chamber at a constant temperature of 1450°F. The flow rate and the diameter of the thermal oxidizer is sized such that an off-gas retention time within the combustion chamber of 0.9 seconds is achieved. This retention time at temperature provides a minimum treatment efficiency of 99 to 99.9% for organics. Figure 2-4 shows the thermal oxidizer as assembled at the LANL site.

A sample collection unit is fitted to the outlet stack such that a sample of the off-gas can be collected isokinetically and routed to continuous emission monitors located inside of the off-gas treatment trailer. The off gas is continuously monitored for total hydrocarbons, carbon monoxide, carbon dioxide, and oxygen content. In addition, other monitors can be added to this system depending upon the materials being treated.

2.4 Auxiliary Systems

The GeoMelt ISV system is controlled via an automated process control system which serves to collect and store data from the various units. In addition, the process control system has the capability via batch logic to automatically maintain the system in a safe and functional operating mode. For instance, the batch logic will automatically start an alternate scrub pump in the event of a pump failure, shut off power if vacuum within the hood is lost, maintain the pH within the scrub tanks, as well as other activities.

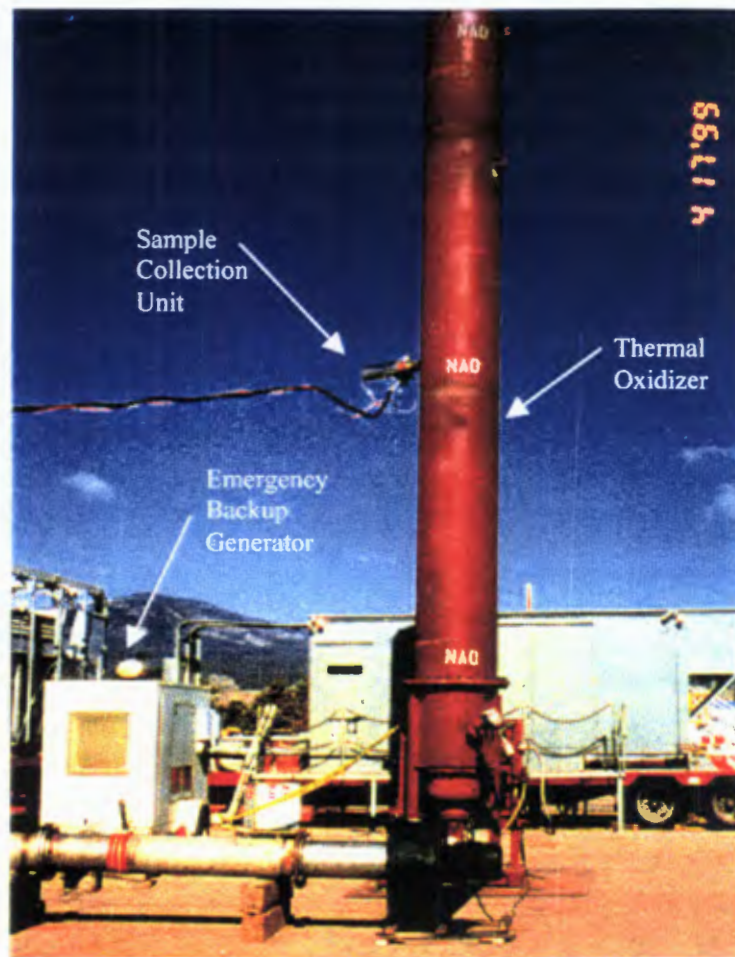


Figure 2-4. Thermal oxidizer used during the cold demonstration

To ensure that off gases being removed from the hood are continually treated, the GeoMelt ISV system is designed with a back-up off-gas treatment system. In the event of a major component failure, such as the main blower, the back-up system can be activated to allow the continuous treatment of the off gases. The skid is fitted with a filter chamber that can contain roughing, HEPA, and/or activated carbon filters. The output of the back-up off-gas treatment system is routed to the thermal oxidizer for final treatment.

In the event of a loss in power from the main utility supply, the ISV system contains a back-up generator configured with an automatic transfer switch. The transfer switch continually monitors the incoming power, and when a drop is detected, the transfer switch will automatically start the generator and switch over to it for incoming feed. The generator is sized such that the system can be put into a safe operating mode while off-gases continue to be treated. This is accomplished by supplying power to the back-up off-gas treatment system, the thermal oxidizer, the process control system and other auxiliary power circuits such as lighting and HVAC. The back-up generator can be seen on the left side of Figure 2-4.

3. NTISV COLD DEMONSTRATION AREA PREPARATION

3.1 Simulated Absorption Bed Activities

LANL-ER contracted with Morrison-Knudsen to construct a simulated absorption bed for the purposes of the cold demonstration. The goal of the construction was to accurately simulate the configuration of the actual absorption beds located within MDA-V. To accomplish this goal, as-built drawings and data gathered during physical excavation within the absorption beds were reviewed and used in constructing an area similar in design to the actual absorption beds. In addition, the materials used in the construction of the actual absorption beds were reviewed such that like materials could be gathered to form the simulated absorption bed. The configuration of constructing the simulated absorption bed can be seen in Figure 3-1.

3.1.1 Simulated Absorption Bed Excavation and Lateral Thermocouple Placement

An area 20-ft wide by 25-ft long was excavated to form the simulated absorption bed. The excavation was made down to a depth of 6-ft. Prior to beginning to backfill this area, an 11-ft deep excavation was performed on the east end of the simulated bed location to allow for the installation of thermocouples (TCs), which were used for monitoring the initial development of the planar melts. Figure 3-2 shows the bed layout and the location of the deep excavation for placement of lateral thermocouples. It should be noted that, although a 20-ft wide by 25-ft long bed was excavated, the target treatment area established for the cold demonstration consisted of an area 10-ft wide by 15-ft long. Figure 3-3 shows the completed excavation. Once the excavation was completed, placement of the thermocouples followed by partial backfilling of the excavation was performed in a stepwise fashion.

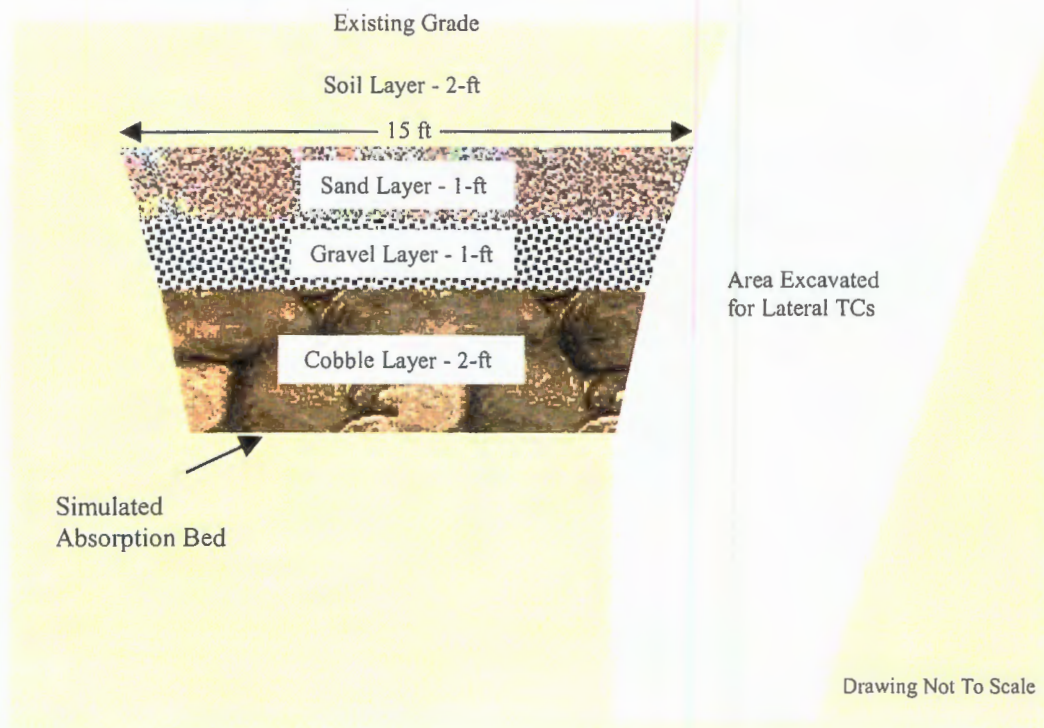


Figure 3-1. Cold demonstration simulated absorption bed configuration

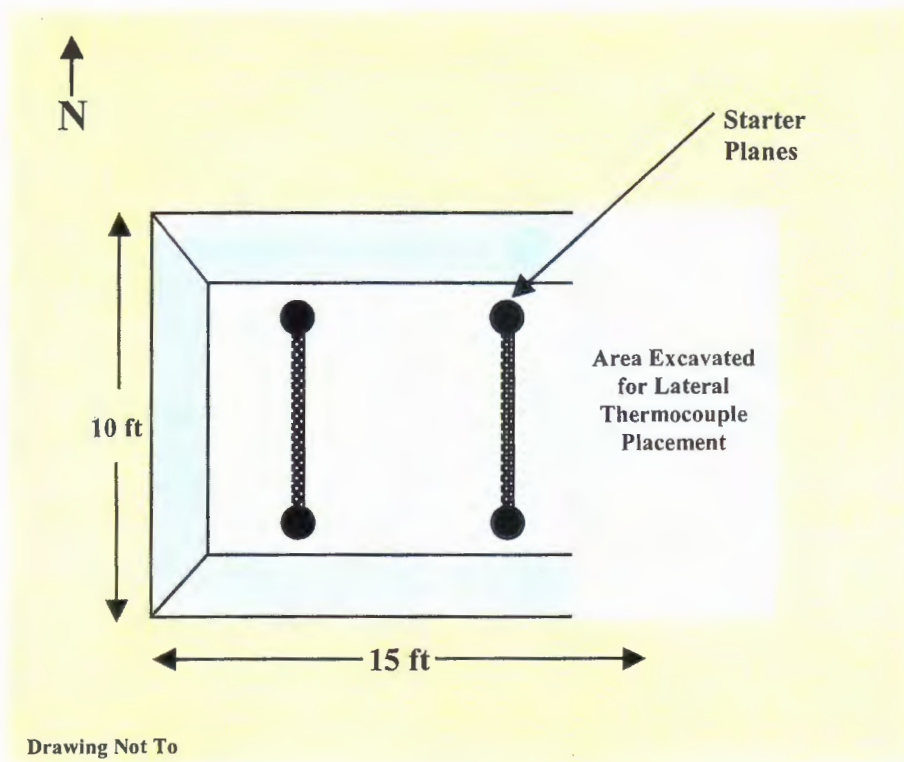


Figure 3-2. Area excavated for the simulated absorption bed



Figure 3-3. Photo of the completed excavation

The first series of TCs placed were located within the 11-ft deep excavation for the purpose of monitoring the development and progress of the melt created around the east pair of electrodes. Type K TCs, which can measure continuous temperatures up to approximately 1200°C, were used to monitor the simulated absorption bed. Type K TCs are used predominantly to determine the edge of the melt as their failure temperature coincides closely with the temperature at which the soils begin to melt. Three sets of TC bundles consisting of four individual TCs each were installed at the 11-ft depth to monitor the initial lateral and vertical progression of the east plane. The bundles were separated by a distance of four feet. The bundles were constructed by taping the four TCs together in a linear fashion such that each TC tip was separated by a distance of 1 ft. The TCs were installed without having to actually enter the excavation. The first of the four TCs in each bundle was located such that they were 6.5-ft from the east/west centerline of the simulated absorption bed. This corresponds to a distance of 3-ft from the east starter plane. The layout of these TCs can be seen in Figures 3-4 and 3-5. This TC configuration resulted in having a total of 12 TCs at the 11-ft depth: three of the TCs 6.5-ft from the east/west centerline, three more 7.5-ft from the centerline, and so on out to 9.5-ft from the centerline.

After placement of the TCs was completed at the 11-ft level, broken tuff backfill was used to cover up the TC bundles and the excavation was backfilled up to the 9-ft depth. Compaction of the area was performed by tamping the area with the bucket of the excavator in approximate 1-ft lifts. At the 9-ft depth, three more TC bundles of four individual TCs each were laid out identically to those described above. The placement of these TCs can be seen in Figure 3-6. This process was repeated again at the 7.5-ft depth.

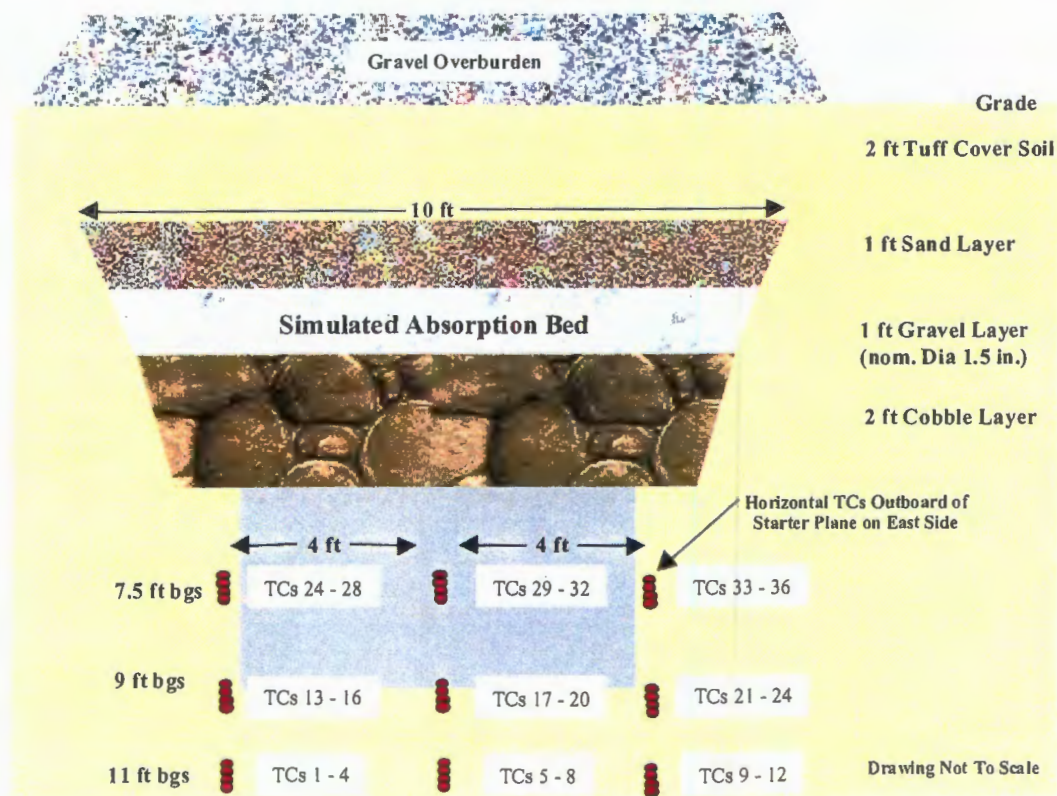


Figure 3-4. Position of lateral TC as viewed from the east side of the bed looking west

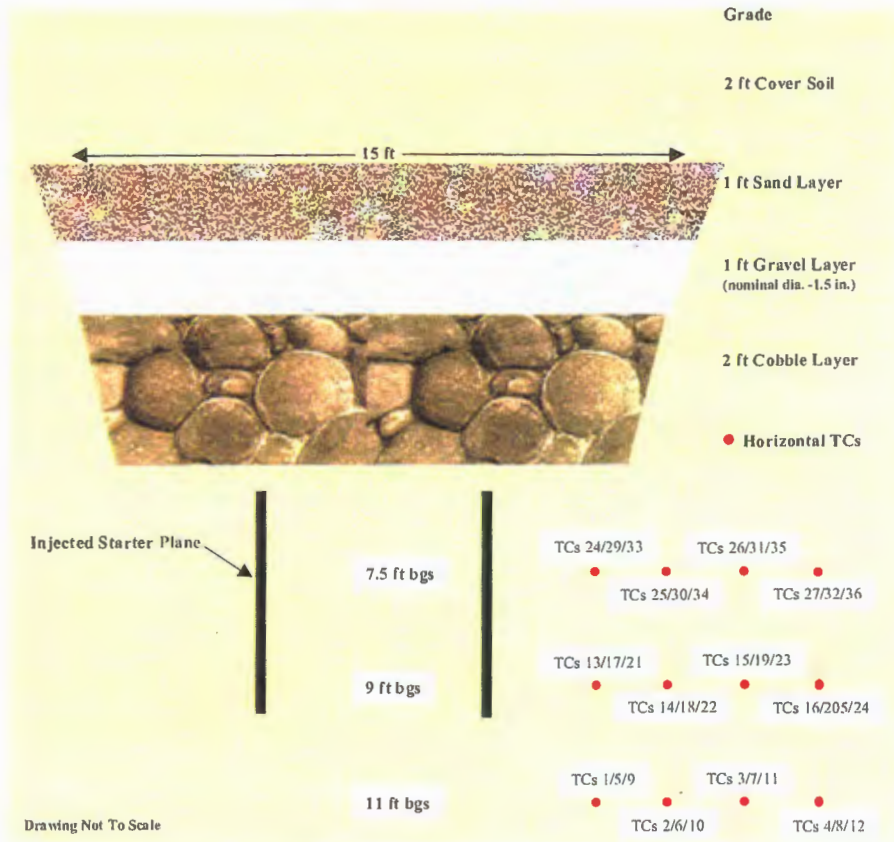


Figure 3-5. Position of lateral TCs as viewed from the south side of the bed looking north



Figure 3-6. Placement of the lateral thermocouples

As can be seen in Figures 3-4 and 3-5, each thermocouple was labeled with a specific number so that the data generated could be correlated to their physical location within the soil column. After all of the lateral thermocouples were installed, the excavation was backfilled to form an area 20-ft wide by 25-ft long by 6-ft deep. This area would serve as the area to be filled with materials representing the make-up of the actual absorption beds found in MDA-V. The 10-ft by 15-ft area of the simulated absorption bed chosen as the target treatment volume for the cold demonstration can be seen demarcated in Figure 3-3 by stakes with orange caps and the yellow line.

3.1.2 Simulated Absorption Bed Construction

Surrogate chemicals were placed on the floor of the simulated absorption bed prior to backfilling the absorption bed. The non-hazardous and non-radioactive surrogates were added to the treatment area to allow confirmation of the vitrified product quality through Product Consistency Testing (PCT) and Toxic Characteristic Leaching Procedure (TCLP) Testing, and to enable determination of the level of homogeneity within the vitrified product. The chemicals chosen to simulate actual radioactive contaminants found in the MDA-V were cesium carbonate (Cs_2CO_3), to simulate the presence of the semi-volatile radioactive cesium, and cerium oxide (CeO_2) to simulate the presence of uranium and plutonium. The amount of Cs_2CO_3 and CeO_2 added to the absorption bed was 6.5-kg and 30-kg respectively. The difference in the amount of surrogates added is due to the different background level of these naturally occurring materials. Because the surrogates added to the absorption bed are typically homogeneously distributed throughout the resultant melt (which will be a significantly larger volume than the original absorption bed), it was necessary to place enough surrogate in the absorption bed so that the final melt concentration would be above both the detection level of the procedure used for analysis and the background concentration of the native soils.

The background concentration of cesium was found to be on average 3.5 ppm, whereas for cerium it was 110 ppm. The background levels of cesium and cerium were determined from samples obtained during pre-test sampling. Details of the pre-test sampling can be found in section 3.7.2. The resulting concentration of cesium and cerium in the simulated absorption bed was significantly greater than the actual concentration of radionuclides present in the actual MDA-V absorption beds. Figure 3-7 shows the chemicals being placed into the simulated absorption bed.

The simulated absorption bed was backfilled with cobble similar to that found in the actual MDA-V absorption beds, once the surrogate chemicals were placed. A review of the physical configuration of the actual absorption beds, which included such items as previous test trenching records and as-built drawings, were used to ensure that representative materials would be used in forming the simulated absorption bed. Cobble with diameters from approximately 4 to 24 inches were obtained from a nearby quarry between Pojoaque and Los Alamos. Sufficient quantities of the cobble were obtained to form a 2-ft layer on the bottom of the simulated absorption bed.

To assist in confirming that the contents within the 10-ft by 15-ft area of the simulated absorption bed were incorporated into the melt, six large pieces of cobble were fitted with TCs. The TCs were attached to the cobble using large hose clamps (similar to those used on automobiles).



Figure 3-7. Placement of the surrogate chemicals on the floor of the simulated absorption bed

The tip of each TC was then inserted between the hose clamp and the cobble and then bent over such that the tip of the TC formed a loop. It was expected that this manner of connecting the TCs to the cobble would ensure a high likelihood of the two staying connected during melting.

The six-instrumented pieces of cobble were distributed in different locations of the simulated bed. Two of the cobbles were placed in the center of the melt area and the other four were placed on the outside of where the four electrodes would later be installed. The placement of the instrumented cobble can be seen in Figure 3-8.

It was planned that as the contents of the absorption bed fed downward and were incorporated into the developing melts, the instrumented cobble will move down likewise and be incorporated. Additional TC wire, which connects the TC to the data acquisition system, was spooled above each cobble to allow the instrumented cobble to feed downward. This would allow the cobbles to move downward without breaking the TC wire as the weight and downward movement caused the TC wires to tighten. In all six cases, several feet of excess wire were spooled directly above each piece of cobble.

Based upon photographs taken during previous excavation activities within an actual MDA-V absorption bed, it was determined that little or no voids existed within the cobble layer. That is, the spaces between the cobble had been silted in during years of absorption bed operation. To minimize the void space in the cobble layer of the simulated absorption bed, top soil that was removed during the excavation of the test bed were spread over the cobble and allowed to infiltrate the spaces. This can be seen being performed in Figure 3-9.



Figure 3-8. Placement of the cobbles with attached thermocouples



Figure 3-9. Addition of soil to fill voids within the cobble layer

The next step in the construction of the simulated absorption bed was to add a 1-ft layer of round gravel. Gravel with a diameter of 1.5-in or less was used to form the gravel layer. The completed gravel addition can be seen in Figure 3-10. The coils of extra TC wire that were connected to the six cobble fitted with TCs can be seen laying on top of the gravel layer.



Figure 3-10. Placement of a 1-ft layer of gravel within the simulated absorption bed



Figure 3-11. Installation of the sand layer in the simulated absorption bed

Following the addition of the gravel, a 1-ft layer of sand was placed directly over the gravel. The completed sand layer is shown in Figure 3-11. A 2-ft layer of backfill material, which remained from the initial excavation, was used to complete the backfilling of the excavation. This consisted of a mixture of broken tuff and the red top soil. This can be seen in Figure 3-12. The final step in the construction of the simulated absorption bed was to level the entire area such that the GeoMelt off-gas hood would set level once it was placed.



Figure 3-12. The completed simulated absorption bed prior to final grading

3.2 Installation of Melt Profile Monitoring Wells

MSE-TA performed various melt profile monitoring activities prior to, during and after the cold demonstration. The melt shape monitoring was performed by using various types of transmitters and receivers, some of which required insertion down 50-ft deep boreholes. To accommodate these activities, Geosafe and its sub-contractor, AGECE, installed four boreholes to a depth of 50-ft. The boreholes were located radially out 25-ft to the north, east, south, and west of the simulated absorption bed center point.

Each borehole was 4-in in diameter and was installed to a depth of 50-ft below ground surface (bgs) using the pneumatic rotary drilling method. The equipment used to perform the boring activities can be seen in Figure 3-13. Cuttings were brought to the ground surface during the drilling operation via a vacuum extraction and HEPA filtration system. All cuttings were contained in HDPE bags and later transferred into lined 55-gal drums. Inside of each borehole, an inner flush threaded 2-in ID PVC well casing sealed at the bottom with a threaded plug and at the top



Figure 3-13. Pneumatic rotary drill rig used to install the melt shape monitoring boreholes

with a plug type cap, was placed. The casing extended from the bottom of the borehole to $\frac{1}{2}$ -ft below grade surface (bgs) and was grouted into the borehole using a bentonite grout. Surface completion consisted of a flush mount monitoring well cover set into a cement apron (see Figure 3-14). The cement apron was installed once the boreholes were checked to be of adequate plumbness.

The plumbness of each borehole was checked to ensure that the borehole probes could be lowered to the bottom of the casing without binding. A tolerance of $\pm 1/4$ in over a distance of 4-ft was provided as the specification. Figure 3-15 shows the testing of borehole plumbness.



Figure 3-14. Completed melt monitoring borehole (minus the cement apron)



Figure 3-15. Vertical plumbness verification of the melt shape monitoring boreholes

3.3 Site Pre-Conditioning By Dynamic Disruption

The Bandelier Tuff at MDA-V is a cliff-forming formation, and consequently, had the potential to form vertical walls above the melt as the melt progressed downward. In addition, the potential of the tuff material to form a bridge over the subsidence volume created by the volume reduction was a concern. This bridging could potentially support the absorption bed materials above the melt and prevent their incorporation into melt. The ability of the tuff and the components of the absorption bed to feed downward into the developing melt was a critical need relative to the subsurface melt initiation. The suspected ability of the tuff formation to form near vertical walls was confirmed by an inspection of the Los Alamos Municipal Landfill, where very tall vertical walls were observed. In addition, the ability of the native top soil to hold a near vertical wall was observed during the excavation of the cold demonstration area, specifically on the end where the 11-ft deep TC trench was dug.

The Bandelier Tuff was preconditioned around the edges, within, and below the simulated absorption bed by the dynamic disruption method. The disruption was performed during the site preparation activities to promote subsidence of the simulated absorption bed and adjacent soils during the melting process. The preconditioning is designed to prevent from having portions of the simulated absorption bed left untreated because of either a bridging potential or from inadequate incorporation of surrounding material.

The equipment used to perform the dynamic disruption preconditioning consisted of 35-ton crane supporting a hydraulic vibrator head. The hydraulic head was connected to a 16-ft long piece of steel rail that was driven into the soil column. Conditioning around the simulated absorption bed was performed on three sides and down the middle of the bed (see Figure 3-16).

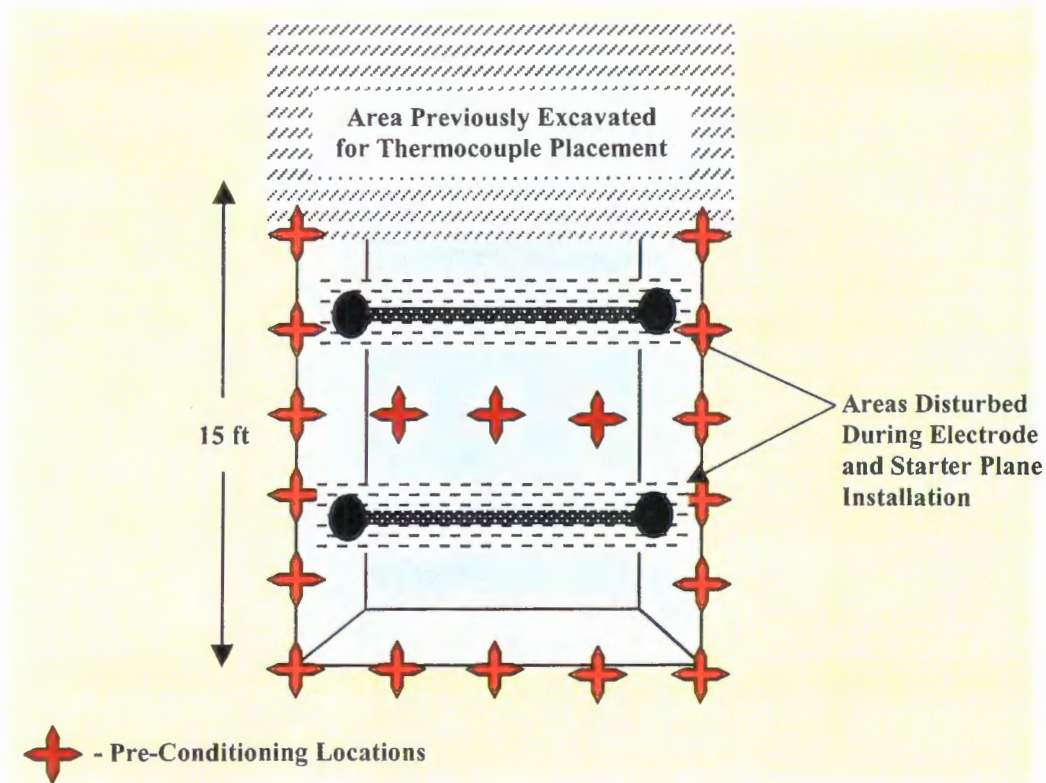


Figure 3-16. Location of preconditioning performed in and around the cold demonstration area

To perform the disruption, the steel rail connected to the vibratory head was moved into position and then the steel was driven in using vibration and the 5-ton weight of the head. Each disruption was performed to a minimum depth of 10-ft below grade. The other side of the absorption bed was already disturbed as a result of the excavation performed for the lateral TC placement. In addition, it was determined that the vibratory placement of the electrode casings and installation of the starter plane would condition the remainder of the inner portion both internal to and below the simulated absorption bed. Penetrations were performed every 3-ft in the area around the simulated bed. Figure 3-17 shows a penetration being conducted. The affected area of soil around each penetration can be seen in Figure 3-18.

Three preconditioning points were also performed down the center of the absorption bed as shown in Figures 3-16 and 3-19. After each preconditioning penetration was performed, a resulting hole was formed, which would stay open until the adjacent area was preconditioned. The adjacent pre-conditioning would then cause the hole to cave in and fill. This enabled the placement of one TC bundle consisting of 7 TCs each, down each of the three center holes. The bundles were positioned such that the TCs were positioned every foot from the 4-ft depth to 10-ft below grade. Figure 3-20 shows a schematic of the vertical TC layout.



Figure 3-17. Dynamic disruption pre-conditioning of the simulated absorption bed area



Figure 3-18. Photograph showing the area influenced around each preconditioning point



Figure 3-19. Pre-conditioning and installation of vertical TCs in the simulated absorption bed

3.4 Electrode Installation

Four graphite electrodes were placed within and below the simulated absorption bed to initiate the NTISV process in the subsurface. To facilitate insertion of the electrodes, four large carbon steel pipes measuring 16-in O.D. by ½-in wall thickness were inserted into the ground to provide a passageway for subsequent insertion of the graphite electrodes. In effect, these pipes served as electrode guide tubes. They were inserted to a depth of 11-ft bgs using a vibratory hammer. AGECE provided the vibratory hammer and drilling equipment used for this process. A 5-ton hammer manufactured by MKT Geotechnical Systems was employed in this application. This hammer provides a vibratory load of 160-tons at a frequency of 1600-cpm. Figure 3-21 shows the third of four casings being installed.

Each electrode guide tube was 16-ft in overall length. Therefore, when the pipe had been fully inserted, a 5-ft section remained above grade. This extra length afforded measurement of the pipe's vertical alignment during and after insertion. The lateral positioning of these guide tubes during the insertion process was also tightly controlled to insure that sufficient tolerances on the 7-ft by 7-ft electrode separation pattern were maintained. As-built measurements indicated that this separation was maintained to within 1½-in between the diagonal casings. Periodically during the insertion process, the pipe was withdrawn and a soil plug removed at grade. This provided the necessary clearance within the I.D. of the pipe for its continued insertion into the ground. This approach was adopted after the original plan of using conical caps on the casings to displace the soil as they were driven in was determined to be ineffective for the soils at the site.

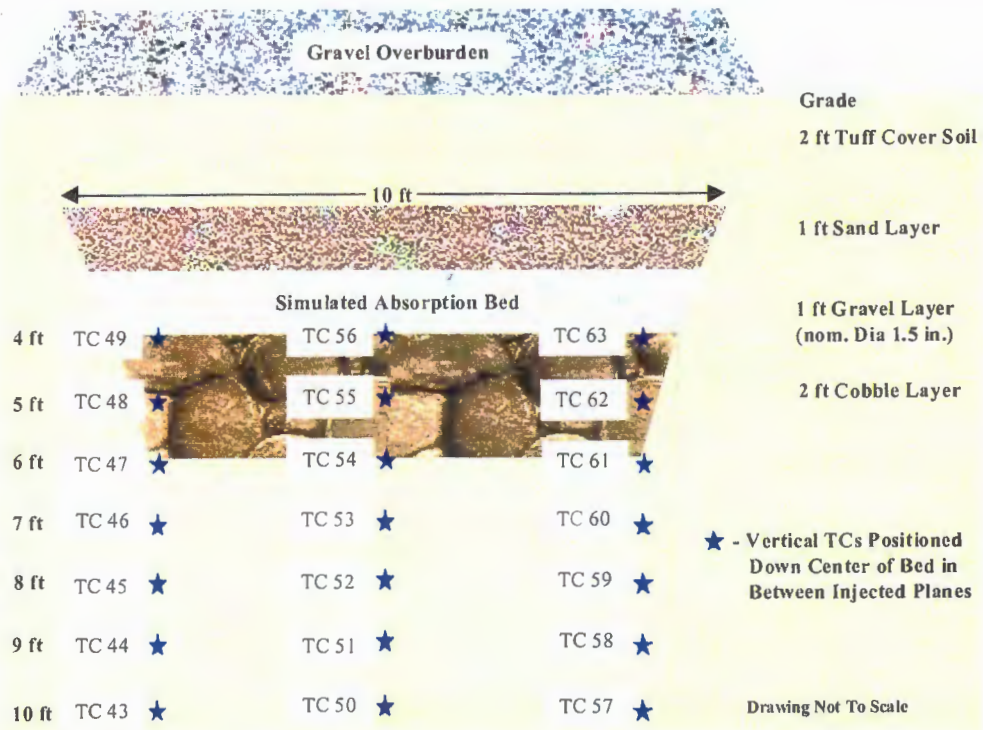


Figure 3-20. Location of vertical thermocouples



Figure 3-21. Installation of the electrode casings

Once the pipes had been properly staged, the clamp used to affix the rim of the pipe to the vibratory hammer was released. Following detachment, a 3-ft segment was cut off each pipe, leaving a 2-ft segment exposed above grade. Two 6-ft electrode segments were then joined to form each of the four electrodes emplaced in the pipes. The electrodes have a 12-in outside diameter. Therefore, once inserted concentrically into the pipe, there remained a 1½-in. cylindrical annulus separating the electrode O.D. and the pipe I.D. This annulus was filled with graphite flake from a depth of 11-ft bgs to approximately 4½-ft bgs. The annular gap was packed during filling using 1 by 2 wooden furring strips to insure that any voids that may have formed during loading of the flake material were collapsed. Once the annular region had been loaded with graphite flake, the vibratory hammer was again attached to the lip of the pipe for the withdrawal process. The pipe was then vibrated and carefully withdrawn from the zone, leaving the electrode and graphite filler material in place (see Figure 3-22). The top surface of the graphite filler material subsided downward during withdrawal of the pipe to fill the volume occupied by the ½-in wall thickness of the pipe. Following complete removal of the pipe, the remaining annular gap between the cavity created by the pipe and the electrode was filled to grade with soil. The soil was also compacted during this process.



Figure 3-22. Withdrawal of electrode casing over the placed electrode

3.5 Starter Plane Installation

Dry soil has a relatively high electrical resistivity. Consequently, to initiate the ISV melting process, an electrically-conductive path needs to be installed between each of the two pairs of electrodes making-up the two-phase circuit. Since, for this application, the melts were to be initiated in the subsurface, these conductive paths were staged using an injection process to introduce a starter material mix into the soil in a prescribed position and configuration. For the NTISV cold demonstration, this material was staged in two vertically-oriented, 3-ft tall planes spanning a depth of 9½-ft bgs to 6½-ft bgs. One plane was staged between the northeast and southeast electrode pair. The other plane spanned the corresponding 7-ft separation between the Northwest and Southwest electrodes.

Each plane was staged by injecting starter material over this depth range using AGECE's drilling rig. The drilling rig consisted of a 4½-in nominal diameter drill bit, fixed to the end of a series of 4-in diameter drill string sections. The unit was used to drill a series of injection borings to the desired 9½-ft bgs depth. The horizontal spacing between each injection boring was approximately 12-in. Five injection borings were required to span the 7-ft separation between electrodes comprising an electrode pair. The three interior borings were spaced 12-in apart. The two end borings adjacent to the electrodes were spaced 11-in off the O.D. of the electrode.

The starter material used to form the starter planes consisted of a mix of water glass (a colloidal suspension of sodium silicate in water), calcium chloride (as a fixative agent) and graphite flake. This material was mixed in the mixer section of AGECE's high-pressure injection system. The mixture was then pumped at high pressure through the stem of the drilling rig and out a pair of nozzles located diametrically opposite one another in the bottom portion of the drill string. To produce a plane of starter material, the drill string was pulled up the injection boring at a prescribed rate. The starter material exiting each nozzle cuts a plane in the soil substrate, filling it and the cylindrical shaft created by the drill string with starter material. The result is a short plane of starter material that has a horizontal cross-section similar to a bowtie. This plane mates-up with the planes injected into adjacent ports to form a continuous plane of starter material between the electrodes.

The appropriate injection pressure, port spacing, nozzle diameter, and withdrawal rate are dependent upon the stratigraphy of the soil into which the planes will be staged. Consequently, a series of test injections were performed in soil adjacent to the NTISV cold demonstration site to determine these parameters for this specific application. For this site, an injection pressure of 5800 psi, boring spacing of 12-in., nozzle diameter of 2.5-mm, and withdrawal rate of 0.17-ft/sec were determined to produce an acceptable path. A single injection using the system with these settings produced a bowtie pattern approximately ¾-in wide at the ends of the bowtie, with an overall span of approximately 14-in. Thus, at a 12-in separation, there was approximately a 1-in. overlap between successive injections. Figure 3-23 shows the result of a test injection performed within the tuff.

The two starter planes were installed using these settings. As indicated above, the planes spanned a vertical depth from 9½-ft to 6½-ft bgs. Each injection port was first drilled down to



Figure 3-23. Starter path injection segment created during field testing within the tuff

depth. The starter material was then injected as the string was withdrawn up the injection port. The five injection ports for the first starter plane staged (the one connecting the northwest and southwest electrodes) were processed in succession, starting at the port adjacent to the Northwest electrode and ending at the port next to the southwest electrode. Figure 3-24 shows the injection of the starter plane between the NW and SW electrodes. There was an approximate 1/4-in annular gap between the O.D. of the drill string and the O.D. of the drill bit. Consequently, some starter material could pass up this annulus to grade during the injection process. During the injection of this plane, approximately 20-gal of starter material was extruded up this annular gap to grade. This material was easily and cleanly collected and deposited in a barrel for subsequent disposal.

It was recognized as desirable to reduce the quantity of spoils to a minimum, however. Therefore, some modifications to the procedure were invoked for the installation of the second starter plane. First, all five injection borings were drilled to depth prior to injecting any starter material. Four of the borings were then plugged with a capped casing while material was injected into the "active" plug. The sequence in which the borings were loaded was also modified. The outboard borings were loaded initially and then the inner borings were installed. The boring adjacent to the NE electrode was loaded first. The corresponding boring adjacent to the SE electrode was loaded next. The three interior borings were loaded in succession, working from south to north. Each port was plugged before and after it was loaded. This procedure dramatically reduced the volume of spoils at grade. Again however, this material was easily collected for subsequent processing. Moreover, as it turned-out, the soil at grade was vitrified during the melting operation, as it was processed concurrently with the target treatment zone.

After completion of the starter plane injection process, resistance measurements were taken between electrodes to confirm that an electrically conductive path had been established. These measurements were repeated for several days following completion of the staging process to

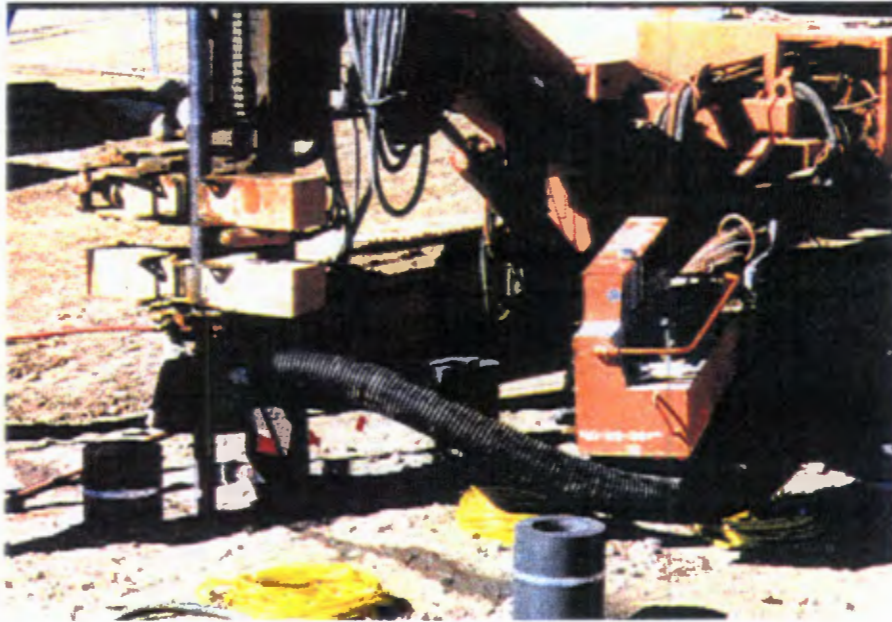


Figure 3-24. Injection of the west starter plane

insure that continuity was being maintained throughout the path's curing process. These measurements were taken by using a Variac to apply a specified AC voltage across a pair of electrodes, and measuring the AC current that passed through the circuit. The path resistance was then determined as the ratio of voltage to current. Table 3-1 presents the results of these measurements (the electrode combinations corresponding to an electrode pair are indicated in bold type).

The final measurements were taken just prior to start-up of the cold demo. These results indicate that, while there was good communication through the east and west starter planes, there was also a completed circuit between diagonally-opposed electrode pairs (i.e.: NW-SE and NE-SW). The simulated adsorption bed was staged for this test, and although attempts were made to "silt-in" the interstitial spaces between the cobbles placed in this simulated bed, the soil was not well packed in these spaces. Therefore, it seems plausible that at the injection pressures employed in staging these starter planes, some portion of the starter material would spread laterally to load the gaps between the cobble. This had the effect of producing a horizontal starter plane that linked all four electrodes. The data clearly indicates, however, that the preferred path was along the planes joining the east and west electrode pairs. It was noted also that the resistance dropped with time. This was likely the result of settling and/or swelling during curing of the starter material. Either of these processes would serve to enhance the connection between electrodes, thereby increasing the conductivity of the path. In any event, it is clear that a good path had been established and that these starter planes could be used to successfully initiate the melting process. The completed cold demonstration area with the electrodes and starter planes installed can be seen in Figure 3-25.

Table 3-1. Resistance of starter planes

Time After Injection (days)	Resistance between the NW-SW Electrodes (ohms)	Resistance between the NW-SE Electrodes (ohms)	Resistance between the NE-SE Electrodes (ohms)	Resistance between the NE-SW Electrodes (ohms)
0	7.6	—	5.7	—
1	6.8	18.9	5.4	18.0
4	3.2	5.6	3.5	7.4
7	2.5	6.3	2.8	4.8
10	2.4	6.5	2.8	4.9
23	2.4	4.9	2.4	5.5

3.6 Installation of the Overburden Layer

The use of engineered overburden has been shown to decrease heat losses and to minimize particulate generation when melting soils in applications similar to the NTISV cold demonstration. To evaluate the effectiveness of overburden for this application, a 2.5-ft layer of washed gravel (with a nominal diameter of 1 to 2-in) was placed over the simulated absorption bed. The boundary of the gravel layer was 20-ft in the north/south direction and 25-ft in the east/west direction. This boundary is represented by the orange outline in Figure 3-25.

3.7 Sampling and Analysis of the Simulated Absorption Bed Materials and Surrounding Soils

Sampling activities during the cold demonstration preparation stage focused on determining the bulk chemistry of the materials to be vitrified and the background levels of the selected surrogates added to the simulated absorption bed. These analyses are discussed below.

3.7.1 Whole Rock Analyses

The goal of analyzing for bulk chemistry is to determine what major components make up the soils and materials used in and around the simulated absorption bed. These components are typically present at percent levels. The chemical composition of the materials to be vitrified affects melt temperature, melt viscosity, mass of off-gas generated from fusion, characteristics of the off-gas (e.g., pH) and electrical conductivity of the melt. These characteristics are all important to establishing proper operational parameters.

Samples were collected of the various layers of material used to build the simulated absorption bed, as well as of the soils surrounding and beneath the simulated absorption bed to properly characterize the area to be treated during the cold demonstration. The procedures used for



Figure 3-25. Simulated absorption bed after the electrode and starter plane installation

collecting these samples are presented in Appendix A. Because the planned melt had a target depth well below the simulated absorption bed area, it was expected that the melt would be composed predominantly of tuff and of the top soil. Therefore, five samples each of these soils were collected and submitted for analysis. Similarly, three samples of the cobble within the absorption bed were collected and submitted. Due to their relatively small volumes, only one sample each of the gravel and sand used in the absorption bed were taken and submitted.

These samples were analyzed using a whole rock method to quantify the bulk composition of the soil and other materials to be treated. This method allows the determination of the quantity of glass forming ions (e.g., Si and Al), as well as the monovalent alkali cations (Na^+ , Li^+ , K^+), which provide electrical conductivity in a silicate melt. The conductivity of the melt is generally proportional to the concentration of these ions, but variations occur because of the complexity of multi-component systems encountered in soil. A review of the pre-demonstration analytical data was performed to determine whether additives may be required to adjust the melt chemistry for any reason. No additives were required prior to treatment of the soils and materials used to configure the simulated absorption bed.

In order to analyze the samples they first must be prepared using a lithium metaborate digestion. A lithium metaborate fusion is the preferred fusion for whole rock analysis in which rock characterization can be made through an analysis of major and minor elements. At Chemex Labs, Inc. the lithium metaborate fusions are carried out in an automated fashion using a Claisse fluxer. The fusion melts can be poured into disks in preparation for X-ray fluorescence analysis or they can be dissolved in acid for subsequent inductively-coupled plasma analysis. Following digestion, the prepared samples are analyzed via inductively-coupled plasma (ICP)-atomic emission spectroscopy (AES). In plasma emission spectroscopy, a sample solution is introduced into the core of an inductively-coupled argon plasma (ICP) at a temperature of approximately 8000 °C. At this temperature all elements become thermally excited and emit light at their characteristic wavelengths. This light is collected by the spectrometer and passes through a diffraction grating which serves to resolve the light into a spectrum of its constituent wavelengths. Within the

spectrometer, this diffracted light is then collected by wavelength and amplified to yield an intensity measurement which can be converted to an elemental concentration by comparison with calibration standards.

The normalized results of the whole rock analyses are provided in Table 3-2. The results of the analyses were also used in a geochemical model that numerically mixes the components (cobble, gravel, soil) in the proportions expected in the field and predicts the resultant product composition. This resultant composition was used to predict melt temperature, viscosity and approximate electrical conductivity. The temperature/viscosity prediction is made using the method developed by Shaw (Viscosities of Magmatic Silicate Liquids: An Empirical Method of Prediction, H.R. Shaw, Amer. J. Sci.272:870-893). This method has been found to be accurate within $\pm 50^{\circ}\text{C}$ for ISV applications provided the soil/rock composition being evaluated is similar to natural magmatic soil/rock compositions. The model predicted that the nominal melt temperature achieved would be in the range of 1900 to 2100 $^{\circ}\text{C}$ depending upon the fraction of each layer that was incorporated to make up the overall melt volume.

Generally, soils with higher concentrations of glass formers (>70%) and lower concentrations of alkali tend to possess a higher melt temperature and also produce a more durable glass due to having a stronger matrix. By totaling the Al_2O_3 and SiO_2 columns for each sample in the Table 3-2, it can be seen that the average level of glass formers for all of the soil types incorporated

Table 3-2. Whole Rock Results of Soils and Materials In and Around the Simulated Absorption Bed

Compound	Tuff (wt %)	Top Soil (wt %)	Cobble (wt %)	Gravel (wt %)	Sand (wt %)
Na ₂ O	4.06	2.85	4.28	2.03	3.23
K ₂ O	4.22	3.60	2.96	1.73	2.87
MgO	0.13	0.71	1.62	1.13	1.44
MnO	0.06	0.06	0.07	0.06	0.05
CaO	0.27	1.02	3.88	2.04	2.84
P ₂ O ₅	0.01	0.01	0.23	0.06	0.12
Cr ₂ O ₃	0.01	0.01	0.01	0.01	0.01
TiO ₂	0.12	0.37	0.55	0.39	0.46
Fe ₂ O ₃	1.67	2.92	3.95	3.48	3.26
Al ₂ O ₃	12.16	13.77	15.71	9.19	13.09
SiO ₂	77.29	74.67	66.75	79.88	72.63
Loss on Ignition	0.50	4.95	1.24	1.16	1.74
Total (excluding LOI)	100	100	100	100	100

into the melt range from approximately 86 to 92 wt %. This level of glass formers indicates that the resulting mixture when melted and allowed to cool will form a very durable leach resistant product.

The loss on ignition (LOI) values in Table 3-2 refers to the weight loss experienced by a sample when it is placed in a furnace at 1010 °C for 1-hr. It is used to give a general indication of the amount of "volatile" species in a sample. The compounds that are removed during this determination include water (both surficial moisture as well as water of crystallization) and organic carbon species. In addition, carbonates decompose to oxides with the loss of carbon dioxide, and sulfates decompose (but usually only partially) to oxides with the loss of sulfur trioxide. Fluorides may also be partially lost. Due to the complex nature of these reactions, the LOI value is best used as a general indicator of the amount of volatile species present. The tuff soils were generally very low in LOI, which would be expected for soils of volcanic origin. The other soils and materials used in simulating the absorption bed are within a range considered to be normal.

3.7.2 Presence of Surrogates in the Simulated Absorption Bed Materials and Surrounding Soils

In order to determine the quantity of surrogates to be added to the simulated absorption bed (see Section 3.1.2), the background concentrations of the surrogates had to be determined in the soils adjacent to and below the simulated absorption bed, as well as within the materials used to construct the bed itself. The results of the baseline analyses would be used to determine the degree of intermixing of the surrogate chemicals within the molten glass and resulting homogeneity in the cooled vitrified product.

The same samples used to determine the bulk chemistry described above were digested via the lithium metaborate fusion method and analyzed via ICP-mass spectrometry (MS). In the ICP-MS method, the plasma is used to generate ions, which are then introduced to the mass spectrometer. These ions are then separated and collected according to their mass to charge ratios. The constituents of an unknown sample can then be identified and measured. ICP-MS offers extremely high sensitivity for many elements and can be successfully applied to a wide range of elements. The ICP-MS procedure provides a detection level of 0.1 ppm for cesium and 0.5 ppm for cerium. As in the bulk chemistry samples, five samples were submitted of the tuff and top soil, three samples of the cobble, and one each of the gravel and sand. Table 3-3 presents the results of this baseline sampling.

Sample	Surrogate 1	Surrogate 2	Surrogate 3	Surrogate 4	Surrogate 5
Tuff 1	0.1	0.2	0.3	0.4	0.5
Tuff 2	0.1	0.2	0.3	0.4	0.5
Tuff 3	0.1	0.2	0.3	0.4	0.5
Top Soil 1	0.1	0.2	0.3	0.4	0.5
Top Soil 2	0.1	0.2	0.3	0.4	0.5
Top Soil 3	0.1	0.2	0.3	0.4	0.5
Cobble 1	0.1	0.2	0.3	0.4	0.5
Cobble 2	0.1	0.2	0.3	0.4	0.5
Cobble 3	0.1	0.2	0.3	0.4	0.5
Gravel	0.1	0.2	0.3	0.4	0.5
Sand	0.1	0.2	0.3	0.4	0.5

Table 3-3. Background Levels of Surrogates in the Simulated Absorption Bed Soils and Materials

Soil Type	Cerium (ppm)	Cesium (ppm)
Tuff	111 ± 3	2.3 ± 0.2
Top Soil	109 ± 5	5 ± 0.3
Cobble	65 ± 8	1.1 ± 0.2
Gravel	40	1.6
Sand	55.5	1.7

4. NTISV COLD DEMONSTRATION TEST OPERATIONS

4.1 Cold Demonstration Operations Overview

Once the GeoMelt-ISV system was interconnected and all of the components individually checked for operability, a readiness checklist was completed to ensure that all steps necessary to initiate the testing were completed. This involved not only verifying that all of the equipment was assembled and operating correctly, but also ensuring that all health and safety and administrative procedures and requirements were met. After approval from all entities involved in the demonstration program, the cold demonstration was initiated.

The off-gas treatment system was started at 1322 hrs on 4/16/99 and allowed to stabilize prior to applying power to the treatment zone. The power supply system was brought on-line at 1407 hrs and the melting process was started. A chronology of the cold demonstration is included in Appendix B, which covers all significant activities during the melt. The melting process continued for 185.7-hrs at which time all of the melting objectives had been met. Power to the melt was terminated at 0735 hrs on 4/24/99. The average power level input to the melt during processing was 971 kW including the graduated start-up. Excluding this graduated start-up period, wherein the power level was slowly increased up to the desired level, the average power input was 1033 kW. The total energy consumed to produce the melt was 165,600 kwh.

4.2 Electrical Performance

Figures 4-1, 4-2 and 4-3 present the voltage, amperage and the power input levels, and the average resistance within the melt. Melting throughout the entire run was well within the typical operating range of the GeoMelt system. Initial heat up of the two starter planes during the start-up process occurred without any difficulties. Both phases were in balance throughout most of the demonstration which can be seen in Figure 4-1. There were some periods where the voltages and amperages for each phase were different such as can be seen during the 20 to 40 hr runtime period. The demand for different voltages is caused by differences in the resistance of one phase as compared to the other (see Figures 4-1 and 4-3). These relatively small differences are typical especially early in the melting process. The resistance of an individual phase is dependent upon several parameters such as:

- the bulk chemistry of the soil near that phase
- the distance between the electrodes
- the quantity of starter path material injected
- the size of melt that develops around each pair of electrodes

As all of these can vary during different stages of the melt, the GeoMelt ISV system is designed to be able to handle both differing and varying loads on each phase. In comparison to other melts performed previously, these results are typical and quite consistent with expectations.

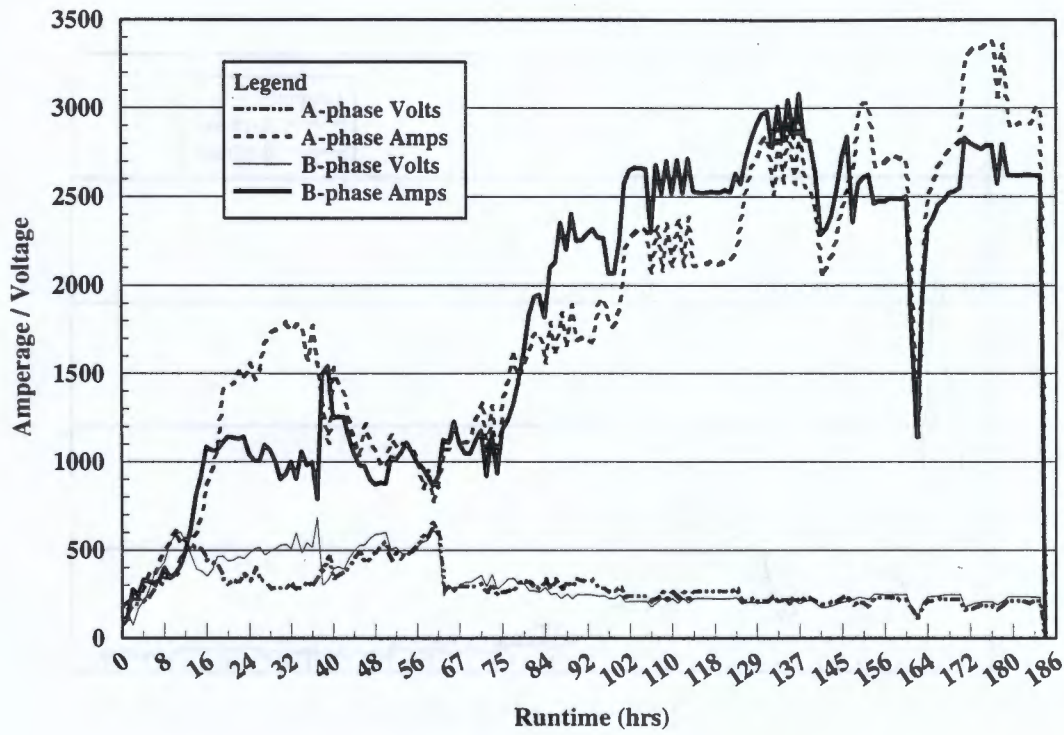


Figure 4-1. Cold demonstration voltage and amperage

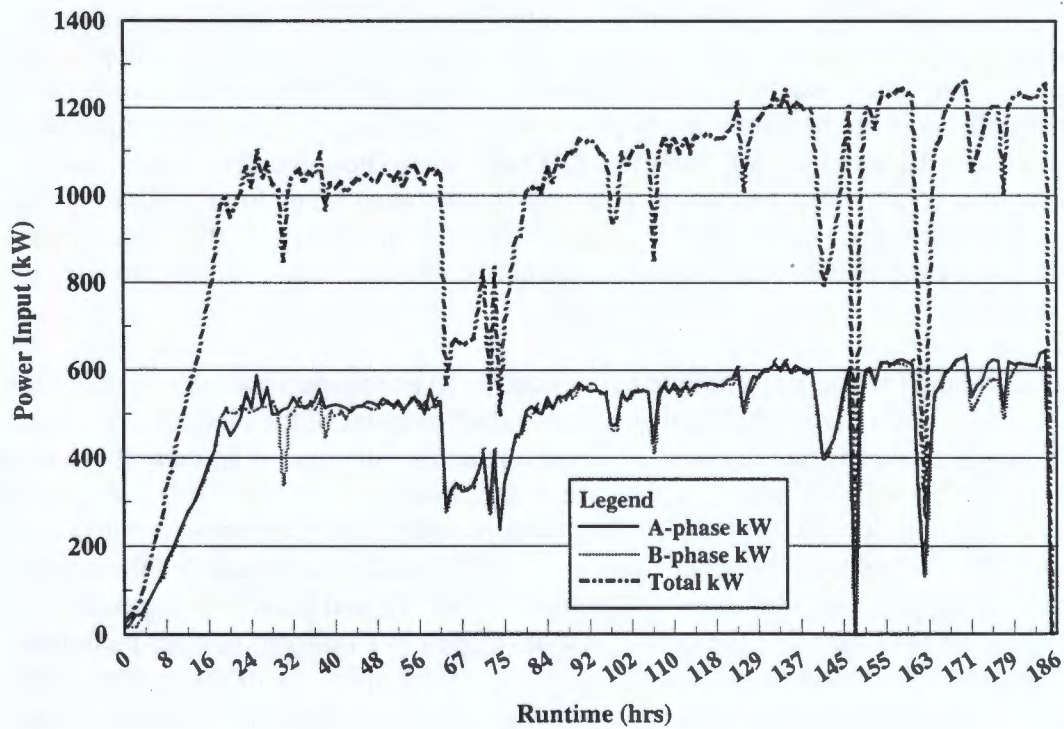


Figure 4-2. Power level input during the cold demonstration

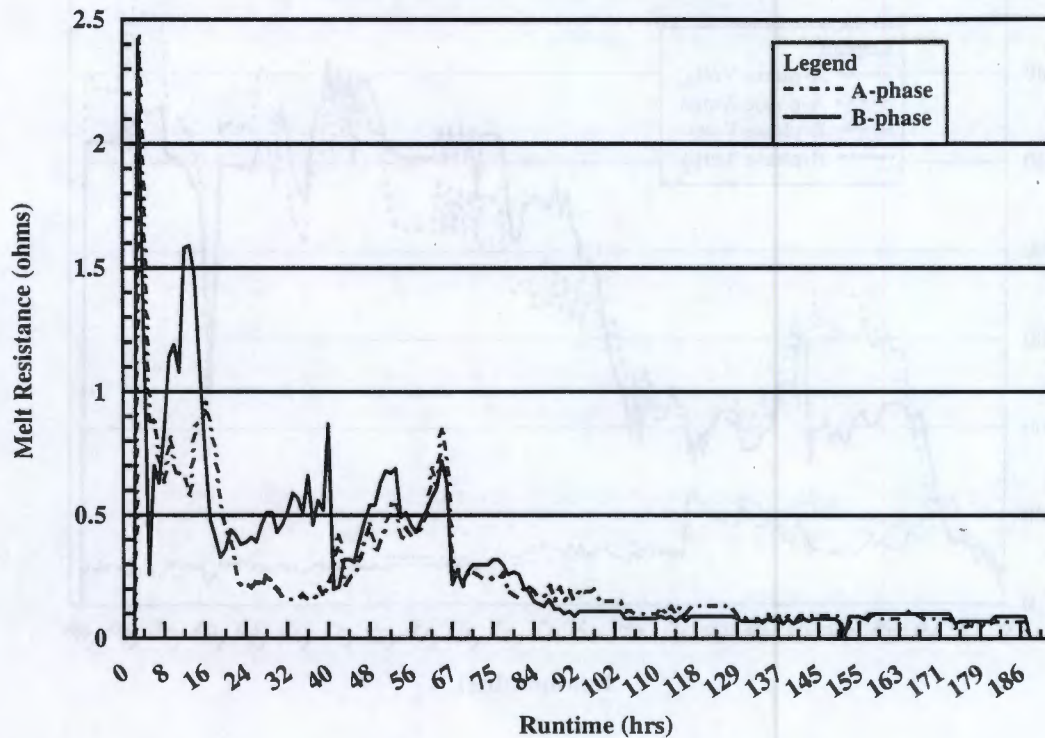


Figure 4-3. Resistances of A and B phases during the cold demonstration

Power input to the melt was maintained at a level below 1250 kW total (see Figure 4-2), which scales up to a power density typical of that applied at larger scales of application. As can be seen, power was initially ramped up to a level of 1000-kW total over a 20-hr period. Following the initial ramp up, power was slowly increased over the duration of the demonstration up to slightly over the 1200-kW level. Periodically power was decreased either to allow the operations personnel to evaluate the melting process or to perform other typical activities such as equipment inspection. Although the voltages and amperages of both phases varied as indicated above, the total power input into each phase was nearly identical during the demonstration.

Power to the melt was also terminated occasionally to enable performance of activities such as the addition of electrodes, inspection and adjustment of the electrode feeders, change of tap positions on the Scott-Tee transformer and the like. Typically these downtimes range from a few minutes, in the case of tap changes, to slightly over 2-hrs for the addition of electrodes. During one of the downtime when the electrodes were lowered, a change in the secondary cable connections was performed which permitted the current to fire across the diagonals of the melt as opposed to the original parallel firing pattern. This was done to ensure that the entire melt developed in a uniform manner including developing a typical slightly rounded bottom. No effect upon any of the electrical parameters could be noticed after the switch to the cross-firing pattern. This switch was easily accomplished by simply switching the secondary cables going to electrodes A2 and B3 at the point where they connect to the bus bar on the transformer. This switch was performed at 148 hrs of runtime.

4.3 Off-Gas Treatment Performance

The off-gas treatment system used during the cold demonstration consisted primarily of the following components:

- off-gas collection hood
- HEPA pre-filter assembly
- cooling chamber
- main HEPA filter unit
- thermal oxidizer

In addition, the GeoMelt ISV system contains the ability to perform wet quenching and scrubbing of the off-gases. However, because of the lack of organics that cause acid gases, these units were only used for a short duration during the cold test to verify their operability and to determine the affect upon the other unit operations. Since this GeoMelt system had never been operated with either the pre-filter in place or with the particular thermal oxidizer procured for use during the cold demonstration, operation of the complete system was performed in order to confirm the design and to gain operating experience.

4.3.1 Particulate Generation and Removal

Particulate generation during the demonstration was greatly reduced as compared to past top-down melts due to the subsurface start-up and the use of overburden. Figure 4-4 shows the particulate loading on the pre-filter and the main HEPA filter throughout the demonstration run. Once particulate accumulation on the main HEPA filter began to occur the pre-filter was valved into service. The pre-filter HEPA was not put into service until 92 hrs into the demonstration. A HEPA filter will usually operate for long periods with little increase in the differential pressure (ΔP) until such time that the entire filter is covered with a fine layer of particulate. Once this occurs, the loading rate typically progresses rapidly up to the maximum ΔP of the filters (typically 8-in H_2O). This affect can be seen in the ΔP rise occurring at 160 hrs and 173 hrs on the plot of the pre-filter ΔP (see Figure 4-4). Alternatively, very rapid increases in the ΔP of the filters can result from dusting events within the hood or from the release of large amounts of water vapor from the melt region.

At a runtime of 122-hrs the ΔP across the pre-filter assembly increased quickly to 8-in H_2O . Such a quick pressure increase is typically due to the filters becoming wet due to condensation forming upon them. However, the operations crew was also in the process of lowering the electrodes at this time, which may have caused dusting within the hood caused by sloughing of surface soils and over burden material into the subsidence hole. As a result of the filter loading, the pre-filter assembly by-pass line was opened which allowed the majority of the off-gas stream to by-pass the filter. The valving to the plugged HEPA bank was also left open such that if condensate was plugging the filter that it would eventually dry out and the ΔP would decrease. At a runtime of 142-hrs, the pre-filter HEPA bank was put back into service. The ΔP of the bank went from a reading

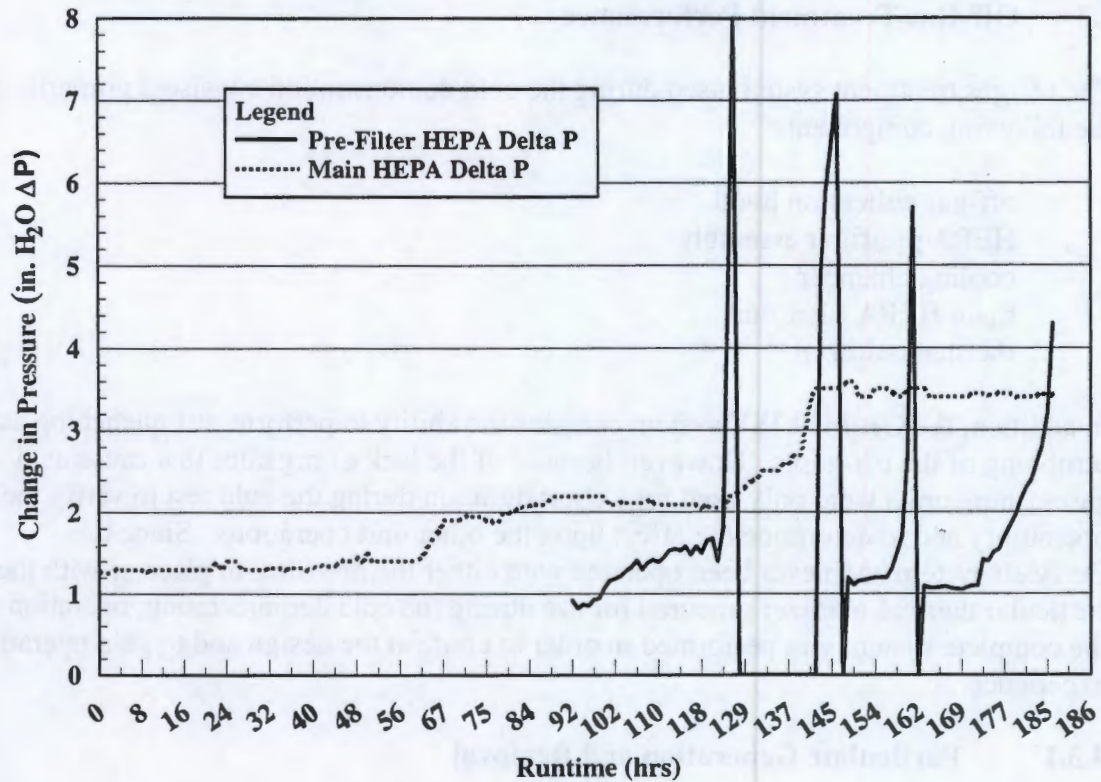


Figure 4-4. HEPA filter loading rate

of 4.9 to 7.1 in 3 hours. Based upon this data, it is believed that the majority of the plugging was not due to moisture, but was most likely due to the dust that was generated as the electrodes were lowered.

The off-gas system is designed with redundancy including a prefilter that has two independent banks of HEPA filters, a wet scrub system, and a final HEPA filter, all of which perform the task of effectively removing particulate from the off-gas stream. Occasionally, as the surface soils feed downward due to subsidence and sloughing, small amounts of dust will be generated and removed to the off-gas system and over time will cause filters to load up. As the prefilter is the initial particulate removal unit in the system, it will load up first. Since it has parallel banks of filters, a filter change-out is easily performed by valving the flow of the off-gas through the other bank while the plugged filter is changed out. Filter change-outs are a typical and routine activity during a melting operation. The installation of new pre-filters during the cold demonstration was performed shortly after the peaks seen at 148 hrs and 162 hrs of runtime. These filter changes can be seen in Figure 4-4 as a peak in the ΔP followed by a sudden drop down to a ΔP of near 1-in H₂O.

It should be noted that the loading rate of the pre-filter increased later in the run as the overburden layer was incorporated into melt. Past operating experience with top-down melting is that HEPA filters require change-out as frequently as 4 to 8 hours when the wet scrub system is not in operation. Thus, the subsurface melting and use of overburden

served to greatly prolong the life of the pre-filters. Prior to the hot demonstration, Geosafe will install the ability to add overburden during the melt process to increase the life of the filters later in the run when the overburden begins to get incorporated into the melt. This will allow the reestablishment of the overburden layer midway through each processing run.

The presence of the pre-filters also greatly increased the life of the main HEPA filter bank. The original set of HEPA filters, which were installed in the main filter housing prior to the start of the cold demonstration, lasted the entire demonstration and were only at approximately 40% of their design loading limit at the end of the run. An increased loading rate was experienced on the main HEPAs during the period of 122 to 142-hrs due to bypassing the pre-filter HEPAs. Once the pre-filter was placed back in-line, the particulate accumulation on the main HEPAs leveled off.

4.3.2 Thermal Oxidizer Operation

Due to low levels of organic contamination found in the area where the simulated absorption bed was constructed, a thermal oxidizer was rented from NAO, Inc. of Houston, TX, and used during the cold demonstration. The thermal oxidizer was used as a final polishing step in the treatment of the off gases. The use of a thermal oxidizer provides the following:

- destruction of any residual organic compounds,
- conversion of carbon monoxide to carbon dioxide
- the elimination of any odors that may be present due to the thermal treatment of soils containing compounds such as sulfur

Operation of the thermal oxidizer is fairly basic in that a control loop monitors the temperature in the combustion chamber and either opens or closes a control valve which adjusts the amount of propane going to the burner. The temperature within the combustion chamber is variable and can be set by the operator. The control temperature was set at 1450°F for the purpose of this test. The organic destruction efficiency for this thermal oxidizer is rated at 99% to 99.9% at this temperature. Figure 4-5 shows the operating temperature of the thermal oxidizer during the demonstration run.

During the first 24-hrs of operation, the combustion chamber of the thermal oxidizer was maintained at a higher than required temperature due to the zero setting on the control valve being out of adjustment. Once this was adjusted, the unit operated very smoothly throughout the remainder of the demonstration.

4.3.3 Off-Gas Emission Sampling

Gases exiting the thermal oxidizer were sampled continuously during the cold demonstration for oxygen (O₂), carbon monoxide and dioxide (CO and CO₂), and total

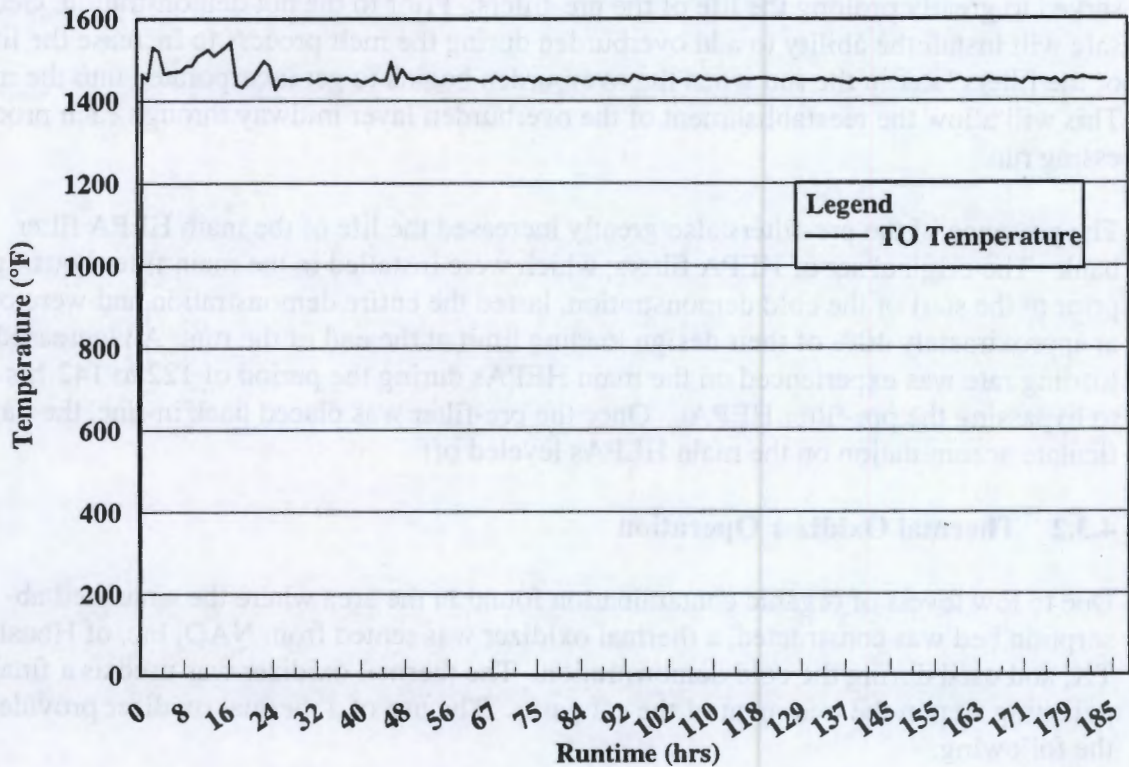


Figure 4-5. Thermal oxidizer operating temperature

hydrocarbons (THC). These compounds are typical when treating hydrocarbons as they either measure:

- a component required for combustion (O_2)
- a combustion product (CO and CO_2), or
- the presence of any unoxidized organics (THC).

The results of the emission monitoring can be seen below in Figure 4-6. It should be noted that the results of the O_2 and the CO_2 are presented in weight percent, whereas, the CO and THC results are in ppm.

The O_2 and CO_2 levels are typical readings when measuring at the discharge of the thermal oxidizer. The propane fuel combustion depletes the O_2 level from 20.9 wt % down to approximately 15 wt %. Likewise, 5 to 8 wt % CO_2 is generated from the combustion of the fuel. The total hydrocarbons measured were between 0 and 1 ppm during the demonstration.

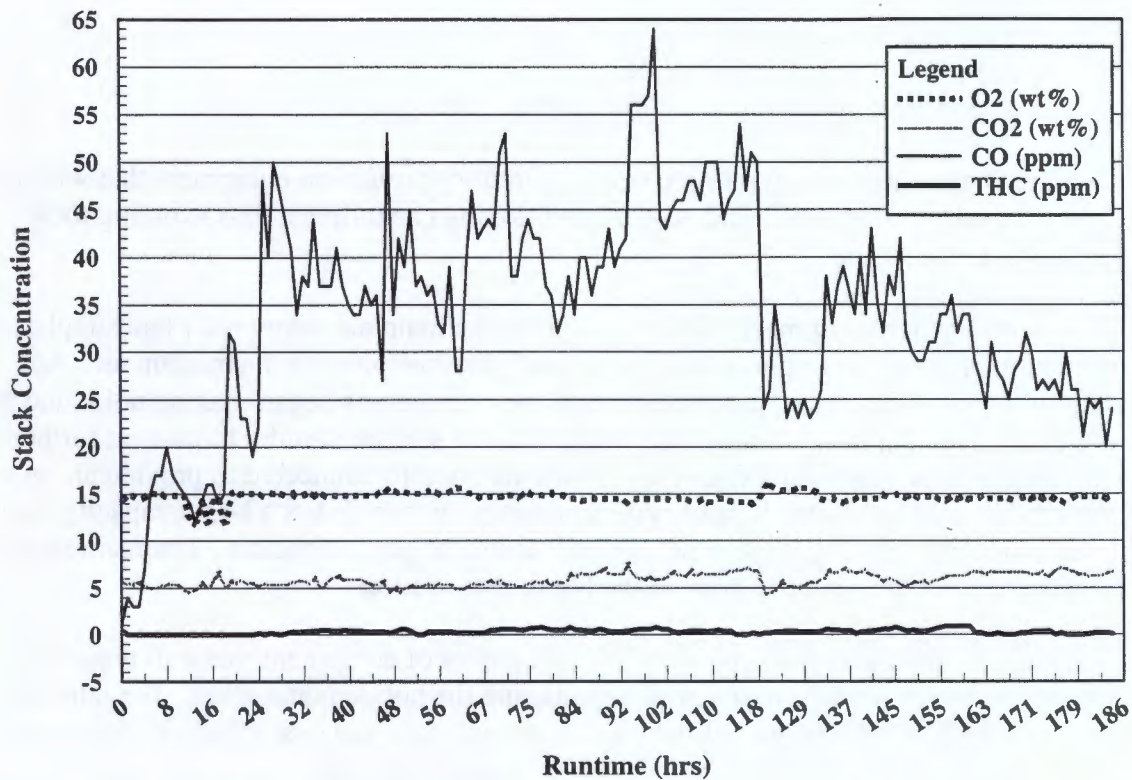


Figure 4-6. Result of off-gas monitoring during the cold demonstration

The level of carbon monoxide, which is generated as a result of partial combustion, was evolved at a level typically between 15 and 65 ppm, which is approximately equivalent to the emission coming from one standard automobile. This level is variable depending upon the temperature setting of the TO. Raising the temperature of the TO will lower the CO level; however, this will dramatically increase the cost of propane consumed.

4.4 System Reliability and Improvements

All major components of the GeoMelt ISV system operated as designed throughout the duration of the demonstration. Only two minor equipment problems were encountered during the cold demonstration. These problems did not cause any difficulties in successfully completing the demonstration as the system is designed to be inherently safe and reliable. However, Geosafe is in the process of resolving the causes prior to the start of the hot demonstration.

The first problem involves an apparent problem with the incoming power. It is suspected that fluctuations in either the voltage or the amperage of the primary power feed caused problems with many of the sensitive equipment such as computer systems and instrumentation. Geosafe personnel discussed the issue with the utility dispatch personnel in hopes of determining a cause. However, in each case the dispatcher reported no problems either with the power being delivered over the grid. Some of the intermittent problems encountered due to the apparent fluctuations include:

- circuit breaker tripping
- computer locking up
- computer circuit boards failing
- erroneous validyne pressure monitoring system data

Geosafe is currently investigating electrical circuitry protection equipment that will provide both surge suppressant and power conditioning capabilities, thus avoiding these problems in the future.

The second minor equipment problem involved the main air compressor that supplies both high pressure air to pneumatic valves and also low pressure instrument air. Approximately 171 hrs into the demonstration, the compressor began making noise and getting hot. The system was immediately taken out of service in order to prevent further damage. An auxiliary compressor was immediately interconnected to provide air on a backup basis. The electrode feed system compressor, which has a larger capacity, was later connected to the system to provide the source of pressurized air. The main system compressor will be repaired prior to the hot demonstration

Performance data was gathered on individual pieces of equipment that will require "fine tuning" or minor modifications prior to initiating the hot demonstration. The adjustments that have been identified will allow for an efficient, safe and cost effective application during the hot demonstration. Some of these changes include:

- Addition of a port which will allow the addition of overburden during processing
- Addition of an in-line heater prior to the pre-filter to prevent condensation
- Installation of a condensate removal pump on both the prefilter housing and the cooling chamber
- Sealing of the auxiliary blower feeding the thermal oxidizer
- Improving the seal between the off-gas hood panels and the electrodes
- Improving the electrical contactor operation on the electrode feeders

4.5 Electrode Performance

The downward movement of the electrodes during the cold demonstration is presented in Figure 4-7. Initially, the electrodes were operated in a gravity feed mode, wherein they were allowed to feed downward as the melts developed beneath them. In this manner, they remain on or near the bottom of the melts. The electrodes begin to move after startup once the melt develops around and beneath them. This typically takes between one to two days depending upon the power level and particular mode of application. During the cold demonstration three of the four electrodes began moving at 60-hrs into the run and the fourth started to move at 80-hrs. The initial downward movement of the electrodes can be significant depending upon factors such as the depth of start-up, the type of soil being melted, and size of electrode. This is predominantly due to the frictional resistance of the soil and overburden above the melt that is surrounding the upper portions of the electrodes. This resistance serves to hold the electrodes in place until such time that enough of the soil subsides. Subsidence of the soil will either lessen the force on the electrodes or cause a vibration from the sloughing which can cause the electrode to shake slightly and "free up". This initial movement was experienced more on the two

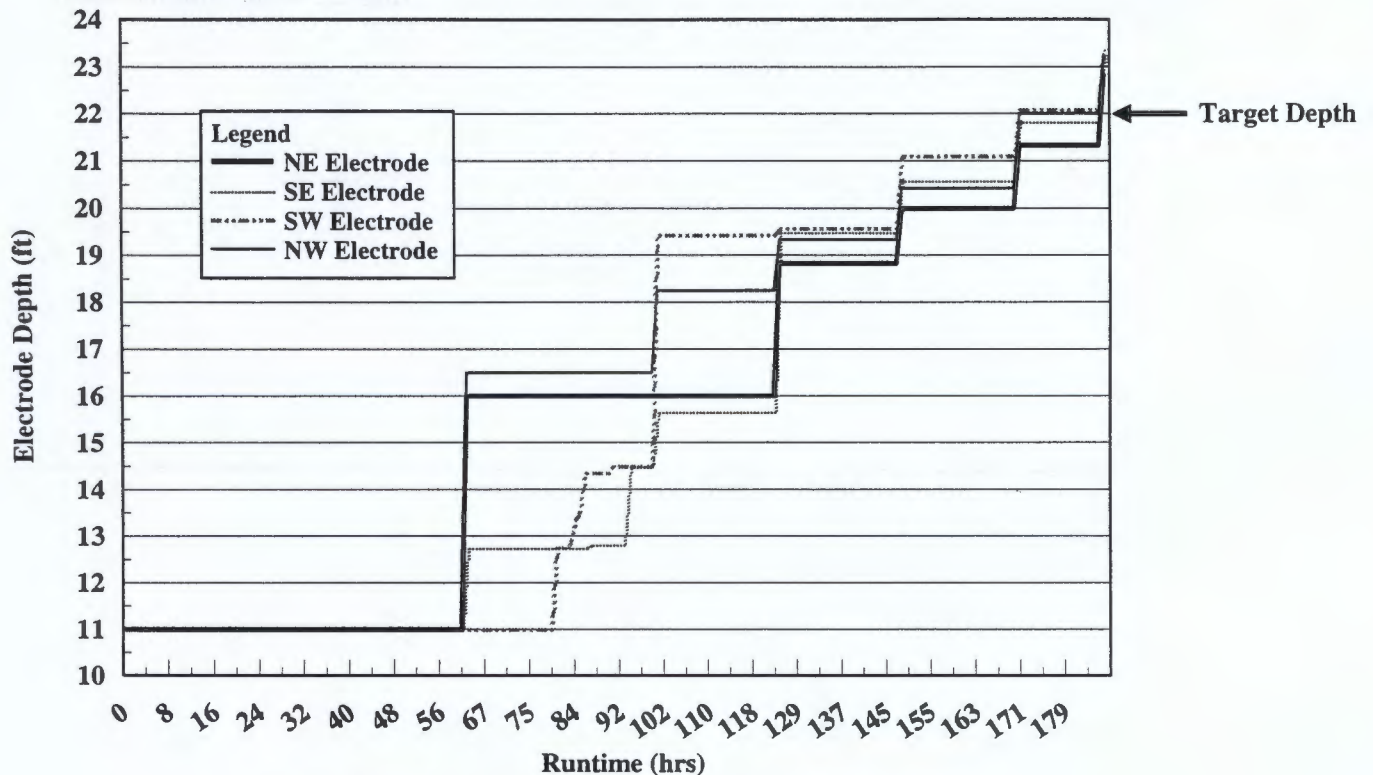


Figure 4-7. Electrode depth during the cold demonstration

north electrodes than on the south. The two north electrodes moved downward from 5 to 5.5-ft initially, whereas the two south electrodes moved down slightly less than 2-ft.

Shortly after the initial movement, the electrodes were gripped using the pneumatic gripping device on the feeders. This was done to ensure that the electrode depths remained relatively close and to ensure that the feeding of the electrodes could be controlled. It is important to ensure that the electrodes are not exposed to excessive force or wear as they are a critical element of the melting process.

To ensure that the electrode feeding could be controlled during the remainder of the run, a crane was used to lower the electrodes typically once per day for the remainder of the demonstration. The final electrode depths all reached or exceeded the target depth of 22 ft. The exact depths were:

- A1 - 22' 10"
- A2 - 23' 2"
- B3 - 23' 4"
- B4 - 23' 3"

The performance of the electrodes and their associated system was considered good throughout the cold demonstration. The amount of oxidation that occurs during the traditional melting process is always a concern and can potentially lead to the breakage of an electrode. During subsurface melting, the overburden and surface soils protect the

electrode from being oxidized and thus, greatly increase their longevity. No observable oxidation was detected on any of the four electrodes used during the cold demonstration.

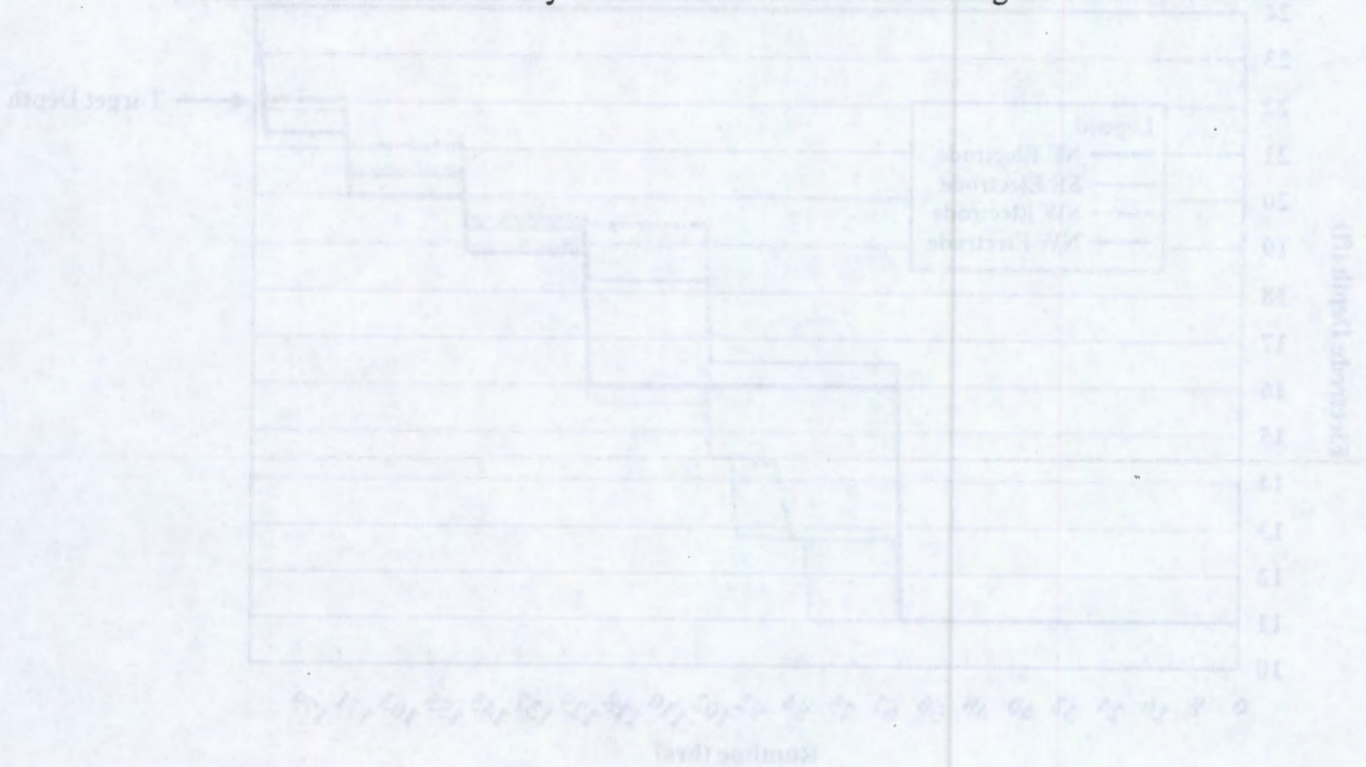


Figure 4-7. Electrode depth during the cold demonstration.

both electrodes than on the south. The two north electrodes moved downward from 2 to 2.5 ft initially, whereas the two south electrodes moved down slightly less than 2 ft.

Shortly after the initial movement, the electrodes were jiggled using the pneumatic tapping device on the leads. This was done to ensure that the electrode leads remained relatively clean and to ensure that the loading of the electrodes could be controlled. It is important to ensure that the electrodes are not exposed to excessive forces or wear as they are a critical element of the machining process.

To ensure that the electrode loading could be controlled during the remainder of the run, a crane was used to lower the electrodes slightly each day for the remainder of the demonstration. The full electrode depth is recorded or estimated the target depth of 22 ft. The crane depth was:

- A1 - 22.10"
- A2 - 22.2"
- A3 - 22.4"
- A4 - 22.3"

The performance of the electrodes and their attached system was considered good throughout the cold demonstration. The amount of oxidation that occurs during the initial machining process is always a concern and can potentially lead to the breakage of an electrode. During subsurface testing, the oxidation and surface soils protect the

5. NTISV COLD DEMONSTRATION PRODUCT EVALUATION

5.1 Post-Test Condition of Treatment Zone and Overburden

This section will describe the appearance, condition and size of the simulated absorption bed area and the vitrified product resulting from the GeoMelt treatment process.

5.1.1 Subsidence Volume

A subsidence volume forms over the treatment zone due to volume reduction when the soils and other materials are melted and incorporated into a melt. The subsidence is primarily due to the elimination of void volume that exists naturally in soil. All voids are eliminated when the soil is converted to a fluid. Any vapor or air that is contained within the soil voids is removed and thermal treated prior to entering the off-gas stream. Another source of volume reduction includes removal of volatile materials during processing (e.g., water, carbonates, organics). The volume reduction of the soil is enhanced during subsurface melting due to the typical downward progression of the melt, as well as from the movement of the soils (and simulated absorption bed contents) downward into the top of the melt.

Typically, the volume reduction resulting from the GeoMelt process is in the range of 20 to 50 percent (e.g., a 15-ft deep melt would develop a vertical depression of 3 to 7.5-ft). The soil bulk density is the primary factor associated with the amount of subsidence created during a melt. The bulk density of the tuff in and around the MDA-V ranges from 0.94 to 1.49-g/cm³. This is a relatively low-density material as compared to most soils, which usually fall in the 1.6 to 2.0-g/cm³ range. However, the preparation of the cold demonstration area also included cobble, gravel, and sand, as well as the surrounding top soil, which are all higher density than the tuff. Considering the wide range of materials included in the area to be treated during the cold demonstration and the fact that the density of the vitrified product is typically 2.5-g/cm³, it was expected that the volume reduction would be in the 30 to 40 percent range.

Figure 5-1 shows the subsidence volume created as a result of processing the simulated absorption bed and the volume of soil beneath it. The depth of the subsidence was approximately 9-ft in the center and averaged 7.5-ft overall. The percent volume reduction is determined by dividing the depth of subsidence by the overall depth of the treatment area, which comes out to be 33 % for the cold demonstration (7.5-ft/23-ft).

The soil's cliff-forming characteristics can be seen in the walls surrounding the subsidence area as they retain a near vertical angle of repose after treatment (see Figure 5-1). The angle of repose will range from 45° for sandy soils to near vertical for soils such as tuff and some high-clay content soils. Soils that have minimal sloughing during treatment can be advantageous in that it allows a smaller diameter hood to be used, which is more cost effective.

One of the electrodes can be seen extending upward out of the subsidence volume in Figure 5-1. This is due to the method in which the electrodes are removed prior to lifting the

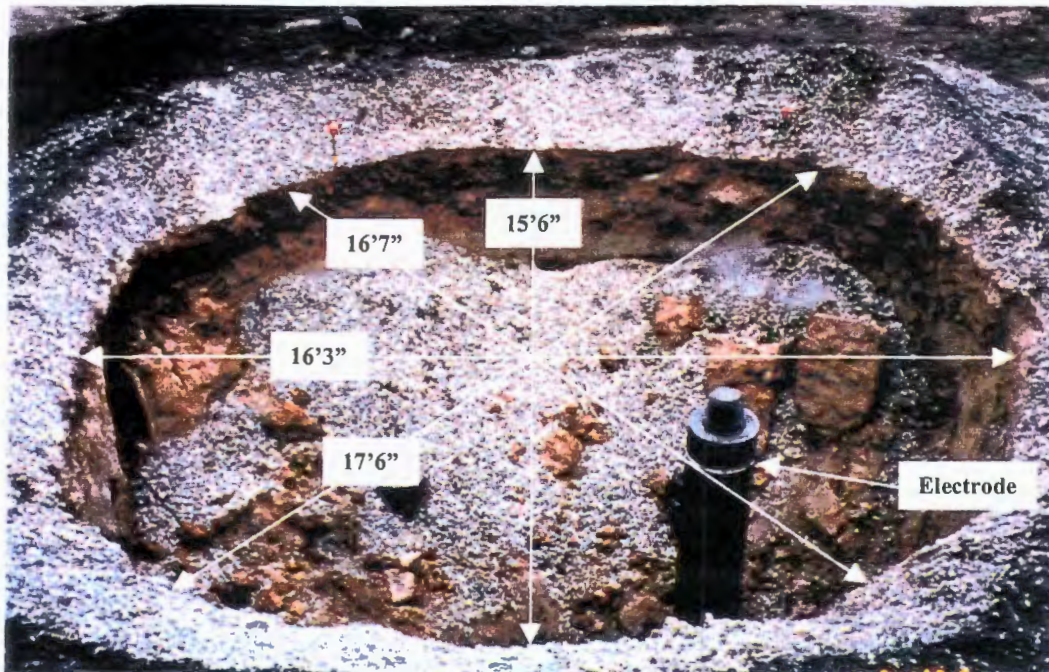


Figure 5-1. Cold demonstration subsidence area

hood off of the demonstration area. The first electrode, which is the one shown in the figure, was unscrewed from on top of the hood. Since the electrodes are connected in 6-ft segments, there is no control at which threaded connection point the electrode will unscrew. Thus, a 6-ft section of electrode was left in the subsidence zone and later removed with heavy equipment. The three other electrodes were removed by breaking the connecting nipple near to the point at which they entered the melt. This allowed removal of all of the electrode sections from the subsidence area.

The dimensions of the subsidence can also be seen in Figure 5-1. The location of the extremities of the subsidence is a good indication that the contents of the bed were completely incorporated into the melt. The dimension of the subsidence completely encompassed the original target treatment volume of 10-ft by 15-ft by 6-ft deep. Additional data, such as the dimension of the melt and presence of any of the simulated absorption bed contents on top of the melt, were gathered during the excavation of the vitrified product. These results are presented in Section 5.1.2.

5.1.2 Vitrified Monolith Size and Shape

Only four weeks were allowed for cooling prior to initiating partial exhuming of the vitrified monolith. The excavation activity was expedited so that samples of the product could be obtained and analyzed as soon as practicable. Typically, it takes approximately 6 to 12 months for a vitrified monolith to cool to near ambient temperature. To allow early exposure and sampling, extra precautions were taken due to the high heat associated with the product and surrounding soil. The excavation of the block, which was performed by LANL-ER and their subcontractor (Morrison-Knudsen), was performed in a step-wise fashion so that dust emissions could be kept under control. Excavating near a

recently completed melt can be very dusty due to the surrounding soil being totally devoid of any soil moisture. A fine water spray was used during the excavation activities to help suppress the dust and to cool the soil and product.

The determination of whether all of the contents of the target treatment volume were incorporated downward into the vitrified product was of primary importance during the excavation to the monolith surface. Visual inspections were made periodically during the excavation both of the monolith surface and of the material being removed. No indication of any of the simulated absorption bed materials (cobbles, gravel, and sand) were found remaining above the vitrified monolith. Only a small amount of surrounding soil and gravel from the 2.5-ft layer of overburden were found immediately on top of the surface of the monolith, and the incorporation of these materials were not targeted.

The surface of the vitrified monolith was surveyed once it was exposed and determined to be 10-ft below grade around the outside edge and approximately 13-ft below grade in the center area. Observations of the surface of the block indicated that it was slightly bowl shaped, which is believed to be due to trapped gases that were slowly released. Gases that enter the melt as vapor from soil moisture or from the decomposition of compounds such as carbonates can potentially be trapped under the surface of the melt. The gases are then forced out by the downward pressure created when the subsidence is backfilled with clean soil. Once the gases escape, the surface of the melt subsides. Figure 5-2 shows the surface of the melt. The melt surface was found to be uniform in depth, width and overall shape.

Trenching was performed along the north and west edges of the vitrified product to determine the side profile of the product. Only two sides were exposed to save costs as the

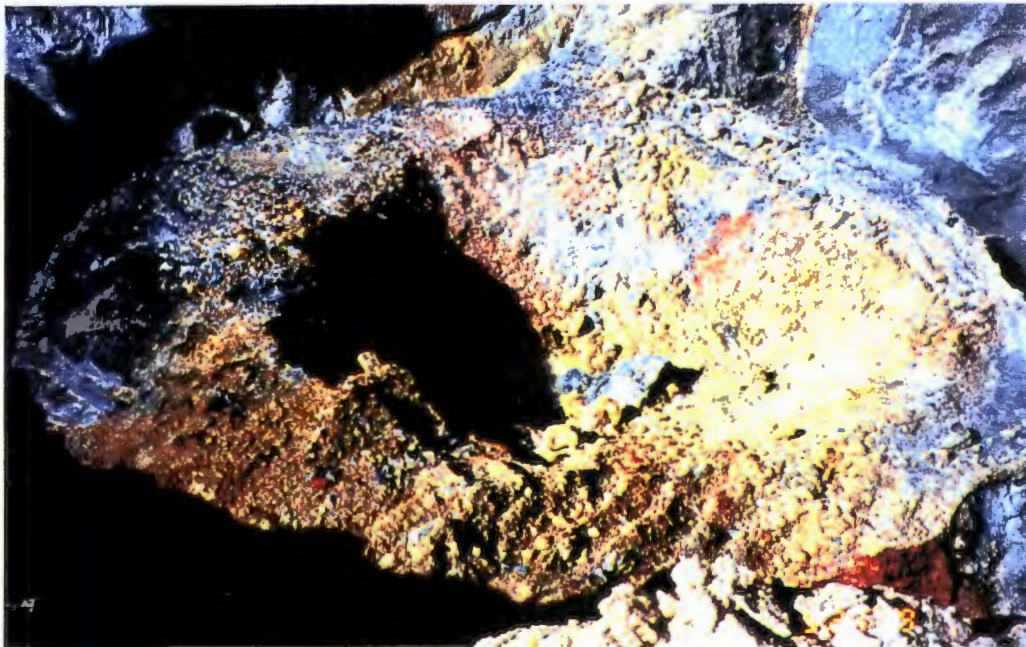


Figure 5-2. Surface of the cold demonstration vitrified monolith

melt and resulting monolith are typically symmetrical in shape. The two trenches were excavated to a depth of 16 to 18-ft which was limited by the depth of the product and reach capability of the excavation equipment.

The shape of the monolith was approximately a square block with slightly rounded shoulders (see Figure 5-3). Measurements taken of the melt width indicated that the monolith was 23-ft wide in the north/south direction and 25-ft wide in the east/west direction. The appearance of the vitrified monolith was typical and there existed no abnormalities associated with the shape.

Although the bottom of the monolith was not exposed during the excavation activity, it is believed that the bottom is relatively flat with a slight upward bowl shape. The depths of all four of the electrodes at the completion of the cold demonstration were within 6-in of each other. This indicates that in the 7-ft by 7-ft separation area of the electrodes, the bottom was consistent. It is believed that the bottom of the melt has a slightly rounded shape because of the behavior of the electrodes during the latter portion of the melt. When the electrodes were lowered to the bottom of the melt late in the run, they all angled in toward the center of the melt. Likewise, the top of the electrodes, which are visible on top of the hood, angled slightly outward away from the center. When the electrodes were lifted off the bottom of the melt slightly the angle would improve and the electrodes would return to a more vertical orientation. This indicates that the bottom of the melt was rounded somewhat, as has been seen during prior melts. It is believed that the bottom shape of the cold demonstration block is comparable to other larger-scale

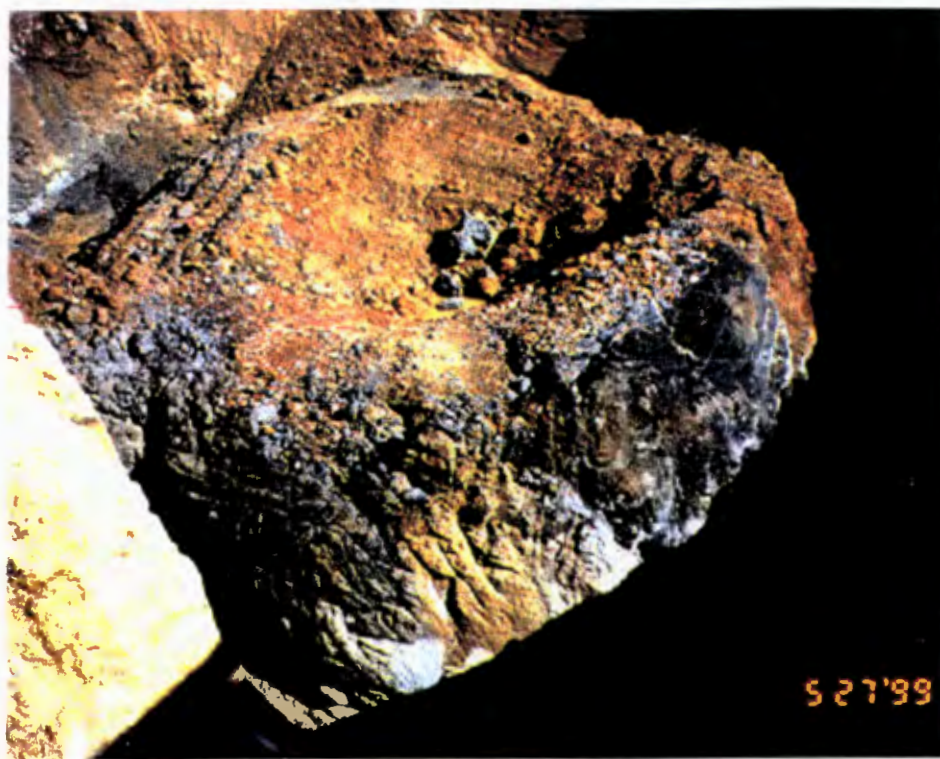


Figure 5-3. Shape of the vitrified product produced during the cold demonstration

GeoMelt products based upon the physical appearance of the two sides and top, as well as, the behavior of the electrodes when contacting the melt bottom.

Figure 5-4 shows the position of the simulated absorption bed prior to treatment as compared to the final location of the vitrified product. The approximate boundary of the subsidence is also shown.

5.1.3 Melt Depth

The depth of treatment of traditional ISV has historically been one of the limitations and as such all previous applications were typically to a depth of <16-ft. A benefit of the sub-surface melt initiation is an increased depth potential due to improved electrode life and efficiency of melting. Thus, a depth objective was established for both the cold and hot demonstrations of 22-ft.

The standard method used to determine the melt depth is to monitor the depth of the four electrodes, which are incremented such that their depths can be monitored as they feed in. The electrodes either rest on the bottom of the melt or periodically are lowered down to the bottom (depending upon the operational mode) to determine the depth at each of the four electrodes. The depths of the electrode are generally considered a good representation of the bottom depth of the melt due to its consistent and symmetrical bottom shaping.

All four of the electrodes exceeded the 22-ft depth at the completion of the cold demonstration. Their final depths ranged from 22-ft 10-in to 23-ft 4-in.

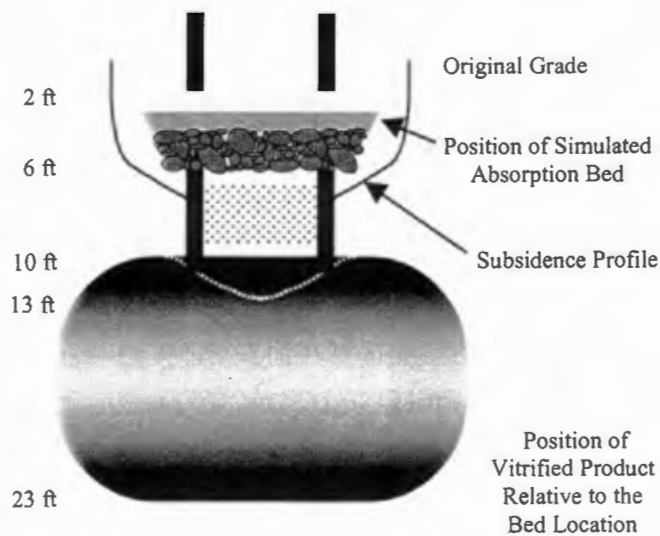


Figure 5-4. Location of the vitrified product compared to the original location of the simulated absorption bed

5.2 Vitrified Monolith Sampling

Excavation of the soil around the monolith enabled a portion of the vitrified product to be removed and sampled. Sampling was performed to:

- confirm the bulk composition of the product.
- determine the concentration of surrogates and degree of homogeneity contained within the product
- determine the product quality by leach testing (PCT and TCLP)
- determine geochemical properties of the product.

An excavator fitted with a hydraulic hammer was used to break small pieces of the northwest corner of the monolith. Initial efforts to obtain samples by striking the monolith with the teeth of an excavator bucket were unsuccessful. This demonstrates the high strength and toughness of the product that is created by the GeoMelt process. Compression testing performed previously on products with similar compositions have reported compressive strengths of up to 50,000 psi.

The approach used for sampling the monolith was to select a quadrant of the product and remove as much of it as possible. Sampling of only one quadrant was performed to save costs as compared to breaking up the entire monolith or performing core sampling through the monolith in several locations. Technically, this approach is acceptable as the melt shape is typically symmetrical and the geochemical properties and contaminant distribution is homogeneous. Random unbiased samples were then collected from portions of the product that was removed and brought to grade. Details of the sampling methodologies can be found in Appendix A. Figure 5-5 shows the equipment used in breaking and removal of the vitrified product. As can be seen in the photo, the excavator operated up to its maximum reach to obtain the product samples. To increase the depth capability of the excavator, a bench was dug such that it could get lower and closer to the vitrified product. However, because of the depth of the product, only a portion of the block could be broken and removed. Figure 5-6 shows the section of the block that was broken and removed to provide samples. It is estimated that 20 to 25 tons of vitrified product was broken off and removed for sampling. Figure 5-7 shows a typical piece of the product removed during the sampling activity.

5.2.1 Bulk Chemistry Testing

Five vitrified product samples were sent to ChemEx Labs, Inc. to determine their overall bulk chemistry. The actual geochemical composition of the product will allow confirmation of the melting properties, as well as, provide useful data regarding the expected melting characteristics of the hot demonstration area. For a description of the whole rock procedure used to determine the bulk chemistry, see Section 3.7.1. The results of the five samples are presented in Table 5-1.

An average of the vitrified product whole rock results was input into a model that predicts a viscosity/temperature curve (see section 3.7.1 and appendix C). The curve indicates that a melt temperature of 2,100°C would generate a viscosity of approximately 100



Figure 5-5. Breaking of the vitrified product during sampling activities

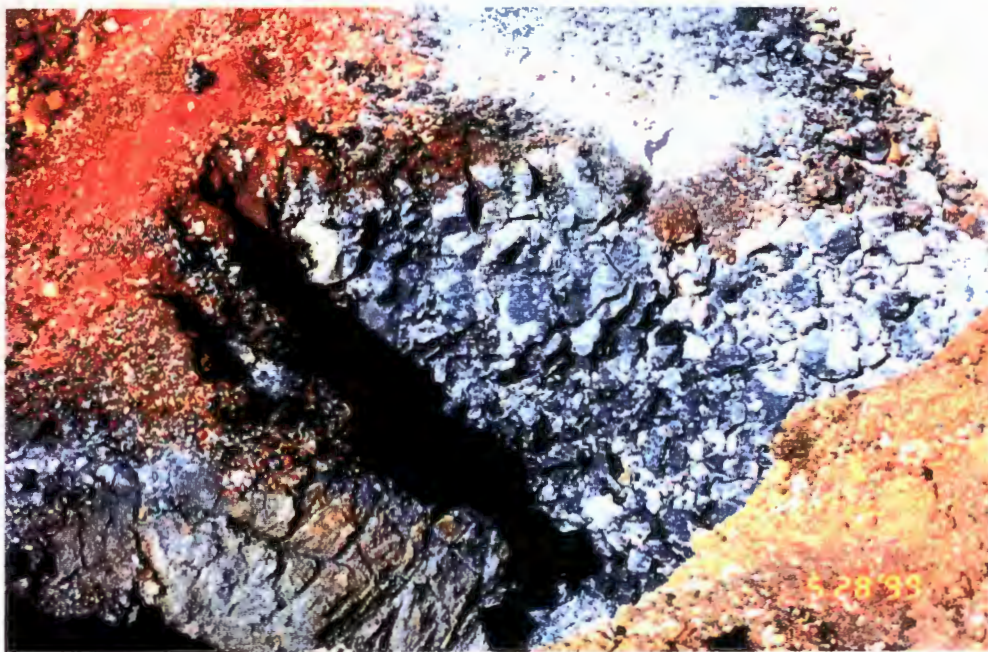


Figure 5-6. Section of the vitrified product removed for sampling



Figure 5-7. Representative sample of the vitrified product

Table 5-1. Post-test glass product sample bulk chemistry results (normalized)

Oxide Compound	NTISV-GB-12 (wt %)	NTISV - GB-18 (wt %)	NTISV - GB-20 (wt %)	NTISV - GB-23 (wt %)	NTISV - GB-26 (wt %)	Average (wt %)
Na ₂ O	3.63	3.63	3.59	3.64	3.57	3.61
K ₂ O	3.65	3.66	3.66	3.66	3.66	3.67
MgO	0.44	0.41	0.45	0.44	0.48	0.44
MnO	0.06	0.06	0.06	0.06	0.06	0.06
CaO	0.88	0.84	0.90	0.90	0.98	0.90
P ₂ O ₅	0.01	<0.01	<0.01	<0.01	<0.01	<0.01
Cr ₂ O ₃	0.01	<0.01	<0.01	<0.01	<0.01	<0.01
TiO ₂	0.20	0.20	0.21	0.20	0.20	0.20
Fe ₂ O ₃	1.49	1.48	1.40	1.43	1.55	1.47
Al ₂ O ₃	12.38	12.45	12.60	12.56	12.79	12.56
SiO ₂	77.25	77.19	77.11	77.09	76.67	77.06
Total	100.0	100.0	100.0	100.0	100.0	100.0

poise. Typically, the viscosity within a melt will be close to 100 poise and the corresponding melt temperature is identified as the T100P or the melt temperature at a viscosity of 100 poise. Although, no actual melt temperature measurements were made during the NTISV demonstration, the model has been validated to be accurate within $\pm 50^\circ\text{C}$ for ISV applications provided the soil/rock composition being evaluated is similar to natural magmatic soil/rock compositions.

The composition of the cold demonstration monolith consists of close to 90% SiO_2 and Al_2O_3 (see Table 5-1). Both of these oxides are glass-forming compounds and are considered to be refractory in nature. Thus, the temperature of the melt would be expected to be high, which would result in a very durable product.

5.2.2 Homogeneity of the Radionuclide Surrogate Distribution

Five random samples were selected from the edge, center and upper portions of the vitrified monolith and were submitted for complete digestion and radionuclide surrogate analysis. It was necessary to completely dissolve the vitrified material to accurately determine the concentration of the surrogates immobilized within the glass matrix. Because the product is very resistant to standard digestions procedures that use strong acids, the lithium-metaborate fusion digestion (described in section 3.7.1) was used. The digested samples were analyzed for Cs and Ce using ICP-MS to determine the levels of the surrogates in the five samples. Table 5-2 presents the results of the surrogate analyses.

Table 5-2. Results of radionuclide surrogate analyses in the vitrified product

Sample Number	Cesium (ppm)	Cerium (ppm)
NTISV-GB-12	33.3	249
NTISV-GB-18	33.0	249
NTISV-GB-20	32.9	249
NTISV-GB-23	33.4	252
NTISV-GB-26	30.9	241
Average in Vitrified Product	33 ± 0.7	248 ± 3
Average Background Value in Tuff Prior to Demonstration:	2.3 ± 0.2	111 ± 3

The amounts of Cs and Ce surrogates added to the simulated absorption bed were based on the need to increase the surrogate concentrations within the product to a level that would be distinguishable above the natural background levels in the soil. This would allow an effective determination of how well the surrogates were distributed throughout the resulting monolith. The targeted increase in concentration levels in the vitrified product above the background soil concentrations were a factor of 2 increase for Ce and a factor of 10 increase for Cs. As can be seen in Table 5-2, these levels were achieved for both

the Ce and the Cs. The level of increase in the product above the background levels for the Ce and the Cs were factors of 2.2 and 14, respectively.

The rise in the vitrified product concentration above the background levels is another indicator that all of the contents of the absorption bed were incorporated downward into the developing melts. Had some of the bed contents and associated surrogates not been incorporated into the melt, the surrogate levels in the vitrified product would have been lower than the targeted concentration level.

The degree of homogeneity within the vitrified product can be seen in Table 5-2. Confidence intervals of 248 ± 3 ppm for the Ce and 33 ± 0.7 ppm for the Cs demonstrate the excellent mixing that occurs during melting. It should be noted that:

- the placement of the surrogates within the absorption bed was at a single depth which was several feet above the location of the finished product. Thus, the surrogates moved downward with the components of the simulated absorption bed and fed into the top of the developing melt(s) and then were uniformly distributed throughout the molten media.
- the samples of the vitrified product were taken from the outer portion of one quadrant due to equipment reach limitations. This is significant in that the outer edges of the melt are typically cooler due to heat loss to the surrounding soils. As a result, the molten product in this region can possess a higher viscosity which can restrict the fluid flow in the outer portions, thus working against homogenization. This data indicates that the convective flow patterns that existed within the cold demonstration melt served to uniformly distribute both the Ce and Cs surrogates, despite this possibility.

5.2.3 Surrogate Retention Efficiency

The high levels of surrogate within the glass are an excellent indication of the immobilization efficiency (or retention efficiency, RE) of these compounds within the glass. Although, a true mass balance is not possible due to off-gas and surrounding soil sampling not being performed, the retention evidence derives from the fact that the concentrations of the surrogates are at or slightly above the targeted levels. The level of immobilization efficiency of actual radionuclides, as well as their surrogates, within a GeoMelt product is well documented. Typically, immobilization (or retention efficiency) of the more refractory radionuclides such as U, Pu, and Sr is >99.99 (Buel et al. 1987 and Geosafe 1996).

Cesium is considered to be a semi-volatile material. Cesium oxide (Cs_2O) decomposes at approximately 400°C , while the boiling point of cesium metal is approximately 705°C . Since the temperature of an ISV melt is 1600°C and above, there is the potential for cesium to volatilize and escape from the system during processing. However, cesium has been shown to be readily incorporated into the glass matrix produced by the ISV process (Spalding 1992). Some of these evaluations include:

- In 1983, conventional top-down ISV was applied at pilot-scale to process a staged, radioactively-contaminated soil volume at the Hanford site in Washington state (Timmerman and Oma 1985). For this test, trace quantities of cesium, as well as a number of radioactive materials, were staged in a plastic container approximately 0.74-m below grade. The target treatment zone was processed in approximately 23 hours. A cesium RE of 99.23% was obtained.
- In a 1987 test, a simulated waste burial trench containing a mixture of actual Oak Ridge National Laboratory (ORNL) Site soil and crushed limestone was treated using the conventional, top-down ISV process (Carter, et al. 1987). The test was performed at engineering scale and involved a target treatment zone staged with non-radioactive cesium (as Cs_2CO_3) and strontium [as $\text{Sr}(\text{OH})_2$] to simulate the presence of the major radioactive materials in the actual burial trench. The entire treatment zone was processed in 8 hours. A RE of 99.996% was obtained for both the cesium and strontium materials in this test.
- Also in 1987, a pilot-scale test was performed on a $3/8$ -scale simulated ORNL Radioactive Liquid Waste Disposal Trench (Spalding and Jacobs 1989). This test involved application of conventional, top-down ISV to process the simulated trench. Non-radioactive Cs_2CO_3 and SrCO_3 were staged approximately 1.5-m below grade in the simulated trench. The trench was composed of crushed limestone surrounded by native ORNL Site soil. The test was conducted over a 110 hour period and produced a vitrified monolith of approximately 20 tonnes. The cesium RE obtained for this test was 99.88%.
- In 1990, conventional, top-down ISV was employed to remediate an actual contaminated soil site at the Hanford Site in Washington state (Luey, et al. 1992). This site (116-B-6A) contained cesium and a number of other radioactive elements, as well as concentrations of various heavy metals (e.g – chromium[VI], lead, and mercury). The process was completed in 288 hours of operation, and produced a 770 tonne vitrified block. The cesium RE obtained for this test was 99.98%
- Another pilot-scale test was performed at ORNL in 1991. This test involved processing another simulated ORNL seepage trench. Trace quantities of radioactive cesium-137, strontium-90, americium-241 and plutonium-239/240 were staged in this test. An RE of 97.6% was obtained for the cesium; for the other radioactive elements, REs in excess of 99.9995% were obtained. The lower cesium RE was attributed to several factors. Chief among these was the influence of the PVC pipe used to stage the cesium on its ultimate volatility. A subsequent investigation (Spalding 1994) suggested that when cesium metal reacts with chlorides (from the PVC), the volatility of the cesium-chloride compound was greatly increased over that of the cesium element alone.
- In 1992, an engineering-scale test was performed to investigate the efficacy of using conventional, top-down ISV to process a liquid waste seepage trench at the ORNL Site (Peterson, et al. 1992). As with the 1987 ORNL engineering-scale test, the target treatment zone was loaded with a combination of ORNL Site soil,

crushed limestone, and non-radioactive Cs_2CO_3 to simulate the radioactive cesium present in the actual waste trench. In addition, a significant quantity of Na_2CO_3 was added to the simulated trench in this test to mimic conditions at the actual ORNL trench. A cesium RE of 99.63% was obtained in this test – somewhat lower than the value obtained in the 1987 engineering-scale test. In this test, the cesium was staged over a larger fraction of the target treatment zone, reducing its nominal burial depth. In addition, several ancillary investigations were performed in this test (e.g. – varying power level during operation). Consequently, this test was performed over a 20 hour period. The reduction in cesium RE obtained in this test was attributed to these two factors.

- A small (1-ton) demonstration was performed at the Brookhaven National Laboratory on a simulated configuration of the chemical/animal pits and glass holes. Neodymium, rubidium, strontium and cesium were added to simulate the presence of radionuclides compounds. The measured RE for the radionuclide surrogates were:
 - neodymium - >99.98%
 - rubidium - >99.98
 - strontium - >99.998
 - cesium - 99.97%
- A large-scale application of the conventional, top-down ISV process was performed at ORNL WAG 7, Pit 1 (Spalding, et al. 1997). Radioactive materials (including cesium and strontium) were processed in this application. The cesium RE obtained for this test was 99.998%.
- A demonstration was performed in 1998 on a 4,500-gal tank that simulated the configuration of one of the V-Tanks at the INEEL (Geosafe 1998). A non-radioactive cesium surrogate was added to the sludge heel that was placed within the tank. Characterization of the off-gas flow, deposition on the various off-gas system components and of the surrounding soils, as well as the vitrified product, indicated a retention level of 99.996%.

This data also indicates that the level of retention increases with scale of application (e.g. the REs obtained for the large-scale applications were 99.98%, 99.998% and 99.996%). This is primarily due to the depths of the melts, however other factors, such as top down versus subsurface melting and melt temperature do play a role. This large amount of data indicates the high likelihood for excellent Cs and other radionuclide retention efficiencies during ISV application at the MDA-V.

5.2.4 Product Quality Testing

Two different leaching tests were used to determine the product durability as measured by its resistance to leaching. Five samples were randomly selected and submitted for leach testing at the Corning Engineering Laboratory, located in Corning, NY. Each sample was prepared and analyzed via the Product Consistency Testing (PCT) and Toxic Characteristic Leach Procedure (TCLP) methods.

5.2.4.1 PCT Evaluation of the Vitrified Product

The PCT method (ASTM C 1285-94) was developed specifically to test the durability of high-level waste glasses during production. The method states that it can also be used to test simulated waste glasses. This test involves grinding the glass to obtain a sample with particle sizes in the range of 0.074-mm to 0.149-mm. A portion of this glass “powder” is then exposed to a leachate consisting of ASTM Type I water at 90°C for a period of 7 days. The mass of leachate to which the sample is exposed is specified to be ten times the mass of the sample. For this application, 4-g samples of the glass “powder” were exposed to 40-ml of leachant. At the conclusion of the 7-day test, the concentrations of the target analytes (in this case Cs and Ce) in the leachate was determined using ICP-MS.

Table 5-3 presents the results obtained for each of the five glass samples. As indicated, the concentration of Cs and Ce in the leachate was less than the detection limit of the analytical procedure for all five samples. This demonstrates the excellent leach resistance and durability properties of the ISV-produced waste form.

Using the detection limit value as an upper-bound estimate of the surrogate concentration in the leachate, the results can be recast into several forms. The Cs and Ce in the leachate results presented in Table 5-3 (columns 3 and 7) can be used to estimate the percentage of Cs and Ce mobilized into the leachate on a wt% basis (columns 4 and 8). This is defined as 100 times the ratio of mass present in the leachate relative to the average value in the product. The results of this calculation are listed in Table 5-3 for each glass sample taken. These values are an upper bound estimate, since the Cs and Ce concentration in the leachate were below the detection limit of 2-ppb and 6 ppb, respectively.

Table 5-3. PCT results for the cold demonstration product

Sample	Ave. Cs in Vitrified Product (ppm)	Cs in leachate (ppm)	Cs Mobilized (wt %)	Normalized Cs Release (g/m ²)	Ave. Ce in Vitrified Product (ppm)	Ce in leachate (ppm)	Ce Mobilized (wt %)	Normalized Ce Release (g/m ²)
GB-1	33 ± 0.7	<0.002	<0.061	<0.011	248 ± 3	<0.006	<0.024	<0.036
GB-3	33 ± 0.7	<0.002	<0.061	<0.011	248 ± 3	<0.006	<0.024	<0.036
GB-4	33 ± 0.7	<0.002	<0.061	<0.011	248 ± 3	<0.006	<0.024	<0.036
GB-6	33 ± 0.7	<0.002	<0.061	<0.011	248 ± 3	<0.006	<0.024	<0.036
GB-7	33 ± 0.7	<0.002	<0.061	<0.011	248 ± 3	<0.006	<0.024	<0.036

< value indicates detection limit

An alternative representation of these results is obtained when the surrogate leachate-to-specimen mass ratio is normalized on the surface area per unit mass for the glass “powder” particles. Mathematically, this is expressed as:

$$\hat{R}_i = \frac{[(C_i - B_i) \times 10^6] \times \rho \times V}{m_i \times A}$$

where: \hat{R}_i = normalized release of analyte i , g/cm²
 C_i = concentration of analyte i in the leachate, ppm
 B_i = concentration of analyte i in the leachate blank, ppm
 ρ = density of leachate, ~1-g/cm³
 V = leachate volume, ml
 m_i = mass of analyte i in the sample, g
 A = surface area per unit mass of the sample, cm²/g

The results of performing this calculation for each of the five samples obtained from this test are presented in Table 5-3 (columns 5 and 9). Again, these values are an upper bound estimate as the surrogates were below the detection limit of the analytical procedure.

5.2.4.2 TCLP Testing of the Vitrified Product

The five samples analyzed for PCT testing were also extracted per the TCLP test as described in 40 CFR 261, Appendix II and in "Test Methods for Evaluating Solid Waste, Physical/Chemical Methods," EPA Publication SW-846. The results of the TCLP test can be seen in Table 5-4. The TCLP is designed to determine the mobility of inorganic (and organic) analytes present in liquid, solid, and multiphase wastes. The TCLP method requires a 100-g sample to first be ground to <9.5-mm and then extracted using enough extraction fluid to equal 20 times the weight of the solid. The extraction fluid used in this procedure is reagent water mixed with acetic acid and sodium hydroxide, which results in an acidic solution with a pH of 4.9. The extraction fluid and ground sample are in contact for 18 ± 2 hrs and then the solution is filtered by passing through a 0.6 to 0.8-µm filter. The resulting extract is then analyzed for the target analytes (in this case Cs and Ce).

All five of the samples submitted for the TCLP test were found to have not leached Cs or the Ce at a level above the analytical detection level. The results of both leach tests performed on samples of the cold demonstration vitrified product are consistent with previous ISV leach results, which far exceed the performance of other waste forms such as high-level waste glass. In addition, ISV glass always surpasses heavy metal land disposal restriction standards by several orders of magnitude.

Table 5.4. Results of TCLP testing of the cold demonstration product

Sample	Cs in Leachate (mg/L)	Ce in Leachate (mg/L)
GB-1	<0.29	<0.056
GB-3	<0.29	<0.056
GB-4	<0.29	<0.056
GB-6	<0.29	<0.056
GB-7	<0.29	<0.056

< value indicates detection limit

5.2.5 Geochemical Evaluation

Samples of the vitrified product were sent to VitChem, located in Issaquah, WA, for geochemical determination. The objectives of this evaluation included, to:

- evaluate the geochemistry of the vitrified product
- compare the chemistry of the product obtained on a microscopic level with that of the whole rock analysis on bulk samples and provide an explanation of any differences (if discovered)
- determine if the vitrified product has crystallized, and if so, describe the type and morphology of crystallized products present
- postulate how crystallization might influence the disposition of contaminant ions for the hot demonstration
- identify, describe and specify the origin of any inclusions found in the product
- discuss the significance of inclusions with respect to the hot demonstration.

Electron microprobe analysis coupled with two forms of spectroscopy was used to document microscopic features and facilitated quantitative analysis of discrete features in the vitrified product. These techniques provided the capability of documenting chemical differences within various portions of the sample. The report submitted is included as Appendix C.

The conclusions of the geochemical evaluation were:

- the cold demonstration produced a hard, durable homogenous glass product
- the high concentration of glass-forming ions has resulted in a vitrified product that is likely to have exceptional chemical durability
- the sample: LANL-1 exhibited three different components in the vitrified product including glass, elemental iron and small black particles believed to be carbon
- the low concentration of iron in the glass compared to that reported by the whole rock analysis on bulk samples indicates that a large portion of the iron oxide in the materials that were melted was reduced to elemental iron
- the reduction of the iron in the NTISV is believed to have been caused by distribution of carbon in the melt.

6. PRELIMINARY COST INFORMATION

One objective of the NTISV demonstration project is to obtain cost data that will enable estimation of large-scale remediation costs for NTISV and enable comparison of the costs to a target level of \$800/ton. Although cost data will be obtained for both the cold and hot demonstrations, the hot demonstration will generate data that is more useful for addressing this objective because:

- the hot demonstration will be performed at a larger scale which is representative of commercial practice, whereas the cold demonstration is not representative (only half as large)
- the hot demonstration will involve the actual treatment of contaminated soils including the treatment of radionuclides
- the hot demonstration will be performed in a portion of Absorption Bed #1 at MDA-V, which is an undisturbed waste trench that received liquid effluent waste from a laundry facility.

The results collected from the hot demonstration will be used in the preparation of an applicability analysis and large-scale cost estimate. Data gathered during the NTISV demonstrations will be used to develop (or refine) the treatment concept, finalize the remedial design and establish the necessary remedial action elements (including sampling, site preparation, mob/demob, vitrification operations, site restoration, and post-ISV sampling and analysis and long term monitoring needs).

Data obtained during the cold demonstration operations phase provides preliminary information regarding the costs of treating the soil types present at the LANL site, which is a significant factor associated with the unit cost of treatment. Direct treatment costs associated with treating the simulated absorption bed volume and the underlying soil down to a depth of 22-ft were:

starter plane injection	\$170/ton
ISV operations	\$456/ton
electrical power	\$ 36/ton
thermal oxidizer rental	\$ 11/ton
propane consumption	\$ 11/ton
Total Unit Cost	\$684/ton

The unit costs presented above include only those costs associated with the treatment process and those preparation steps that are repetitive (such as the injection of the starter planes). Not included are mobilization and demobilization costs, document preparation and other administrative costs, equipment modifications costs, sampling and analysis and reporting.

The comparable unit cost for the hot demonstration is expected to be equal to or lower than that of the cold demonstration due to the experience gained during the cold demonstration, as well as the fact that the operational costs typically decrease with increasing scale.

7. REFERENCES

- American Society of Testing Materials. 1994. Standard Test Methods for Determining Chemical Durability of Nuclear Waste Glasses: The Product Consistency Test (PCT). ASTM C 1285-94.
- Brouns, R.A., J.L. Buelt, and W.F. Bonner. 1983. "In-Situ Vitrification" U.S. Patent #4,376,598.
- Buelt, J. L., C. L. Timmerman, K. H. Oma, V. F. FitzPatrick, and J. G. Carter. 1987. In Situ Vitrification of Transuranic Waste: An Updated Systems Evaluation and Application Assessment. PNL-4800, Suppl. 1, Pacific Northwest Laboratory, Richland, Washington.
- Carter, J.G., S.O. Bates, and G.D. Maupin. 1987. In Situ Vitrification of Oak Ridge National Laboratory Soil and Limestone. PNL-6174. Pacific Northwest Laboratory, Richland, WA.
- Geosafe Corporation, 1998. Treatability Study for Planar In Situ Vitrification Of INEEL Test Area North V-Tanks. Geosafe Corporation, Richland, Washington.
- Geosafe Corporation, 1996. Pillot-Scalle Treatability Testing of the in situ Vitrification (ISV) Technology on Contaminated Soil and Debris from the Chemical/Animal Pits and Glass Holes at Brookhaven National Laboratory. Geosafe Corporation, Richland, Washington.
- Luey, J., et al. 1992. In Situ Vitrification of a Mixed-Waste Contaminated Soil Site: The 116-B-6A Crib at Hanford. PNL-8281. Pacific Northwest Laboratory, Richland, WA.
- Peterson, M.E., T.D. Powell, and C.L. Timmerman. 1992. Engineering-Scale In Situ Vitrification of Simulated Oak Ridge National Laboratory Liquid Waste Seepage Trenches. PNL-7988. Pacific Northwest Laboratory, Richland, WA.
- Shaw, H.R. 1972. "Viscosities of Magmatic Silicate Liquids: An Empirical Method of Prediction." *Amer. J. Sci.*, **272**, pp. 870 – 893.
- Spalding, B.P. and G.K. Jacobs. 1989. Evaluation of an In Situ Vitrification Field Demonstration of a Simulated Radioactive Liquid Waste Disposal Trench. ORNL/TM-10992. Oak Ridge National Laboratory, Oak Ridge, TN.
- Spalding, B.P., et al. 1992. Tracer-Level Radioactive Pilot-Scale Test of In Situ Vitrification for the Stabilization of Contaminated Soil Sites at ORNL. ORNL/TM-12201. Oak Ridge National Laboratory, Oak Ridge, TN.

- Spalding, B.P. 1994. "Volatilization of Cesium-137 from Soil with Chloride Amendments during Heating and Vitrification." *Environ. Sci. Technol.*, **28**, pp. 1116 – 1123.
- Spalding, B.P., et al. 1997. In Situ Vitrification Demonstration at Pit 1, Oak Ridge National Laboratory. Volume 1. Results of Treatability Study. ORNL/ER-425/V1. Oak Ridge National Laboratory, Oak Ridge, TN.
- Timmerman, C.L. and K.H. Oma. 1985. "A Pilot-Scale Test Using In Situ Vitrification." *Nuclear Technology*, **71**, pp. 471 – 481.
- United States Environmental Protection Agency. 1986. Test Methods for Evaluating Solid Waste. SW-846, 3rd edition, Office of Solid Waste and Emergency Response, Washington, DC.

APPENDIX A

Sample and Analysis Plan

Sampling and Analytical Plan

The goal of the sampling and analytical plan is to provide representative and statistically valid data for the cold demonstration evaluation of the planar-ISV process for the simulated absorption bed. In order to achieve this goal, adherence to strict protocol is required and provide in this section. Thorough steps have been outlined below in regard to sample acquisition, quality control, field sampling, and handling & sample analysis. These methods have been incorporated to ensure that the methodology for collecting and testing representative samples is followed, that the quality control procedures are in place to evaluate the information content of the analytical data, and to determine the necessity or the effect of corrective action procedures.

The sampling and analytical procedure outlined in this plan is primarily targeted at performing product quality evaluations. Thus, pre-test soil sampling and post-test vitrified product sampling will be performed to quantify and determine the homogeneity of the surrogates used in this testing within the vitrified product and also the products resistance to leaching.

All samples generated as a result of this testing will be labeled with the operators initials, date, time, test number, and sample description. Section 1.1.1 provides Sample Storage Requirements, Sample Custody Protocol, Sampling Equipment and Technique, Sampling Equipment Decontamination Procedures, and Sample Composite procedures to be used during to performance of this test.

1.1 Sample Handling Techniques

1.1.1 Sample Storage Requirements

The sample storage requirements for all samples taken during the test are for all samples to be placed in specially cleaned glass or plastic containers provided by the chosen analytical laboratory and stored in secured ice chests at 4°C. All samples to be analyzed for chemical characteristics shall be sent via overnight delivery to the laboratory. Additional samples not analyzed will be held from time of collection by the analytical laboratory until data review and issuance of the final report.

1.1.2 Sample Custody Protocol

Sample custody will be the responsibility of Geosafe personnel from the time of sample collection until the samples are shipped to the analytical laboratory. Thereafter, custody will be maintained by the laboratory.

Samples will be kept in appropriate containers and labeled to uniquely identify each sample. A Field Sampling and Collection Form will provide an inventory and field sampling record for each sample collected during test operations. A chain of Custody Record Form will provide the formal custody record. The Request for Analysis Form documents the required analyses to the sender and the laboratory. Sample Labels and Custody Seals are also used to ensure proper identification and security of the samples as the custody changes during the project. Every sample sent to the laboratory for analysis has a typed analytical result which serves as the final stage of the custody and documentation record for the sample.

Samples will be kept at 4°C ($\pm 2^\circ\text{C}$) in an ice chest and will be shipped to the analytical laboratory in a secured chest. Chain of Custody forms will be handled as follows:

- one copy retained by the sampling team
- one copy provided to the Geosafe Project Manager
- original included with the sample shipment
- one copy retained by the analytical laboratory.

The laboratory custodian, after taking inventory of each shipment, will sign and date the original custody form. He will make a note on the custody form of any discrepancy in the samples and will also maintain a log in which all samples are recorded and described. The samples will be maintained in custody until the final report is submitted and approved.

1.1.3 Sampling Equipment and Technique

Stainless Steel Soil Trier

A trier consists of a stainless steel tube cut in half lengthwise with a sharpened tip that allows the sampler to cut into sticky solids and loosen the soil. The trier size must be at least twice the diameter of the particle size obtained. The following procedure shall be utilized for obtaining every soil sample:

1. Clean the trier according to the steps outlined in Section 3.5.3.1.4.
2. Insert the trier into the soil at angle of 0 to 45° from the vertical. Rotate the trier to cut a core of the material. Remove the trier with the concave side up.
3. Transfer the sample to the sample jar using a stainless steel spatula.
4. Clean the trier and spatula (Section 1.1.4) label and store the sample (Section 1.1.1).

The samples shall be obtained from the sample grid locations as described in SW-846 for obtaining random unbiased samples. It should be noted that multiple triers of the same dimension and construction can be used in order to avoid timely decontamination procedures. However, once a single trier is used, it must be decontaminated before obtaining another sample.

Alternative Soil Sampling Method

Samples obtained of the surrounding soils, as well as the materials to be added to the simulated absorption bed may be collected via random grab samples. These samples shall be collected using a clean sample collection tool (hand trowel) or by using the sample container as a scoop.

Wipe Sample Equipment

Wipe sampling equipment consists of wiping a cheese cloth across a desired surface using teflon coated forceps to handle the cloth. The following procedure shall be used for obtaining every wipe sample:

1. Don clean, unused disposable latex sample gloves.

2. Obtain cheese cloth and fold in half three times.
3. Obtain clean (see Section 1.1.4) forceps and grasp cloth with the forceps, approximately 1-cm from, and parallel to, the triple folded edge.
4. Saturate cloth with hexane or appropriate solvent.
5. Wipe surface sample vertically and horizontally (two swaths each direction).
6. Each swath is 5.5-cm wide, overlapping 0.5-cm (this method of wiping surface areas provides a consistent area of 100 cm², if desired, and eliminates cross-contamination of surface areas).
7. After the surface area has been wiped, any torn fragments from the cloth remaining on the sample surface are dabbed off using the cloth to prevent loss of recovery from the sample area.
8. The cloth is then placed in an 8-ounce glass sample container and labeled appropriately. The forceps are held over the mouth of the sample jar and rinsed with hexane, collecting the rinsate in the jar to remove any residual surface contaminant that may have been picked up by the forceps.
9. Prior to obtaining the next sample, the cleaning procedure is repeated and new sample gloves are donned.

Note: For wipe sampling ISV off-gas system pipe, don new disposable latex gloves after disassembly of the pipe, and follow above procedure.

Vitrified Product Sample Equipment

Precise core samples of the vitrified product will be collected to accurately map concentrations of contaminants incorporated within the glass and illustrate the distribution. In cases where this is necessary, a hollow tip diamond bit core drill is required. To obtain the glass sample the following procedure should be utilized:

1. Spread a 10 x 10 foot plastic sheet on a flat surface to provide a clean working area.
2. Draw map of ISV block, locating sample points.
3. Perform core sampling of the ISV block.

4. Disassemble core drill and obtain select glass pieces (approximately 2 x 2 x 2 inches) and place in glass containers provided by the laboratory or composited as specified in section 1.1.4. Use teflon coated or stainless steel forceps for handling the samples. The forceps and core drill should be decontaminated prior to and in between each sample according to the procedure in Section 1.1.4.
5. Seal and label samples accordingly.
6. Archive remaining pieces of vitrified block product into plastic and prepare for return shipment to client.

Alternative Vitrified Product Sample Equipment

For glass samples where precise location is not a requirement, physical breaking of the vitrified block and selecting pieces of glass to be sent to the laboratory is appropriate. For obtaining a glass sample the following procedure should be utilized:

1. Collect pieces of the vitrified product using appropriate equipment and layout such that size reduction can be performed.
2. Don protective clothing as specified in the Safety Plan, particularly full faceshield, eye protection, and leather gloves.
3. Use sledge hammer and wedge to break block open. (Note: Heavy Equipment may be utilized to initially break the block and obtain large pieces of the vitrified product.)
4. Obtain select glass pieces (approximately 2 x 2 x 2 inches) and place in glass containers provided by the laboratory. Use teflon coated or stainless steel forceps for handling the samples. The forceps should be decontaminated prior to and in between each sample according to the procedure in Section 1.1.4.
5. Seal and label samples accordingly, note approximate locations within the block.

1.1.4 Sampling Equipment Decontamination Procedure

All sampling instruments (soil trier, spatula, forceps) will be decontaminated prior to and in between each sample to prevent cross-contamination according to the following steps:

1. Wipe excessive contaminant (dirt, grease, etc.) off with a towel or cloth soaked with soapy water, hexane, or acetone, whichever is appropriate for the contaminant.
2. Wash with alconox until all visible contaminant has been removed.
3. Rinse three times with deionized or distilled water.
4. Rinse two times with methanol.
5. Rinse two times with acetone.
6. Wipe with clean laboratory wipes to remove any excessive acetone and air dry.

1.1.5 Sample Composite Procedure

The following procedure should be followed when sample compositing of soils is required:

1. Obtain a large clean stainless steel mixing bowl.
2. Place equal volume aliquots of all samples required for the composite sample into the mixing bowl. The soil/sample material should be removed from its original sample container through the use of a disposable wooden tongue depressor. Each sample should have its own tongue depressor in order to prevent cross-contamination between samples.
3. Thoroughly mix the soil/sample material in the bowl using a clean stainless steel spatula.
4. Remove sample from mixing bowl and place in sample jar.
5. Decontaminate mixing bowl and spatula and dispose of tongue depressors prior to compositing next sample.

1.1.6 Statistical Equations for Representative Sampling

The following equations shall be used to calculate the mean concentration, the standard deviation, and the confidence interval for the samples obtained in Sections V and VII. The equations given are adopted from the "Test Methods for Evaluating Solid Wastes" (SW-846), 3rd Edition, Volume II, Chapter Nine. The equations are:

Mean Sample Concentration:

$$\bar{x} = \sum_{i=1}^n X_i / n$$

where: X_i = individual sample measurement
 n = number of sample measurements.

Standard Deviation:

$$s^2 = [(\sum_{i=1}^n X_i^2 - (\sum_{i=1}^n X_i)^2 / n) / (n-1)]$$

$$s = (s^2)^{0.5}$$

$$s_x = s / (n)^{0.5}$$

Confidence Interval:

$$CI = \bar{x} \pm t_{.20} s$$

where: $t_{.20}$ = student t value (for $n=4$ samples, $t = 1.638$)

Number of Samples:

$$n = (t_{.20}^2 s^2) / (RT - \bar{x})^2$$

where RT = regulatory threshold value.

1.2 Test Sampling

Details regarding the sampling plan for each type of sample is discussed further below.

1.2.1 Pre-Test Sampling

All of the materials used in this test will be obtained from uncontaminated sources. Surrogate compounds will be used to simulate Cs and transuranics to assist in the determination of the vitrified product volume. Although it is unlikely that these uncontaminated pre-test materials will contain significant amounts of the chosen surrogates, all of the pre-test materials will be sampled for these compounds prior to testing. This is necessary to be able to ensure a proper mass balance closure.

Pre-Test Soils Sampling

Samples of the site soils sent to Geosafe will be collected and analyzed for the surrogates chosen. The pre-test soil stockpile will be randomly sampled with a stainless steel soil trier that will be decontaminated between each sample to prevent cross contamination. Section 1.1.3 provides the instructions for obtaining the samples and decontamination of the trier. The sample results will be used to determine if any of the surrogates are present and if so, to determine baseline values to compare post test results with.

Samples collected of the tuff will be labeled as follows:

<u>Sample #</u>	<u>Parameter</u>	<u>Method</u>	<u>Detection Limit</u>
NTISV-1-T1 through NTISV-1-T5 Plus NTISV-1-T11	metals	6010	0.1 mg/kg

A split sample will be taken of NTISV-1-T1 and will be labeled NTISV-1-T11. Samples NTISV-1-T1 through NTISV-1-T5 and NTISV-1-T11 will be analyzed for cesium and cerium initially. Upon completion and receipt of the analytical results, the sample mean, variance, and 80 percent confidence intervals will be calculated and verified that 5

samples are sufficient to calculate the 80 percent confidence interval for the surrogate metals. Section 1.1.6 provides the equations for calculating the parameters listed above.

Samples collected of the top soil will be labeled as follows:

<u>Sample #</u>	<u>Parameter</u>	<u>Method</u>	<u>Detection Limit</u>
NTISV-1-BF1 through NTISV-1- BF 5 Plus NTISV-1- BF 11	metals	6010	0.1 mg/kg

A split sample will be taken of NTISV-1- BF 1 and will be labeled NTISV-1- BF 11. Samples NTISV-1- BF 1 through NTISV-1- BF 5 and NTISV-1- BF 11 will be analyzed for cesium and cerium initially. Upon completion and receipt of the analytical results, the sample mean, variance, and 80 percent confidence intervals will be calculated and verified that 5 samples are sufficient to calculate the 80 percent confidence interval for the surrogate metals. Section 1.1.6 provides the equations for calculating the parameters listed above.

Samples collected of the cobble used in the simulated absorption bed will be labeled as follows:

<u>Sample #</u>	<u>Parameter</u>	<u>Method</u>	<u>Detection Limit</u>
NTISV-1-C1 through NTISV-1-C3	metals	6010	0.1 mg/kg

Samples NTISV-1- C1 through NTISV-1- C3 will be analyzed for cesium and cerium initially. Upon completion and receipt of the analytical results, the sample mean, variance, and 80 percent confidence intervals will be calculated and verified that 5 samples are sufficient to calculate the 80 percent confidence interval for the surrogate metals. Section 1.1.6 provides the equations for calculating the parameters listed above.

One samples each will be collected of the gravel and sand used in the simulated absorption bed and will be labeled as follows:

<u>Sample #</u>	<u>Parameter</u>	<u>Method</u>	<u>Detection Limit</u>
NTISV-1-G1 and NTISV-1- S1	metals	6010	0.1 mg/kg

Samples NTISV-1-G1 and NTISV-1- S1 will be analyzed for cesium and cerium.

Natural Oxide Content of Soil (Whole Rock Analyses)

The geochemical properties of materials to be treated by ISV are an important factor to be considered when evaluating ISV applicability. Chemical composition of the materials to be vitrified affects melt temperature, melt viscosity, mass of off gas generated from fusion, characteristics of the off gas (e.g., pH) and electrical conductivity of the melt.

A whole rock analysis is used to quantify the bulk composition of the soil. Particular attention is paid to the concentration of glass-forming ions, and ions which serve as fluxing agents in the melt. The monovalent alkali cations (Na^+ , Li^+ , K^+) provide electrical conductivity in a silicate melt. The conductivity of the melt is generally proportional to the concentration of these ions, but variations occur because of the complexity of multi-component systems such as in soil. Experience in melting various soils has shown that if the sum of the monovalent alkali cations is within the range of 2 to 5 wt%, ISV processing proceeds without electrical difficulty. The presence of large cations such as Na^+ and Ca^{+2} also reduces the viscosity of the melt by physically separating the glass-forming cations and reducing the number of glass-forming bonds in the melt. Therefore, the addition of Na as an electrical flux also reduces melt viscosity and operating melt temperature. Performing the whole rock analysis also provides the silica, aluminum, iron, and calcium content.

Prior to initiating any vitrification project, the bulk chemistry of each waste component (e.g., soil and simulated bed contents) to be treated is analyzed. These analyses are then

used in a geochemical model that numerically mixes the components in the proportions expected in the field and predicts the resultant product composition. This resultant composition can then be used to predict melt temperature, viscosity, and approximate electrical conductivity. It can also be used to predict crystallization behavior.

The temperature/viscosity prediction is made using the method developed by Shaw (["Viscosities of Magmatic Silicate Liquids: An Empirical Method of Prediction"], H.R. Shaw, Amer. J. Sci. **272**:870-893). This method has been found to be accurate within 50°C for ISV applications provided the composition being evaluated is similar to natural magmatic compositions.

The pre-test samples submitted for surrogate analyses will also be analyzed for whole rock.

1.2.2 Post-Test Sampling

After the ISV melt test is complete, samples will be collected of the vitrified block.

All samples should be obtained under the procedures set forth in Section 1.2.2 of this Sampling and Analytical Plan. The sampling procedure is a random sampling scheme adopted from the Environmental Protection Agency's SW-846 Test Methods for Evaluating Solid Waste, 3rd Edition, Volume II, Chapter Nine. In addition, all statistical calculations will be made in accordance with the guidelines specified in SW 846, Vol. 2, Chapter 9.

Analyses of Tracers Remaining in Vitrified Product

Once the vitrified product has cooled sufficiently, collection of vitrified product samples will be performed. Five vitrified product samples will be collected for analysis of the surrogates immobilized in the product. These samples will be labeled as follows:

<u>Sample #</u>	<u>Parameter</u>	<u>Method</u>	<u>Detection</u>
<u>Limit</u>			
NTISV-GB-01 through NTISV-GB-05 and NTISV-GB-06 (split of core 1)	Metals	XRF & ICP/MS	0.1 mg/kg

Submit samples NTISV-GB-01 through NTISV-GB-05 for metals analyses listed above. In addition, one QC sample will be split into two halves and analyzed for the metal tracer. The blind split QC sample will be labeled NTISV-GB-06. The sample locations will be determined to samples from the center areas as well as the outer edge portions of the block

Product Leach Testing

Samples will also be collected from the above mentioned vitrified product composites and submitted for leach testing using either the product consistency testing (PCT) method (ANS/ANSI Method 16.1) and the toxic characteristic leach procedure (TCLP) test (U.S. EPA Method 1311). Samples NTISV-GB-07 through NTISV-GB-11 shall be submitted for the following analyses:

<u>Sample #</u>	<u>Parameter</u>	<u>Method</u>	<u>Detection Limit</u>
NTISV-GB-7 Through NTISV-GB-11	Metals	PCT & TCLP	0.1 mg/kg

APPENDIX B

Cold Demonstration Operations Chronology

NTISV COLD DEMONSTRATION MELT CHRONOLOGY

4-16-99

- 1322 Hours, Geosafe started the control system trends and began the off-gas system
- 1407 Hours, the main disconnect was closed and power was turned on to the melt. The beginning tap setting was PP-4
- 2317 Hours, a standard tap change was made from PP-4 to PP-6

4-17-99

- 850 Hours, the propane level was checked and observed to be 74% full or 8880-gal (12000-gal x 0.74)
- 1003 Hours, thermocouple #50 failed meaning that it was now in the melt
- 1017 Hours, made a tap change back from PP-6 to PP-4 for a better power factor and improved control
- 1033 Hours, minor improvements to the computer system were completed.
- 1910 Hours, thermocouple #51 failed
- 2100 Hours, thermocouple #43 failed

4-18-99

- 406 Hours, made a tap change to PP-3 to improve the power factor
- 447 Hours, determined that surge protectors are needed to protect the LPU's
- 530 Hours, thermocouples #44 and #52 failed. Noted that the hood camera had temporarily stopped operating
- 824 Hours, powered down to reset the hood camera
- 936 Hours, thermocouple #42 failed
- 1051 Hours, made a tap change to PP-4 as A phase was voltage limited
- 1211 Hours, thermocouple #45 failed
- 1402 Hours, thermocouples #58 and #53 failed
- 1415 Hours, powered down to perform a tap change to PP-6
- 1610 Hours, thermocouple #46 failed
- 1416 Hours, powered down to perform a tap change to PP-6 to improve the power factor
- 2300 Hours, thermocouple #47 failed

4-19-99

- 230 Hours, observed movement on electrodes A1 and B4 from 11-ft to 16-ft and 16-ft 7-in, respectively, both electrodes were then gripped
- 504 Hours, electrode A2 moved and was gripped at 12-ft 10-in
- 720 Hours, three gallons of condensate was drained from the cooling chamber
- 904 Hours, thermocouple #9 failed
- 0907 Hours, thermocouple #54 failed
- 1301 Hours, thermocouple #5 failed

4-19-99 continued

- 1549 Hours, shut down power to re-align the contactor on the A1 electrode as it was beginning to heat up. Cleared the area and powered back up
- 1920 Hours, the crane arrived on site to assist in normal electrode lowering operations. No movement was detected. Electrodes A1, A2 and B4 were left in the gripped position while electrode B3 was allowed to gravity feed and catch up to the depths of the other electrodes. After properly clearing the area power was turned back on
- 2246 Hours, Shut down power to re-align the contactor for electrode A2. Also observed that electrode B3 had been gravity feeding as is standard and was at a depth of 12-ft 9-in

4-20-99

- 200 Hours, electrode B3 was observed to be at a depth of 13-ft 2-in
- 423 Hours, un-gripped electrode A2 to allow it to catch up with the depth of the other electrodes. The depth of A2 is 12-ft 10-in
- 445 Hours, powered down to perform a tap change to PP-2 to improve the power factor
- 1036 Hours, drained an estimated 5 gallons from the cooling chamber
- 1121 Hours, observed that electrode A2 had moved to a depth of 14-ft 6-in. At this time the A2 electrode was placed in the gripped position
- 1648 Hours, powered down to use the crane for electrode movement
- 1700 Hours, observed that the subsidence area around the electrodes was symmetrical and uniform. Approximately 4-ft in depth
- 1745 Hours, Electrode B4 was lowered to a depth of 18-ft 3-in and then raised back to 17-ft. Electrode A1 went to a depth of 16-ft and was adjusted to 15-ft 9-in. Electrode B3 was lowered to a depth of 19-ft 5-in and was adjusted back to 17-ft. Electrode A1 showed no movement and was gripped at 15-ft 8-in
- 1815 Hours, Power was turned back on and power was gradually brought up to 1100 kW
- 1900 Hours, observed standard off gassing around the electrodes
- 2209 Hours, powered down to re-align the contactors on electrode feeder A1
- 2300 Hours thermocouple #59 failed

4-21-99

- 1603 Hours, thermocouple #56 failed
- 1627 Powered down for electrode addition and depth observations. Electrode A1 was lowered to a depth of 18-ft 10-in and an additional electrode section was added. Electrode A2 was lowered to a depth of 19-ft 6-in and an additional electrode section was added. Electrode B3 was lowered to a depth of 19-ft 7-in and an additional electrode section was added. Electrode B4 was lowered to a depth of 19-ft 4-in and an additional electrode section was added
- 1800 Hours, waited to turn on power while MSE collected tomography data
- 1825 Hours, normal pre-filter loading was observed and thought to be condensation
- 2028 Hours, power back on to the melt

4-22-99

- 210 Hours, thermocouple #11 failed
- 648 Hours, drained an estimated 6 gallons of condensate from the cooling chamber
- 905 Hours, thermocouple #6 and #33 failed
- 1033 Hours, observed standard sloughing on the south side
- 1305 Hours, thermocouple #18 failed
- 1604 Valved pre-filter HEPA from bank#1 to bank #2 as the #1 bank had reached the change out criteria of 7.0 ΔP
- 1622 Hours, turned off power for daily electrode lowering
- 1655 Hours, the electrodes were lowered to the following depths:
 - A1 20-ft 6-in
 - A2 20-ft 7-in
 - B3 21-ft 1-in
 - B4 20-ft 5-in
- 1745 Hours, new HEPA filters were installed in the pre-filter
- 1818 Hours, while power was down the cables from electrode A2 and electrode B3 switched to the standard Scott-Tee cross firing mode
- 1845 Hours, started up the wet scrubbing portion of the off-gas system to demonstrate total system performance and to ensure that it is operable for the hot demonstration.
- 1939 Hours, powered down to adjust the contactors on the electrode A1 feeder
- 2000 Hours, thermocouple #1 failed
- 2120 Hours, observed that the main air compressor was getting hot and so the back up air compressor was valved in

4-23-99

- 45 Hours, ran the air supply for the main system from the Electrode feed system and put the green compressor in standby
- 653 Hours, power is at 1100 kW
- 908 Hours, thermocouple #62 failed
- 1015 Hours, the #2 bank of pre-filter was changed out and is now ready for operation.
- 1300 Hours, power is at 1200 kW.
- 1607 Hours, power was turned off to lower the electrodes The depths of the electrodes were as follows:
 - A1 21-ft 4-in
 - A2 21-ft 10-in
 - B3 22-ft 1-in
 - B4 22-ft
- 1650 Hours, power was turned back on

4-24-99

735 Hours, power was shut off to the melt as all the objectives of the cold demonstration test were met and the test was completed

0750 Hours, electrodes were un-gripped. The depths of the electrodes were as follows:

A1	22-ft 6-in
A2	23-ft 0-in
B3	23-ft 2-in
B4	23-ft

0835 Hours, took one final electrode depth measurement. Below are the final electrode depths

A1	22-ft 10-in
A2	23-ft 2-in
B3	23-ft 4-in
B4	23-ft 3-in

903 Hours, the #1 bank of the pre-filter reached its change-out criteria and thus, the pre-filter was switched to bypass

1150 Hours, the thermal oxidizer was shut off and valves were placed in the off position

1205 Hours, the off-system was shut off

COLD DEMONSTRATION SUMMARY

Power on to Melt	4-16-99 @ 1407 hrs
Power off to Melt	4-24-99 @ 0735 hrs
Total melt run time	185 hrs
Total power consumed	165,600 kWh
Peak ISV Melt Power Demand	1257 kW
Electrode Depth A1	22-ft 10 -in
Electrode Depth A2	23-ft 2 -in
Electrode Depth B3	23-ft 4 -in
Electrode Depth B4	23-ft 3 -in
Electrode target depth	22-ft
Waste scrub solution transferred	0
Condensate solution	110 gal
Scrub filters used	0
HEPA filters used (pre-filter)	6
HEPA filters used (main system)	3

APPENDIX C

Geochemical Evaluation

FINAL REPORT

**GEOCHEMISTRY OF VITRIFIED PRODUCTS FROM A NON-TRADITIONAL IN
SITU VITRIFICATION DEMONSTRATION AT MDA-V SITE AT THE LOS
ALAMOS NATIONAL LABORATORY**

PRESENTED TO:

**Geosafe Corporation
2952 George Washington Way
Richland, WA 99352**

PRESENTED BY:

**Dale M. Timmons, R.G.
VitChem
23252 S.E. 54th Place
Issaquah, WA 98029**

August 3, 1999

LIMITATIONS

This report and the data it contains was prepared by VitChem for the exclusive use of Geosafe Corporation and the U.S. Department of Energy for evaluating site conditions, regulatory impacts and technology application of non-traditional in situ vitrification. The VitChem investigation was performed using the standard of care and level of skill ordinarily exercised under similar circumstances by reputable geologists currently practicing in this and similar localities. VitChem makes no other warranty, expressed or implied regarding the conclusions or professional advice provided in this report.

Signed report (ten copies) issued to:

Mr. Brett Campbell
Geosafe Corporation
2952 George Washington Way
Richland, WA 99352

Submitted by:

Dale M. Timmons, R.G.

TABLE OF CONTENTS

1.0	Introduction	1
2.0	Project Methods	2
3.0	Sample Description	3
4.0	Whole Rock Analysis	3
5.0	Electron Microprobe Analysis	4
5.1	Quantitative Analysis	5
6.0	Melt Temperature	7
7.0	Conclusions	8
	References	8

List Of Tables

Table 1:	Normalized Mean Bulk Composition of Vitrified Mass	4
Table 2:	Comparison of Bulk Analysis with WDS Analysis	5

List of Figures

Figure 1A and 1B:	Color Photograph	9
Figure 2:	Electron Photomicrograph	10
Figure 3:	Viscosity Curve	11

GEOCHEMISTRY OF VITRIFIED PRODUCTS FROM A NON-TRADITIONAL IN SITU VITRIFICATION DEMONSTRATION AT MDA-V SITE AT THE LOS ALAMOS NATIONAL LABORATORY

1.0 Introduction:

This report has been prepared by VitChem in response to a request by Geosafe Corporation for geochemical analysis of vitrified products produced from a non-traditional in situ vitrification (NTISV) demonstration performed at the Los Alamos Laboratory (LANL). The demonstration includes a "cold" and a "hot" demonstration (non-radioactive and radioactive respectively). The cold demonstration has been completed.

The cold demonstration was performed at the Material Disposal Area V (MDA V) located at the LANL Site. The MDA V site is located in Technical Area 21 along its northern boundary, immediately east-southeast of the town of Los Alamos. The MDA V site encompasses an area of 0.88 acre. It contains three liquid absorption beds constructed to receive waste effluent from the Delta Prime laundry facility that was previously used for cleaning clothing that was contaminated with radionuclides. The cold demonstration was performed in an area adjacent to the absorption beds in uncontaminated soil for purposes of demonstrating a unique application of the technology. The hot demonstration is planned to take place within one of the absorption beds.

A simulated absorption bed was constructed for the cold demonstration. The vitrification process for the cold demonstration was initiated by injecting conductive starter material (graphite slurry) in the subsurface through which an electrical current was passed to initiate melting. Two parallel planar melts were formed and spaced so that they merged midway through the melting period. Melting was initiated at a depth of 6.5 to 9.5-ft bgs and continued to 22-ft.

Following the demonstration, the vitrified monolith was excavated and samples of the vitrified product were collected. Samples were subjected to whole rock analysis, the Product Consistency Test (PCT), Toxic Characteristic Leach Procedure (TCLP) testing and one sam-

ple was selected for electron microprobe analysis. These analyses were performed to evaluate the homogeneity chemistry and chemical durability of the product. This report focuses on the geochemistry of the vitrified product. The PCT and TCLP results will appear in a separate report by Geosafe Corporation.

The objectives of this study are:

1. Evaluate the chemistry of the vitrified products.
2. Compare the chemistry of the product obtained on a microscopic level with that of whole rock analysis on bulk samples. Describe and explain any differences (if discovered).
3. Determine if the vitrified product has crystallized and if so, describe the type and morphology of crystallized products present. Postulate how crystallization might influence the disposition of contaminant ions for the hot demonstration.
4. Identify, describe and specify the origin of any inclusions found in the product. Discuss the significance of inclusions with respect to the hot demonstration.

2.0 Project Methods:

Geosafe provided several samples of the vitrified product. Because of the similarity of the samples, one representative sample was selected for study. The assigned sample number is LANL-1.

The evaluation methods on Sample LANL-1 consisted of:

1. Sample collection of vitrified material from the vitrified mass.
2. Physical description, cataloging and photography of the vitrified sample to document its physical appearance including texture and color.
3. Preparation of electron microprobe thin section and electron microprobe analyses including X-ray energy dispersive spectroscopy (EDS) and wavelength dispersive spectroscopy (WDS) with quantitative analysis and photographs.
4. Interpretation of the data and reporting.

Electron microprobe analysis coupled with EDS and WDS were used to document microscopic features and facilitated quantitative analysis of discrete features in the vitrified product. WDS provides enhanced detection limits for selected elements. These techniques provided the capability of documenting chemical differences within various portions of the sample.

3.0 Sample Description:

Sample LANL-1 was collected from the interior of the vitrified mass. The sample is irregularly shaped and approximately 8 cm on a side. Its color is medium dark gray (N4)¹, vitreous with a waxy appearance, and exhibits a conchoidal fracture. Few inclusions are visible, however, when held up to the light, thin cross-sections exhibit small inclusions. The inclusions are so small (<1 mm in diameter) that characterizing them in hand specimen is difficult. The inclusions are sparse and occupy significantly less than 1% of the sample volume. No unmelted rock particles were identified in LANL-1.

Figures 1A and 1B consist of two optical color photographs. 1A was taken at low magnification and 1B was taken at high magnification. For both figures, the fine scale is millimeters and the coarse scale is 1/16 in. Color and texture are accurately represented in these photographs.

The sample is physically durable, appears non-porous and is difficult to break with a hammer. There were no cracks observed in the sample other than those created by breaking the sample during collection.

4.0 Whole Rock Analysis:

Many samples were collected for analysis from different portions of the main body of the vitrified mass. The samples were collected from various locations in the vitrified mass in order to provide a representation of the mass. In addition to whole rock parameters, the concentrations of surrogate analytes (Ce and Cs) were evaluated. Table 1 shows the normalized mean composition from whole rock analysis. A discussion of the results of the Ce and Cs analysis is provided in Geosafe's report under separate cover.

Table 1. Normalized Mean Bulk Composition of Vitrified Mass (wt%)

Oxide	Concentration
SiO ₂	77.11
TiO ₂	0.21
Al ₂ O ₃	12.53
Fe ₂ O ₃	1.46
MgO	0.44
CaO	0.90
Na ₂ O	3.62
K ₂ O	3.67
Cr ₂ O ₃	<0.01
MnO	0.06
P ₂ O ₅	<0.01

5.0 Electron Microprobe Analysis

Sample LANL-1 was subjected to electron microprobe analysis. A microprobe thin section was prepared by mounting a slice of the sample on a glass slide, grinding it to a thickness of 30µm and then polishing it with diamond paste. This slide was then examined with a JOEL 733 Superprobe electron microprobe.

Differences in shades of gray in the electron photomicrographs correspond to differences in average atomic number of the features observed (equating to density). Lighter shades are denser than darker shades. Differences in density can be attributed to differences in chemistry and/or crystallization differences. These differences were examined in part by acquiring EDS spectra of back-scattered electrons. EDS spectra reveal the elements that are present in the target area of the sample and semi-quantitatively identify the relative concentration of the elements from the height of the spectral peak.

In addition to EDS, WDS analysis was performed on selected targets in the sample. WDS provides better detection limits than EDS and better resolution of the emission peaks. EDS resolution is about 180 eV (corresponding to about 0.2 wt% of the element) and WDS resolution is about 6 eV.

Initial examination of Sample LANL-1 with the electron microprobe included identification of the fundamental features in the sample. Several features were identified and include:

1. Glass
2. Vesicles
3. Small particles (i.e., <100 μ m) of iron
4. Very small (<5 μ m) dark irregularly-shaped particles
5. No unmelted rock or mineral fragments were observed.

Figure 2 is a backscattered electron image of Sample LANL-1. This photomicrograph shows spherical iron droplets (I), vesicles (V), and glass. Most of the material in this image is glass (medium gray background). The locations: G-1 and G-2 correspond to locations at which WDS analyses were performed. The iron was identified by acquiring an EDS spectrum on the large droplet in the center of the image. This spectrum showed only an Fe peak. This type of feature has been observed in ISV melts in the past.

5.1 Quantitative Analysis

Quantitative analyses using WDS was performed on the glass at locations G-1 and G-2 in Figure 2. Table 3 shows the results of the WDS analyses at each of these locations and compares these results with the normalized bulk analysis.

Table 2: Comparison of Bulk Analysis with WDS Analysis

Oxide	Bulk Analysis	G-1 WDS Analysis	G-2 WDS Analysis
SiO ₂	77.11	79.91	78.20
TiO ₂	0.21	0.24	0.21
Al ₂ O ₃	12.53	13.14	12.68
Fe ₂ O ₃	1.46	0.34 (FeO)	0.32 (FeO)
MgO	0.44	0.43	0.43
MnO	0.06	0.08	0.06
Na ₂ O	3.62	1.52	2.99
CaO	0.90	0.89	0.91
K ₂ O	3.67	4.06	4.17
Cr ₂ O ₃	<0.01	NA	NA
P ₂ O ₅	<0.01	NA	NA

< - Below Detection Limits

NA - Not Analyzed

The differences between the mean bulk composition from the NTISV monolith and the WDS analyses are relatively minor with the exception of the concentration of iron. After converting the oxide concentrations to elemental concentrations, the concentration of Fe in the bulk analysis is 1.02% and the concentration in the glass from WDS analysis is 0.26%. This is a significant difference and appears to be the result of iron reduction that took place during the NTISV cold demonstration.

In Figure 2 there are numerous white spots visible in the image. During the examination of the sample with the microprobe, 12 of these white spots were selected at random and an EDS spectrum was acquired using a 1 μ m electron beam. The EDS spectrum acquired from each of the 12 white spots showed the presence of Fe only. The reduction of Fe from the melt would result in Fe concentrations in the glass lower than that reported in the bulk analysis. This is because the WDS analysis is acquired from one small spot on the polished surface on the glass and does not include iron inclusions.

The image in Figure 2 is a digitized image consisting of 250,000 pixels. To estimate the true quantity of iron present in the Figure 2 image the white and gray pixels were counted and their sums compared. Based upon the pixelization of the image, the small spots of Fe represent 1.27% of the area of the image. It can be reasonably assumed that the Fe spots are randomly distributed so that the area occupied by Fe in Figure 2 can be assumed to be equal to the volume occupied by Fe in the vitrified product. The average density of elemental Fe is 7.5 g/cm³ and the average density of glass produced by ISV is 2.5 g/cm³. Taking into account the density differences, the pixelization would indicate that the Fe concentration is 3.8%. This is clearly too high and probably the result of two factors. The first factor is that the iron particle in the center of Figure 2 is by far the largest particle found in the sample and is probably skewing the concentration. The second is that some of the Fe particles are so small that a single pixel is probably larger than the particle. Thus, it is difficult to accurately estimate the concentration of Fe in this product using WDS.

There are small black spots visible in Figure 2 in addition to the black vesicle. Attempts to acquire EDS spectra were attempted on several of these spots. Each attempt resulted in a spectrum that was characteristic of the glass. The black color on the image is indicative of a

low atomic number or a void. Clearly, some of the circular dark areas are vesicles. However, some of the black areas do not have the morphology indicative of void space or vesicles. Vesicles in this size range tend to have spherical morphology due to the very high surface tension in this size range. It is believed that some of these dark areas consist of particles of carbon originating from the graphite starter material. There are several reasons for this belief including:

1. Carbon has a low atomic number and would result in a very dark gray or black spot in the electron photomicrograph.
2. The detector on the electron microprobe is only capable of detecting elements with atomic number greater than 11 (sodium). Attempts to detect elements lighter than this would result in spectra characteristic of surrounding media (in this case the surrounding glass).
3. The black spots are finely disseminated and in some cases appear to have a flake-like appearance. This is the morphology that would be expected from the presence of graphite particles used in the startup procedure.
4. A relatively large quantity of graphite start-up material was injected into the subsurface prior to initiating the demonstration. The vast majority of this material was incorporated into the melt during processing.
5. Although reduction of Fe from the graphite electrodes has been observed in the past, this usually results in an accumulation of small amounts of reduced iron in close proximity to or below the electrodes and only slight reductions in Fe concentrations in the product. The very fine dissemination of small iron particles is not characteristic of reduction caused by electrodes.

6.0 Melt Temperature

The calculated temperature-viscosity curve shown in Figure 3 (Shaw, 1972⁸) predicts a viscosity of 118 poise for a melt with the bulk composition shown in Table 1 at a temperature of 2,100°C. No melt temperature measurements were made during the NTISV demonstration. Consequently, the validity of the calculated viscosity curve cannot be verified. The composi-

tion of the NTISV monolith consists of close to 90% SiO₂ and Al₂O₃. Both of these oxides are glass-forming ions and are considered refractory. Thus, the temperature of the melt would be expected to be high.

7.0 Conclusions:

Observations made of Sample LANL-1 result in several interpretations and conclusions. These include:

1. The NTISV demonstration produced a hard, durable homogenous glass product. The high concentration of glass-forming ions has resulted in a vitrified product that is likely to have exceptional chemical durability.
2. The sample: LANL-1 exhibited three different components in the vitrified product including glass, elemental iron and small black particles believed to be carbon.
3. The low concentration of iron in the glass compared to that reported by the whole rock analysis on bulk samples indicates that a large portion of the iron oxide in the materials that were melted was reduced to elemental iron.
4. The reduction of the iron in the NTISV is believed to have been caused by distribution of carbon in the melt

REFERENCES

1. Geological Society of America, Rock Color Chart, Boulder, CO, 1970.
2. Shaw, H.R., 1972, Viscosities of Magmatic Silicate Liquids: an Empirical Method of Prediction., Amer. J. Sci., 272, 870-93

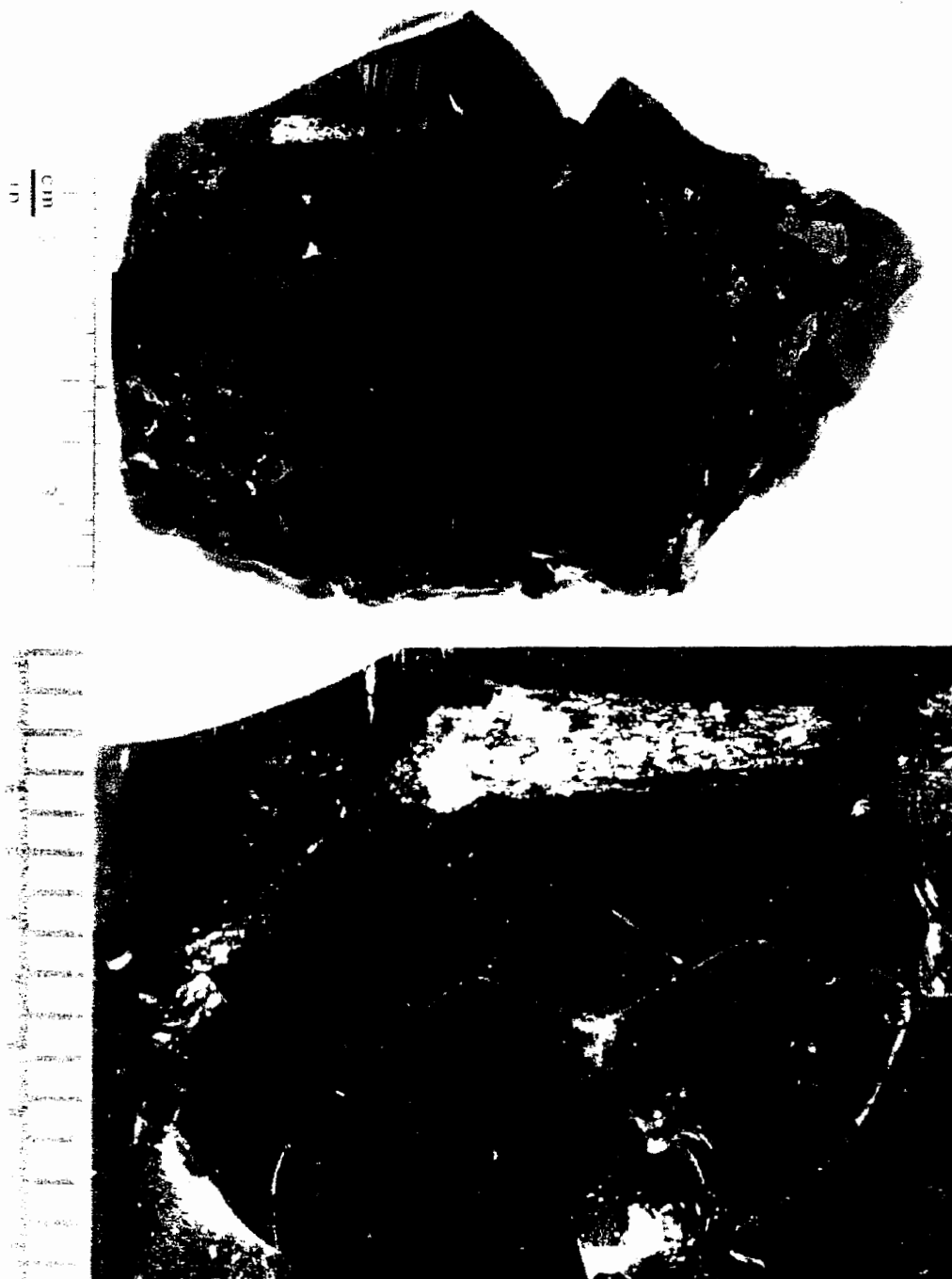


Figure 1A and 1B. Sample LANL-1

This photograph shows of Sample LANL-1 at low magnification. The scale at the right shows mm (fine scale) and 1/16th in. (coarse scale). The sample is black to grayish black with a waxy appearance and conchoidal fracture. Few inclusions are visible.

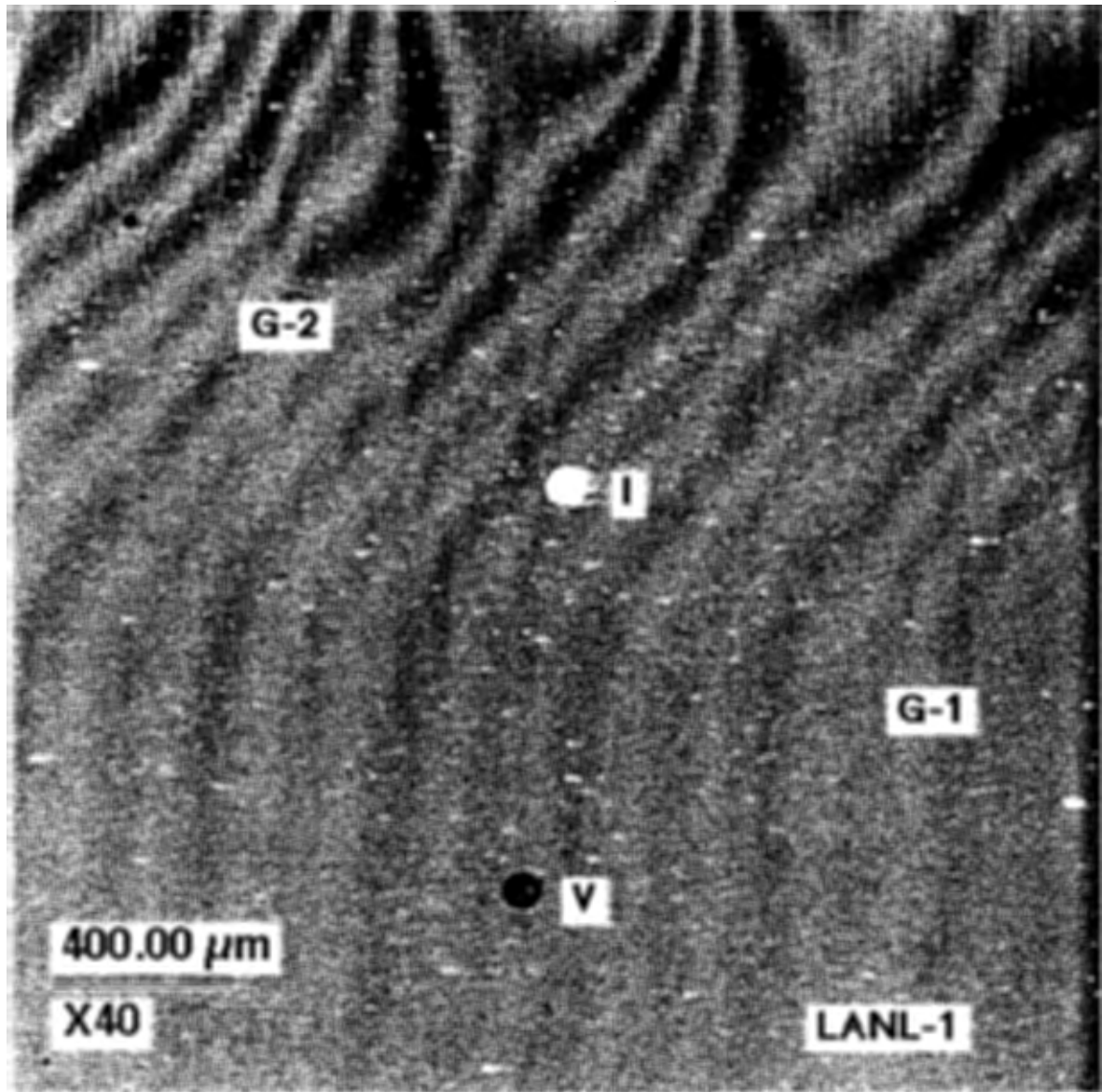


Figure 2. Sample LANL-1

This electron photomicrograph shows iron ("I" and small white specks), vesicles (V) and glass (medium gray background). The iron particle was that largest found in the sample. WDS analyses were conducted at the locations: G-1 and G-2. Many of the tiny black particles are believed to be carbon originating from the graphite starter material that was used to initiate the NTISV cold demonstration. Based upon whole rock and WDS analysis, this product is homogeneous on a macroscopic level and with the exception of distribution of iron, on a microscopic level as well.

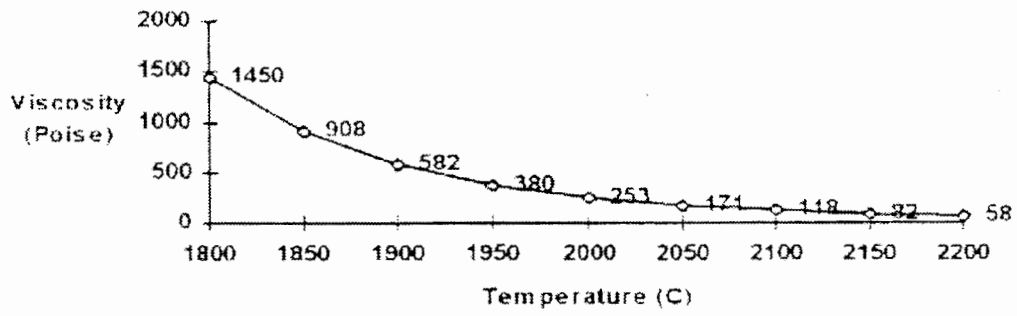


Figure 3. Predicted Viscosity of Cold Demonstration Molten Glass